TOPOLOGY ORIENTED SECURITY AND VULNERABILITY ANALYSIS IN POWER SYSTEMS

YOUWEI JIA

Ph.D

The Hong Kong Polytechnic University

2015

The Hong Kong Polytechnic University

Department of Electrical Engineering

TOPOLOGY ORIENTED SECURITY AND VULNERABILITY ANALYSIS IN POWER SYSTEMS

YOUWEI JIA

A thesis
submitted in partial fulfillment of the requirements for
the degree of Doctor of Philosophy

May 2015

CERTIFICATE OF ORIGINALITY

I hereby declare that this thesis is my own work and that, to the best of my knowledge and belief, it reproduces no material previously published or written nor material which has been accepted for the award of any other degree or diploma, except where due acknowledgement has been made in the text.

_____(Signed)

____Youwei JIA_____(Name of student)

To my parents,

Guanru Zhao and Yongling Li,

and my sister,

Youjing Jia

Abstract

Successful development of smart grid demands strengthened system security and reliability, which requires effective security analysis in conducting system operation and expansion planning. Classical *N-1* criterion has been widely used in the past to examine every creditable contingency through detailed computations. However, the adequacy of such approach becomes doubtful in facing with many recent blackouts where cascading outages are usually involved. This may be attributed to the increased complexities and nonlinearities involved in operating conditions and topological structures in the context of smart grid development. Thus far, existing literatures on multiple contingency (*N-k*) analysis show a lack of comprehensiveness to address topological changes of transmission networks in different contingency scenarios, and post-contingency risk (e.g. risk of potential cascading failures), etc. Most existing methods are less effective to accommodate more stringent security standards, which suffer from heavy computational burden, inaccuracy of *N-k* contingency screening, or both of them. Further, in large-scale electric power networks, such security analysis can be even more intractable due to massive data involved and the combinatorial explosion problem.

In this thesis, a comprehensive study is conducted to deal with the security threats particularly from *N-k* contingency induced topological changes in transmission network and cascading risk in the post-contingency phase. The need of effective and efficient

analytical approaches is highlighted in Chapter 1, where research background and incentive of this study are introduced in details. Chapter 2 presents an overview of existing research works concerning security issues of modern electric power network in a static sense, where tricky challenges and open problems are also identified. Motivated by previous works, a topology oriented security study is presented in Chapters 3 and 4, which cover two parts—underlying network robustness and resilience analysis, and *N-k* induced cascading contingency screening. Chapter 3 focuses on structural issues including topological vulnerability analysis, identification of network separations, network partitions in the smart grid environment, and percolation phenomena as critical phase transitions in power transmission network. Other than event based analysis, Chapter 3 provides high level statistical solutions based on complex network theory. In Chapter 4, a new and efficient *N-k* contingency screening framework is proposed, which comprises cascading failure simulation module (CFSM) for post-contingency analysis, risk evaluation module (REM) based on data mining techniques, and contingency screening module (CSM) for listing out different Pareto optimal fronts containing high-risk multiple contingencies. This framework comprehensively combines topological aspects and detailed steady-state cascading simulations. The effectiveness of this framework is demonstrated through two case studies on New England 39-bus system and IEEE 118-bus system.

It is concluded in Chapter 5 that incorporating topological analysis of underlying networks into steady-state power system security evaluation is an effective and promising way of *N-k* induced cascading contingency screening. Experimental results demonstrate a high potential of this framework for practical application on system planning. Meanwhile, Chapter 5 also indicates the future works to further extend this framework to fulfill emerging requirements in future smart grids.

List of Publications Arisen from the Thesis

Technical Papers in Refereed Journals

[1] **Youwei Jia**, Zhao Xu, Siu-Lau Ho, Zhao Yang Dong, "An hybrid approach for k-way partitions in smart grid based on Laplacian spectrum and self-organizing map". *Industrial Informatics, IEEE Transaction on*. (Submitted in 2015) (Remark: this is an awarded paper in *IEEE Student Paper Contest, Hong Kong, 2014/15*, which is also selected as one of top three papers representing Hong Kong Section to participate *IEEE Region 10 Paper Contest*)

[2] **Youwei Jia**, Zhao Xu, Loi Lei Lai, Kit Po Wong, "Risk based Power System Security Analysis Considering Cascading Contingency". *Industrial Informatics, IEEE Transaction on*. (Submitted in 2015)

[3] **Youwei Jia**, Zhao Xu, Zhao Yang Dong, David Hill, "Spectral Clustering based Approach for Detecting and Forecasting Uncontrolled Separation in Power Transmission Network", *Chaos: An Interdisciplinary Journal of Nonlinear Science*. (Submitted in 2015)

[4] Zhao Xu, Yang Gao, Songjian Chai, Jian Zhao, **Youwei Jia**, Ming Niu, Yujun Li, "Towards Intelligent Power Grid of The Future". *IEEE Systems, Man, and Cybernetics Magazine* (Submitted in 2015)

[5] **Youwei Jia**, Meng Ke, Zhao Xu, "N-k Induced Cascading Contingency Screening", *Power System, IEEE Transaction on*, vol. PP, pp. 1-2, 2014.

[6] **Youwei Jia**, Yang Gao, Zhao Xu, Kit Po Wong, Loi Lei Lai, Yusheng Xue, Zhao Yang Dong, David J. Hill, "Powering China's Sustainable Development with Renewable Energies: Current Status and Future Trend", *Electric Power Components and Systems*, (Accept to be published)

[7] Nan Sheng, **Youwei Jia**, Zhao Xu, Siu-Lau Ho, Chi Wai Kan, "A Complex Network Based Model for Detecting Isolated Communities in Water Distribution Networks", *Chaos: An Interdisciplinary Journal of Nonlinear Science*, 23(4), 043102

Conference Papers in Refereed Proceedings

[1] **Youwei Jia**, Zhao Xu, Loi Lei Lai, Kit Po Wong, "A Novel Network Partitioning Approach in Smart Grid Environment", *IEEE International Conference on Systems, Man, and Cybernetics*, October 10-13, 2015. (Submitted in 2015)

[2] Weicong Kong, Zhao Yang Dong, Guo Chen, **Youwei Jia**, "A rule based domestic load profile generator for future smart grid." *Power Engineering Conference (AUPEC), 2014 Australasian Universities. IEEE, 2014*.

[3] **Youwei Jia**, Zhao Xu, "A Graph-algebraic Approach for Detecting Islands in Power System", In *Innovative Smart Grid Technologies Europe (ISGT EUROPE), 2013 4th IEEE/PES, pp. 1-5. IEEE, 2013*.

[4] **Youwei Jia**, Zhao Xu, "Security Analysis of Physical Structure of Smart Grids-A Complex Network Perspective", in *Advances in Power System Control, Operation and Management (APSCOM 2012), 9th IET International Conference on, 2012, pp. 1-4*.

[5] **Youwei Jia**, Zhao Xu, "Novel Structural Vulnerability Assessment of Power Grids based on Complex Network" (in Chinese), *The Fifth Nanshan Academic Forum for PhD Candidates from Shenzhen, Hong Kong, Macao and Taiwan*, Shenzhen China, December, 2012

[6] **Youwei Jia**, Zhao Xu, "Risk Assessment Based on Information Entropy of Cascading Failure in Power Systems", in *Power and Energy Society General Meeting, 2012 IEEE, 2012, pp. 1-5*

[7] **Youwei Jia**, Zhao Xu, "Study of Grid-connected Single Phase Micro Photovoltaic Inverter", *The Fourth Nanshan Academic Forum for PhD Candidates from Shenzhen, Hong Kong, Macao and Taiwan*, Shenzhen China, December, 2011

[8] **Youwei Jia**, Yuan Li, "A 200-W Grid-connected Single Phase Micro-Photovoltaic Inverter and its Control Strategy", in *Power and Energy Engineering Conference (APPEEC), 2012 Asia-Pacific, 2012, pp. 1-4*.

[9] Youming Cai, **Youwei Jia**, Yuan Li, "Circuit Analysis of A Single Phase Micro-Photovoltaic Inverter", in *Power and Energy Engineering Conference (APPEEC), 2012 Asia-Pacific, 2012, pp. 1-4*

Acknowledgements

I would like to express my heartfelt gratitude to my chief supervisor, Dr Zhao Xu, for his continuous guidance, encouragement, care, support and patience throughout my entire graduate study. He is one of the most important persons in my life. Without him, I may end up in a completely different path.

I am grateful to my co-supervisor, Professor Siu-lau Ho, for his support and advice over the years.

In addition, I would like to sincerely thank my parents and sister for their unconditional love and support.

Finally and most importantly, I would like to acknowledge the support from Ph.D studentship awarded by The Hong Kong Polytechnic University.

Table of Contents

List of Tables

List of Figures

Nomenclature

Acronyms

CFSM	cascading failure simulation module
CI	correctness index
CSM	contingency screening module
DBI	Davies-Bouldin Index
DNNE	decorrelated neural network ensembles
MAPE	mean absolute percentage error
NERC	North American Reliability Corporation
PAM	power adjacency matrix
PNIP	power network interdiction problem
PTN	power transmission network
QEA	quantum inspired evolutionary algorithm
QMEA	quantum inspired multi-objective evolutionary algorithm
REM	risk evaluation module
RF	receptive field
RMSE	root mean square error
RVFL	random vector functional link
SC	spectrum closeness
SE	spectrum entropy

SOM	self-organizing map

Symbols

A	adjacency matrix
A_{power}	power adjacency matrix
E_{ave}	average efficiency
e_{ij}	efficiency of edge (i-j)
Cap_i	the capacity of node i
α	tolerance coefficient of a network
Ld_i	load of node i
P_i	real power injection of node i
Q_i	reactive power injection of node i
V_i	bus voltage of node i
$\mathcal{G}$	abstract graph of electric power network
$\mathcal{N}$	set of all vertices
$\mathcal{E}$	set of all edges
$S_{shortest}$	a set comprising all edges through the shortest path between a pair of vertices
ε_{ij}	electrical efficiency of path (i, j)
N_G	set of all generation nodes

N_L	set of all load nodes
E_{norm}	normalized overall efficiency
D	degree matrix
W	weighted adjacency matrix
L_{sym}	normalized Laplacian matrix (symmetric form)
L_{rw}	normalized Laplacian matrix (related to random walk)
$\mathcal{K}$	Kohonen map
$\eta(t)$	learning rate of SOM
$\Theta(\cdot)$	neighborhood function
S_{pareto}	Pareto set
p_c	threshold of percolating transition
$N_{lattice}$	size of lattice
θ	fraction of generation nodes in a PTN
γ	fraction of connecting nodes in a PTN
μ	fraction of load nodes in a PTN
G_j	sub-grid j
ΔD_m	total load shed
ΔV_m	total voltage violation
$R_{\{N-k\}}$	risk of a *N-k* contingency

$\hat{R}_D$	averaged risk in terms of load shedding
$\hat{R}_V$	averaged risk in terms of voltage violation
$\mathcal{F}_i$	N-k contingency vector
$\mathcal{T}$	risk dataset
α_i	weight of *i*-th base network
$b_i(\cdot)$	*i*-th individual learner
$b(\cdot)$	ensemble collective function
$\mathcal{D}$	training dataset
z	ensemble size
λ	regularizing factor
$g(\cdot)$	squashing basis function
β_{ij}	the output weight of the *j*-th hidden neuron in the *i*-th base learner
e_i	decorrelated error of the *i*-th individual learner
H_{corr}	hidden correlation matrix
B_{ens}	global output weights matrix
T_h	hidden-target matrix
$\mathcal{F}_i$	feature vector of contingencies
$\mathcal{T}$	risk vector of contingencies
$\tilde{y}_v$	prediction value of DNNE

Chapter 1 Introduction

1.1 Background of Research

Modern power system is now evolving towards smart grid with increased penetration of renewable energies, highly inter-connected physical network structure, as well as integration of information and communication technologies [1-4]. Advanced monitoring and control technologies to tackle flexible operating conditions with renewable generations [5, 6] and interactive demand sides [7] become widely deployed. Admittedly, smart grids make power transmission much more efficient while it also comes with significant concerns on operation security and reliability. Moreover, the trend of liberalization of electricity market can drive the whole grid to operate near its limits. Therefore, the development of smart grids places higher demand on security analysis in both planning and operation phases.

Generally, power systems are operated in accordance with *N-1* security criterion[1]. Such criterion is intended to inhibit contingencies with one component outage. However, the inadequacy of classical security assessment methods based on *N-1* has come to light after many blackout events happened over the past few years. For instance, large blackouts occurred in North America on August 14th, 2003 [8], Europe on November

[1] N-1 security criterion in power system requires that any single outage of one electrical component out of *N* will not result in violation of branch thermal limits and bus voltage.

12th, 2006 [9], Brazil on November 10th, 2009 [10], and India on July 30th, 2012 [11]. Even though such blackout events are infrequent, they usually give rise to devastating consequences to society. Meanwhile, power system failures always come along with negative impacts on other fundamental infrastructures, such as water supply, communication, and transportation, etc. According to previous records, complicated cascading behaviors in power systems were involved in the most blackout events [12]. Furthermore, since those power grids are *N-1* secure, most of those cascades are initiated by multiple component failures in combination. Consequently, robust power system operation necessitates more strict security criterion, which shall effectively consider multiple contingencies and even bear with various potential cascading outages.

In fact, the electricity industries in many countries have been revising the reliability standards from classical *N-1* security to more stringent *N-k* (where $k \geq 2$) security against potential cascading outages. For example, North American Electric Reliability Corporation (NERC) Standard FAC-011-2 [13] emphasizes that system operating limits should be established such that all single contingencies and certain multiple contingencies do not result in uncontrolled successive loss of system elements. This also highlights the need of developing reinforced security assessment framework to support future grid development.

Since cascading outages of electrical components in power systems frequently contribute to widespread blackouts, it is imperative to study and manage the cascading

risk when conducting security assessment for system planning. Thus far, a variety of simulation models have been established based on different cascading mechanisms to assess the risk or even reproduce blackout events. However, this topic is always challenging and remains open due to the complex and uncertain nature of outage propagation. Moreover, lack of trusted benchmarking cases and historical blackout data makes the existing methods and models fairly hard be effectively validated. In addition, a tremendous amount of cascading paths yielded by different models make it tough to accurately evaluate the consequence of cascading failures.

1.2 Incentive of Thesis

By far, most research works have focused on classical *N-1* contingency analysis while limited works have been done on multiple contingency analyses. Meanwhile, probabilistic or risk based analysis of potential cascading outages are rarely involved in existing works. Obviously, traditional methods cannot meet the ever enhanced security needs. To fulfill more stringent security standards, an effective security assessment framework should simultaneously consider both multiple contingencies and their potentially induced cascading failures. Under such new requirement, there are two major issues needed to be resolved. One of the confronted challenges is the combinatorial explosion of multiple contingencies. Notably, the number of contingency to be considered in an *N-k* security analysis is $N!/(x!(N-x)!)$, which can be extremely large even for a small *k*. For example, for a power grid with 10000 components, *N-3*

contingency analysis would require more than 1.6×10^{11} rounds of simulation, which is computationally costly and even infeasible. Obviously, detailed analysis of all possible N-k contingencies by exhaustive enumeration is not practical. Secondly, there are a tremendous number of possible cascading paths with different probability in post-contingency phase. Thus, the integration of risk evaluation of potential cascades thereby adds an extra multitude of complexity in addition to *N-k* security analysis alone.

In response to the aforementioned challenges, complex network theory provides a new perspective to investigate security assessment in terms of structural vulnerability of power grids. Complex network based models can simulate the cascading process based on network evolution rules [14-16] without explicit modeling of power flows. Such high-level models can well accommodate the uncertainty and complexity involved in cascading failures from a network topology perspective, and can provide some rough indication of structural vulnerability of power grids. Nevertheless, they can also be misleading since significant electrical properties and principles (e.g. Kirchhoff's laws and Ohm's Law, etc) are neglected. By capturing more electrical features, different approaches have been proposed to enhance complex network based models so as to investigate the topological vulnerability of power grids taking practical engineering considerations into account.

Given above analysis, a comprehensive security assessment framework developed from a network topological perspective while taking various practical considerations into account is developed in this thesis, which consists of two parts:

1) Analysis of topological robustness and resilience of power transmission networks (PTNs) based on complex network theory.

By capturing more electrical features (i.e. load flow sensitivity), a novel complex network based model is proposed for power grid structural vulnerability analysis. To effectively identify the weak portions that would cause system uncontrolled separation, a spectral clustering based approach is developed. In the context of "self-healing" capability in smart grid, a hybrid approach for k-way network partitions is developed accordingly. Lastly, some "small-world" properties of power grids are investigated in this thesis. A percolation model is constructed to quantitatively evaluate the grid resilience to electrical component outages.

2) Risk based *N-k* contingencies screening considering potential cascading outages.

To tackle the issues rooted from *N-k* combinatorial explosion, a sufficient number of credible contingency cases are considered for big data analysis of these contingencies. An advanced algorithm of decorrelated neural network ensembles (DNNE) is proposed to learn *N-k* contingencies under different operating conditions and predict the corresponding cascading risk. In considering the uncertain and complex nature of potential cascades following each *N-k* contingency, Monte Carlo simulation method is adopted to provide a high-level statistical solution for cascading risk evaluation. Lastly,

a new screening approach based on quantum inspired multi-objective evolutionary algorithm (QMEA) is proposed, which is capable to effectively capture a bunch of Pareto fronts of contingencies with different rankings in a large search space.

1.3 Thesis Layout

The remainder of this thesis is organized as follows:

Chapter 2 reviews the previous research work of steady-state security analysis including conventional models of power system contingency screening and complex network theory based methods for topological vulnerability assessment. The drawbacks of existing methods for power system interdiction problems are discussed in context of new industrial security standards. In addition, different types of models for cascading failure simulation are reviewed. As an effective way of network structure analysis, the strengths and weakness of complex network theory utilized in power system analysis are also discussed.

The robustness and resilience of power transmission network is discussed in Chapter 3, in which four types of applications based on complex network theory are presented— i) a novel structural vulnerability assessment method is proposed, where power flow sensitivity matrix is incorporated; ii) to identify the uncontrolled system separation in advance, a spectral clustering based approach is proposed; iii) to enhance "self-healing" control in the context of smart grid, a k-way partitioning method is proposed based on

Laplacian spectrum and self-organizing map (SOM) algorithm; and iv) a "small-world" percolation model is proposed to quantitatively evaluate the network resilience of power transmission network.

In Chapter 4, an advanced *N-k* contingency screening method is proposed, which consists of cascading failure simulation module (CFSM), risk evaluation module (REM), and contingency screening module (CSM). CFSM generates cascading risk database containing different operating scenarios, which is used to train DNNE in REM. A well-trained REM can efficiently assess the cascading risk of an *N-k* failure using simple matrix calculation. By formulating the interdiction problem as a multi-objective optimization problem, QMEA employed in CSM can screen out high-risk multiple contingencies in different levels.

Finally, Chapter 5 concludes this thesis. Some prospective extensions for future work are also summarized.

The overall structure of this thesis is illustrated in the schematic diagram shown in Fig. 1.1.

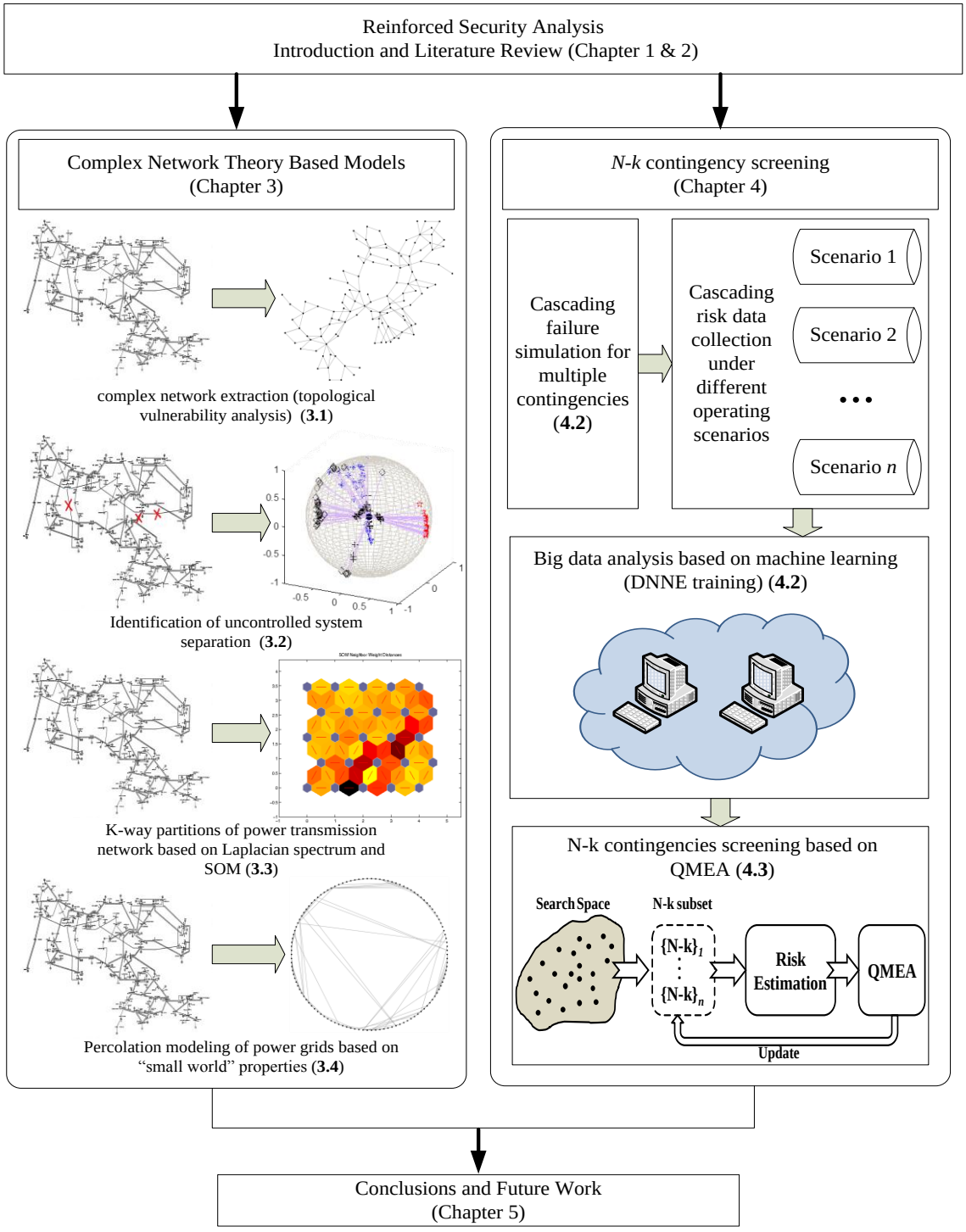

Fig 1.1 Illustration of the overall structure of this thesis

Chapter 2 Overview of Steady-State Security Analysis in Power System

2.1 Introduction

As introduced in Chapter 1, electricity reliability organizations, e.g. NERC, have enhanced the operational security standards, which require that "Transmission Operators shall actively operate to protect against instability, uncontrolled separation, or cascading outages resulting from multiple outages". Under such context, a comprehensive security assessment framework is proposed including two modules for identification of uncontrolled system separation, and *N-k* induced cascading contingencies screening respectively. In [17], Mili and Dooley argue that the conventional concept of *N-1* security is evolving towards to a new concept of network resiliency to system events with substantial risk. Unlike traditional models for *N-1* or a credible set of *N-k* contingency analysis, the method proposed in this thesis jointly considers the potential cascading risk caused by multiple transmission line outages and network resilience to component outages from the topological perspective. Conventional works based on load flow for contingency analysis are comprehensively reviewed in Section 2.2. Complex network, as a useful theory to investigate the structural vulnerability and network evolution, is employed in the proposed framework. Related studies are reviewed in Section 2.3.

2.2 Conventional Works on Contingency Analysis

2.2.1 Load flow based power system interdiction problem

In recent years, the urgent need of more detailed security analysis by evaluating the long-term impacts of multiple contingencies has drawn much attention around the world. The *N-k* contingency analysis is also known as power network interdiction problem (PNIP). Solving PNIP is always challenging and somewhat intractable due to the heavy computational burden involved. The existing literatures dealing with PNIP can be roughly categorized into two classes.

The first category focuses on establishment of high performance computing platforms to accommodate the heavy computational burden. Some pioneering work, for example, [18-21], exploited the use of parallel processing based on adequate pools of computers interconnecting together. The computational capability for system analysis is obviously strengthened by doing so, whereas the limitations of those works were exposed since they are less extendable and require significant hardware system upgrade for larger or more complex electric networks. Subsequently, some more advanced computing strategies were proposed, for example, pervasive grid computing platform reported in [22], which is further improved and even more powerful than previous computing paradigms. Nevertheless, exhaustively simulating all contingency cases under different operating scenarios in a large-scale power system is still infeasible, and less valuable due to its nature of time consuming.

The second category includes a number of tailor-made algorithms, which intrinsically reduce the computational complexity or the dimension of PNIP. In [23], a method using event trees based on substation configuration data was proposed to identify a number of multi-failure combinations. In order to reduce the elapsed time of power flow calculation during simulations, line outage distribution factors were adopted in [24] to identify N-k contingencies that result in overload of transmission lines. By scaling down the dimension of PNIP to only focus on a specific set of the highest-impact or the most severe multiple contingencies, some optimization based screening algorithms have been proposed, such as, a mixed-integer linear model based on discrete and non-convex optimization reported in [25]; an extreme events screening method based on optimal graph partitioning reported in [26], and its extended version illustrated in [27], where a mixed integer nonlinear programming model is used, and so forth. Such optimization based approaches can identify *N-k* contingencies with respect to different objectives in acceptable durations, whereas the results are sensitive to the formulation of objectives. Without loss of generality, a "random chemistry" algorithm has been applied to contingency analysis in [28, 29] to generate all unbiased collections of multiple contingencies for statistical analysis.

To sum up, exhaustive enumeration based methods can yield comprehensive results but are highly demanding on computing power. Tailor-made approaches are promising that can effectively reduce the dimension of PNIP, while the results can be significantly subject to the formulation of objectives and system models etc.

2.2.2 Risk assessment of cascading failures

Cascading outages are the main causes of wide-spread blackouts [30]. Cascading behaviors in power system are complicated and difficult to be assessed. In evaluating the risk of cascading failures, considerable research efforts have been devoted and a number of commercial tools are developed and used in the current electrical industries [31]. For example, CAT (Cascade Analysis Tool) based on AC power flow is adopted in the US; and ASSESS based on DC or AC steady state plus dynamic simulations is adopted in the UK.

Thus far, a number of cascading simulation models (such as hidden failure model [32, 33], branching process model [34-36], CASCADE model [37], OPA model [38-41] and its extended / improved models [42-44], Manchester model [45, 46], stochastic model [47, 48], etc.) have been proposed to simulate system behaviors in different ways by different researchers. All existing methods and models are capable of capturing only a subset of cascading mechanisms [49]. Thus, there is no perfect method or model for analyzing cascading failure, which can address every single aspect in both academic and industrial areas. Nevertheless, based on different engineering considerations, it is fairly valuable to explore various combinations of cascading mechanisms to model system behaviors under different operating scenarios. Some typical research-grade models are reviewed as follows:

1) Hidden failure model. This model was developed by Chen and Thorp, which mainly focuses on thermal overload and generator re-dispatch. The concept of hidden failure is referred to as the incorrect or inappropriate actions of a relay or a relay system. Hidden failure model uses fast simulation technique and heuristically identifies potential failure of protection system in a probabilistic manner. The outage probability of electrical components (e.g. transmission line) depends on thermal overload causing the hidden failure of relay systems.

2) OPA model. OPA model is jointly developed and named by Oak Ridge National Laboratory, Power Systems Engineering Research Center at the University of Wisconsin and University of Alaska. This model simulates both cascading behaviors of a power system in a fast process, and system development (e.g. growing load demand) and engineering responses in a slow time scale. In the simulation model, the initial failure is generated randomly. Once a failure occurs, the generation and load in the power system are re-dispatched based on DC load flow. The subsequent line outages are randomly selected in a group of overloaded lines. Such process is iterated until cascade ends.

3) Manchester model. This model comprehensive includes a wide range of cascading failure interactions, such as tripping of transmission lines, generator instability, under frequency load shedding, voltage collapse, re-dispatch of

active and reactive resources, etc. Beside the network data for load flow calculation, the probabilities of electric component failures (e.g. tripping of generators based on under voltage protection, tripping of transmission lines based on hidden failure of protection systems, etc) are also included as the input for this model. In some extended versions, some non-system-level faults (e.g. weather conditions, natural disasters, etc) are also modeled. The termination criterion for cascading failure simulation is set in the model. Monte Carlo trials are frequently used to analyze different cascades until the termination criterion is satisfied.

4) Branching process model. This is a high-level probabilistic model which globally provides a statistical solution of transmission line outages and a total amount of load shed. This type of model does not retain the topological data and no load flow calculation is needed.

Among the models illustrated above, hidden failures due to malfunction of relay are regarded as an important reason for cascading development. Therefore, in this thesis, hidden failures of protection system caused by thermal overload are assumed to be the main inducement of fault propagation in cascading analysis.

2.3 Topological Models for Power System Analysis

2.3.1 Structural vulnerability assessment and weak portion identification for uncontrolled system separation

Incorporating complex network theory into power system analysis has provided novel and useful solutions to many practical issues [50]. Initially, physicists developed complex network theories such as Erdos-Renyi random networks in their researches on abstract networks to mathematically analyze the structure and linkage of networks [51-53]. Because of the abstract nature, the classical complex network theory is unable to fully address physical properties of many practical networks. Motter et al studied internet and power system networks and found the robust-but-fragile feature under cascade-based attacks [54, 55]. Simultaneously, some complex network based models were reported to investigate the structural vulnerability of power grids [50, 56]. These works mainly focus on the physical topologies and structural connection of networks, while mostly neglecting specific electrical features and interactions of network components governed by engineering principles.

Even though cascading failures in both theoretical complex network and practical power grids have some similar features, such as criticality and power laws [57, 58], the failure propagation mechanisms of them can be quite different. Therefore, purely topological models based on complex network theory may not be able to reflect detailed power system behaviors. Nevertheless, this theory is useful for statistical studies of

topological properties by considering the PTN as an abstract graph. The PTN design aims at transferring electric power from generation sides to demand sides. Undoubtedly, the functionalities of PTN are significantly dependent on the topological structure, which is greatly affected by their organizational complexities and interplays among all electrical components[58]. In [59], Barabasi-Albert discovered that the scale-free network which is characterized by heterogeneous structures and non-uniform degree distributions, possesses some important features such as robustness against random failures as well as vulnerability to attacks on their hubs, i.e. nodes with high degree, high connectivity. Once the network is changed by e.g. component outages, the network functionality may be significantly weakened. In [60], Watts has demonstrated the small-world features of the typical electric power network. Based on the topological statistics, the cascading models in complex network have been reported in [54, 61, 62]. In [63], Hines and Blumsack generalize the concept of betweenness[2] in electric power network by considering electrical distances, which also reveals the scale-free properties of the power grid structure. In recent years, specific features and interplays of electric components in PTNs have been studied in [64-66] from a complex network perspective, which deserves further research efforts.

To the author's best knowledge, there have been few applications of complex networks to tackle the challenging issue of uncontrolled network separation in power

[2] "*betweenness"* is measured to indicate the importance of link or node based on complex network theory, which is proportional to the number of least distance paths though the link or node.

systems. Previously, some research works revealed that large and highly interconnected power systems possess small-world features, where different parts are highly interdependent to each other and interact directly or indirectly. One particular property of a small-world network is that the network distance or connectivity can be greatly affected by topological changes [67]. One failure in a part may notably propagate to other parts then split or even collapse the whole network. Previous researches are fairly valuable for system islanding detection while those works are principally based on qualitative analysis.

Detecting system separations in PTNs is closely related to the graph-partitioning research, where many relevant algorithms and approaches have been developed thus far. As a pioneering work, Girvan and Newman proposed an iterative method based on the concept of *betweenness* [68-70], which can well recognize network splitting patterns by recursively removing edges with the largest betweenness. This approach yields very good partitioning results but is computationally heavy and time consuming. In [71], a divisive algorithm is reported that can well handle triangular or higher order arcs i.e. loops exposed in networks. Proposed in [72], Wu-Huberman algorithm is based on the idea of voltage drop, which can be fast but still involve iterative computations. Based on a *q*-state Potts Hamiltonian, Reichard-Bornholdt method is reported in [73], which is a pioneering approach for identifying fuzzy communities. In [74], Capocci-Servedio-Colaiori-Caldarelli method combines spectral properties of networks with correlation measurements to detect the closeness of communities.

By applying graph-partitioning algorithm to islanding detection in PTNs, the need of computing efficiency and detecting accuracy is accentuated in this thesis. Therefore, a tailor-made improved spectral clustering algorithm is proposed in Chapter 3 (Section 3.2) to capture an insight of emerging topological separation in PTNs.

2.3.2 Network partitioning

Power grids normally comprise of several synchronous interconnected sub-systems, which are usually referred as "control area". Each of them is controlled by its respective control entity (e.g. regional transmission organization). Traditionally, these areas are formulated considering asset ownerships, as well as policies and regulations etc. that govern power system operation. Direct application of the existing control areas can simplify the network partitioning tasks, but may not guarantee satisfactory performances, for example, system restoration in a later stage. This is because the conventional way of network partitioning may not best fit with the evolving topology and operation conditions of the power grids from a perspective of power balance.

Thus far, a lot of research works have been reported in literatures on intentionally dividing power systems into several areas for particular purposes. As pioneering works in the field, [75] and [76] propose a partitioning method of "tearing" down the large-scale power systems to reduce the computational complexity. To be specific, many approaches of network partitioning are subsequently proposed to tackle different applications with big data and heavy computations such as resource adequacy

assessments[77], area-based voltage stability assessment and control[78-80], electricity market (e.g. zonal pricing[81]) and reserve scheduling, and so forth. Another important application of power system partitioning (or termed as "islanding" in some literatures) is for planning and operational security analysis. Some of these approaches e.g. [26, 27, 82] are based on steady or quasi-steady state analysis to address generation-load imbalance problems. Meanwhile, several studies utilize synchronization of complex network[83] or simulation methods (e.g. slow coherency approach[84, 85]) to identify the dynamic coherent sub-networks in power systems. In recent years, some studies have reported that partitioning methods can also be utilized to facilitate the integration of wind power sources in power grids [86].

In the context of smart grid, different network partitioning algorithms are proposed regarding planning[87], security control[88] and system reconfiguration[88, 89], etc. In traditional power systems, islanding boundaries for security control and subsequent reconfiguration are predetermined according to control area boundaries or transmission operators. In most cases, this can be less effective since the operating conditions and topological structure of PTNs are not properly considered. In this thesis, an effective network partitioning approach for smart grid is proposed, which is inspired by some previous works in [80, 87, 90]. In [87], an electrical distance based partitioning method was proposed to reflect network topology when considering different network attributes. In [90], the electric network is partitioned based on generation-load imbalance to identify combinations of multiple contingencies. Voltage stability was considered in the

partitioning problem in [80] for reactive power planning. In the proposed approach in this Thesis, one attempts to efficiently partition the PTNs to contribute to system planning and provide useful solutions for intentional islanding or reconfiguration from a "self healing" perspective. It should also be noted that the real power flow is a good reflection of the operational conditions and the reactive power flow has strong influences on voltage profile. Consequently, the network topology, real and reactive power flows are jointly considered in this approach. Detailed illustrations and discussions will be addressed in Chapter 3 (Section 3.3).

2.4 Summary of This Chapter

In this Chapter, steady-state security analysis based on traditional power system models and topological models are comprehensively reviewed. Accommodating the heavy computational burden, as well as uncertainty and complexity involved in cascading contingencies, has been indicated for further research work. Complex network, which serves as a useful theory to study the electric network topologies, is also highlighted in this Chapter. Motivated by previous research works, some network robustness and resilience evaluating models, and an *N-k* induced cascading contingency screening framework are proposed in this thesis, which are illustrated in details in Chapters 3 and 4 respectively.

Chapter 3 Robustness and Resilience of Power Transmission Network

3.1 Structural Vulnerability Assessment based on Complex Network Theory

3.1.1 Introduction

Electric power network has been considered as one of the largest manmade complex networks over the world. Effective protection and reliable operation of such fundamental infrastructure all rely on the prior identification of crucial and/or weak portions of the whole network. This section mainly deals with the impact of removals (or component failures) of network links and studies the overall structural vulnerability via "efficiency" loss oriented perspective.

Traditionally, topological models based on complex network theory are developed to describe an abstract graph with a group of nodes connected by edges. The topological connection can be expressed mathematically by an adjacency matrix $\boldsymbol{A}$:[a_{ij}]. If an edge connects node i and j, a_{ij} is 1, otherwise a_{ij} is equal to 0. This matrix also represents the efficiency of each edge. Based on the complex network theory, the definition of efficiency for each edge is the inverse of the shortest distance between node i and j (i.e. $e_{ij}=1/d_{ij}$), which means that a shorter distance of edge reflects higher efficiency [91].

Structural vulnerability analysis of complex networks significantly depends on this matrix. The average efficiency of a network is calculated as:

$$E_{ave} = \frac{1}{N(N-1)} \sum_{i \neq j} e_{ij} \tag{3-1}$$

where E_{ave} denotes the average efficiency, N is the total number of nodes and e_{ij} is the efficiency of each edge.

According to complex network theory, the load of a node is defined as "betweenness", namely the number of the shortest paths through it. The capacity of each node is expressed as:

$$Cap_i = \alpha \cdot Ld_i(0) \tag{3-2}$$

where Cap_i is the capacity of node i, α is the tolerance of the network, and $Ld_i(0)$ is the initial load of node i.

In reference [12], it is stated that removals of a bunch of nodes can trigger a cascading process. The functionality of networks is continuously weakened and the whole system would tend to evolve to a new stable state. In electric power network, the malfunction of a small group of nodes or even a single node will cause the whole network successively to be deteriorated. Based on complex network theory, network evolution process can be modeled as following—a node is initially removed randomly or intentionally; afterwards, the shortest distances between nodes will change

accordingly and the load of each node will be redistributed. The sequence of dynamical behaviors could be mathematically illustrated as the following iteration rule [16]:

$$e_{ij}(t+1)=\begin{cases} e_{ij}(0)\dfrac{Ld_i(t)}{Cap_i}, Ld_i(t)>Cap_i \\ e_{ij}(0), Ld_i(t)\le Cap_i \end{cases} \tag{3-3}$$

where *t* denotes the iteration step. By means of this iteration method, the efficiency of edges connected with an overloaded node will be reduced. It will recover to the initial efficiency when the nodal load returns to normal. This iterative process will continue until the whole network evolves to a new stable state. The structural vulnerability can be qualitatively assessed according to overall efficiency loss under different nodal or edges' removals.

3.1.2 Proposed complex network model

Traditional complex network based models inaugurate a new research direction of vulnerability analysis for electric power networks. However, those models fail to address sufficient electrical features and operational principles. In order to improve the accuracy and efficiency of structural vulnerability assessment based on complex network, a few of engineering considerations are taken into account in the proposed model.

A. Power adjacency matrix (PAM)

Generally, a PTN consists of generation buses, load buses (i.e. demand sides), electrical facilities (e.g. transformers, relays, breakers, etc.) and physical links (i.e. transmission lines). Secure and reliable operation of power systems aims to transfer electric power from generators to different loads. Based on the concept of complex network, PTNs can be extracted into directed or non-directed graphs with vertices connecting by edges. In this model, a PTN is regarded as a non-directed graph, where generators are considered as source vertices; loads are considered as sink vertices; and transmission lines and transformers are considered as weighted edges. This is reasonable as bi-directional power flows exist in most electric components of PTNs such as transmission lines. Mathematically, a PTN can be denoted by $\mathcal{G}(\mathcal{N},\mathcal{E})$, where $\mathcal{N}=\{n_1,n_2,...,n_{|N|}\}$ is the set of all vertices and $\mathcal{E}=\{edge_1,edge_2,...,edge_{|E|}\}$ is the set of all edges. Each edge corresponds to a pair of vertices (n_i,n_j) .

In power system, nodal power injection is calculated as [92]:

$$\begin{cases} P_i = V_i \sum_{j\in i} V_j (G_{ij}\cos\theta_{ij} + B_{ij}\sin\theta_{ij}) \\ Q_i = V_i \sum_{j\in i} V_j (G_{ij}\sin\theta_{ij} - B_{ij}\cos\theta_{ij}) \end{cases} \quad i = 1,2,3,...n \qquad (3\text{-}4)$$

where P_i and Q_i represent the real and reactive injection power of node i respectively, and V_i is bus voltage of node i.

The incremental active and reactive power can be formulated as Eq (3-5). Detailed derivation can be referred to Appendix-A.

$$\begin{bmatrix} \Delta P \\ \Delta Q \end{bmatrix} = \begin{bmatrix} H & N \\ J & L \end{bmatrix} \begin{bmatrix} \Delta\theta \\ \Delta V / V \end{bmatrix} \tag{3-5}$$

In a high-voltage power system (i.e. transmission system), real power flow is mainly subject to the bus angle while reactive power is mainly subject to bus voltage magnitude. Therefore, Eq. (3-5) can be simplified as:

$$\left.\begin{aligned} \Delta P &= H \cdot \Delta\theta \\ \Delta Q &= L \cdot \Delta V / V \end{aligned}\right\} \tag{3-6}$$

H and L are specified as:

$$H = L = \begin{bmatrix} V_1 & & 0 \\ & V_2 & \\ & & \ddots \\ 0 & & V_n \end{bmatrix} \begin{bmatrix} B_{11} & B_{12} & \cdots & B_{1n} \\ B_{21} & B_{22} & & B_{2n} \\ \vdots & \vdots & \ddots & \vdots \\ B_{n1} & B_{n2} & \cdots & B_{nn} \end{bmatrix} \begin{bmatrix} V_1 & & 0 \\ & V_2 & \\ & & \ddots \\ 0 & & V_n \end{bmatrix} \tag{3-7}$$

where B_{ij} is the entry of susceptance matrix.

According to $\boldsymbol{H}$ matrix, $h_{i,j}$ ($i \neq j$) not only indicates the topological connection of power system, but also reflects the power transmission capability of each edge. Based on the classic concept of adjacency matrix, a new and symmetric matrix, termed as *power adjacency matrix* (denoted as A_{power}), is proposed to generalize the topological and electrical features of PTNs.

B. Improved complex network based model for electric power networks

A directed graph is constructed based on PAM. Each entry of this matrix represents the efficiency of a corresponding edge. In this model, *betweenness* of nodes is still utilized to characterize the load distribution. The electrical efficiency of a path from generation bus to load bus is defined as the harmonic composition of a sequence of edges, which can be expressed as:

$$\varepsilon_{ij} = \left(\sum_{(n,m)\in S_{shortest}} 1/e_{nm} \right)^{-1} \tag{3-8}$$

where $S_{shortest}$ is the set of all edges through the shortest path between a pair of vertices. ε is the *electrical efficiency* of path (*i, j*)

The overall efficiency of the whole network is defined as the averaged efficiency of all paths from generation nodes to load nodes, which is expressed as follows:

$$E_{ave} = \frac{1}{|N_G||N_L|} \sum_{i\in N_G} \sum_{j\in N_L} \varepsilon_{ij} \tag{3-9}$$

where $\boldsymbol{N_G}$ and $\boldsymbol{N_L}$ denote the sets of generation nodes and load nodes, respectively. The overall efficiency can be normalized as:

$$E_{norm} = E_{ave} / E_{ave}(0) \tag{3-10}$$

where $E_{ave}(0)$ is the overall efficiency at the initial state.

Based on PAM, the iterative rule for evolution of PNTs is adjusted accordingly as:

$$h_{ij}(t+1)=\begin{cases} h_{ij}(0)\dfrac{Ld_i(t)}{Cap_i}, Ld_i(t)>Cap_i \\ h_{ij}(0), Ld_i(t)\le Cap_i \end{cases} \tag{3-11}$$

According to Eq.(3-11), if node *i* is overloaded in *t*-th step, the efficiency of edge (*i*, *j*) will be decreased in (*t+1*)-th step. This may lead to a redistribution of nodal loads.

3.1.3 Numerical simulation results

In this section, the structural vulnerability of IEEE 118-bus system is investigated by both traditional and the proposed models. This system can represent a complex transmission network, which consists of 54 generation buses, 64 load buses and 186 branches. Since the size of this testing system is reproducible, the simulation conclusion could be pervasively applied to larger PTNs.

In this case, single node removal strategy is firstly applied to mimic the disturbance caused by electrical components being out of service. Normally, transmission line outage is much more common than nodal outage in power systems. Therefore, subsequent single edge based attack is adopted to trigger network evolution for vulnerability analysis. Simulation process follows the flowchart shown in Fig. 3.1. Random and load-based intentional attacks are applied to both traditional and proposed models.

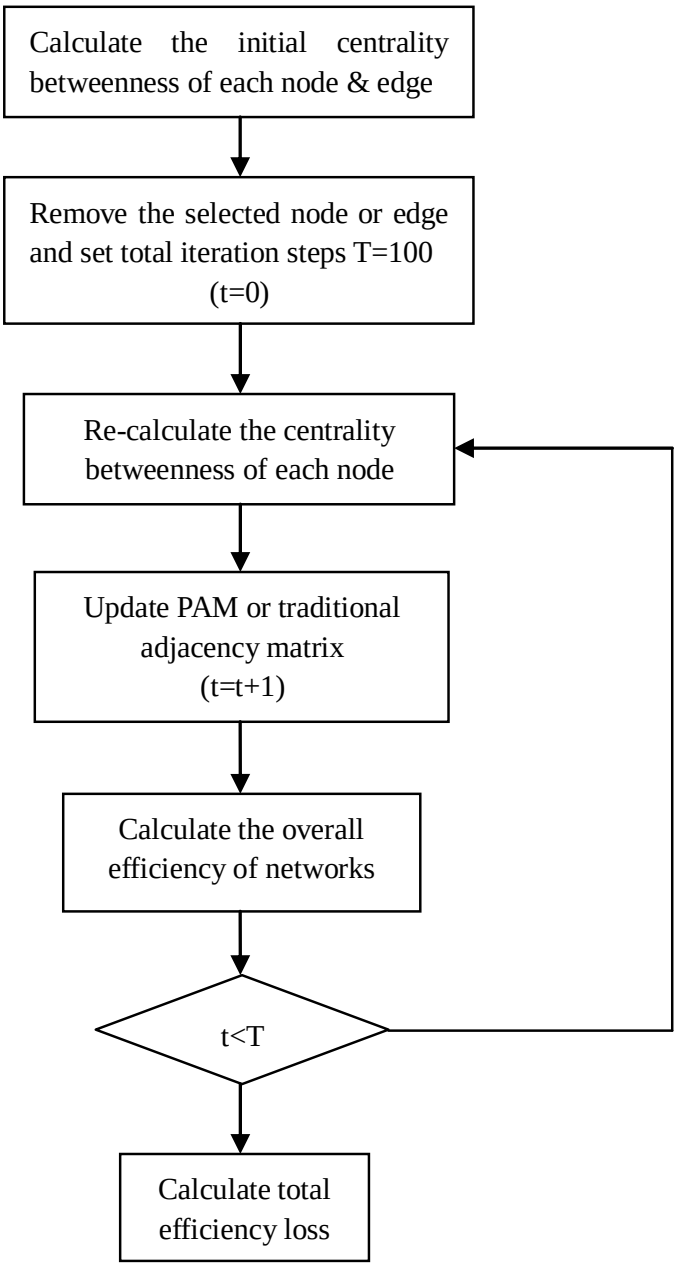

Fig 3.1 flowchart of simulation process of network evolution

Figs 3.2~3.3 and Figs. 3.4~3.7 illustrate the dynamical behaviors of IEEE 118-bus system after initial disturbance of nodal attacks and edge based attacks, respectively.

Network efficiency curves are obtained by averaging 100 individual random removals. Load-based intentional attack is also applied to a single edge with the highest centrality betweenness.

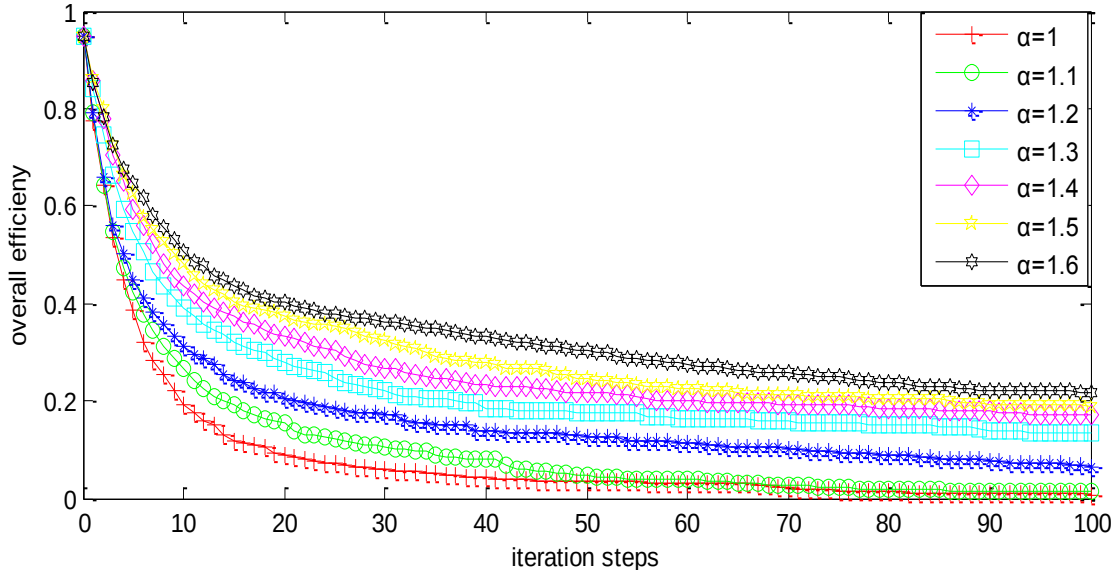

Fig 3.2 Efficiency curve based on random failure (node No. 38) in traditional model

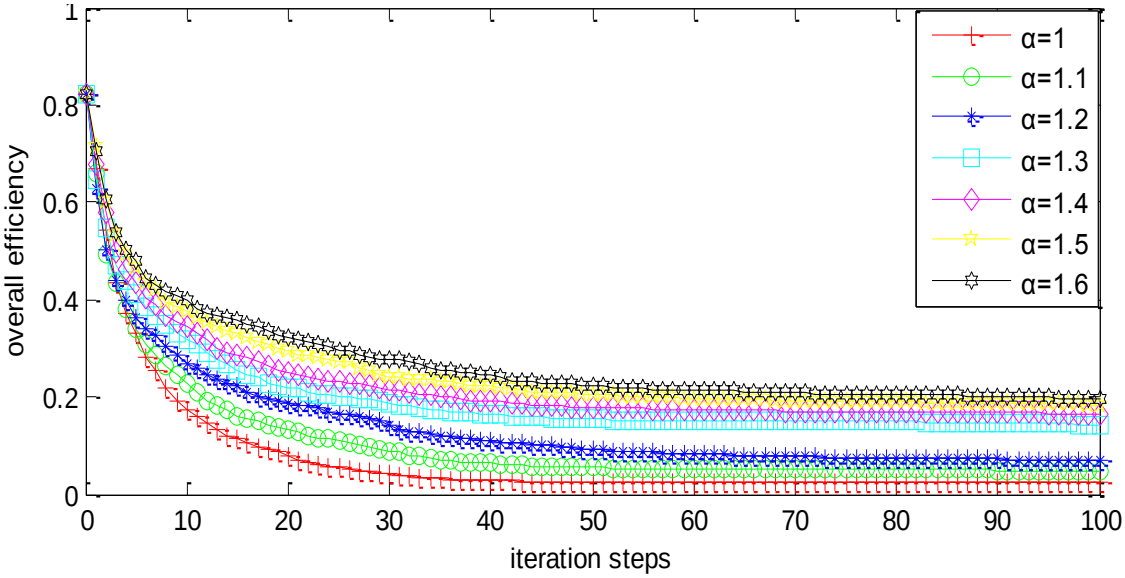

Fig 3.3 Efficiency curve based on random failure (node No.38) in the proposed model

In the node based attack simulation, bus No.38 is initially removed. Figs. 3.2 and 3.3 show the dynamical behaviors from iteration step t=0 to t=100. When the tolerance of node is increased, the overall efficiency of the whole network at the stable state is increased in different levels based on traditional and proposed models. Obviously, simulation based on proposed model converges to stable state faster than that of traditional model. For instance, it can be seen in Figs. 3.2 and 3.3 that traditional model needs more than 90 iteration steps to reach stable state (when α =1.6), while only less than 40 steps are taken by the proposed model.

In the edge based attack simulation, a single edge is removed randomly or intentionally (by selecting the one with highest centrality betweenness). Figs. 3.4-3.7 demonstrate the dynamical behaviors of the testing network based on traditional and the proposed models, respectively. Similar conclusions can be drawn that simulation relying on the proposed model is much more efficient, especially for high network tolerance.

Fig. 3.8 shows the total efficiency loss at stable state for both traditional and proposed models. It is obvious that the trends of simulation curves obtained by these two models are roughly similar. However, there still exist some slight differences. For example, when tolerance α=1.1 in random attack condition, the total efficiency loss obtained from traditional model is increased to nearly 1. That is to say, generally the whole power system will suffer a blackout if an initial removal of a node may trigger a

cascading failure. However it is well known that even the most critical blackout in history did not break down the whole transmission network. The curve obtained by the proposed model is hereby more reasonable.

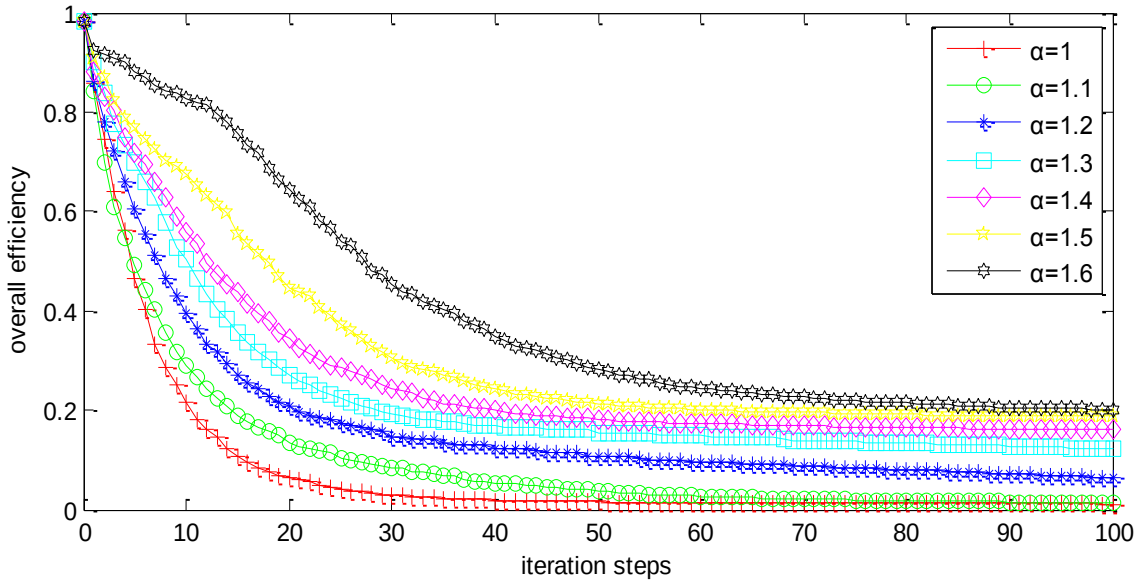

Fig 3.4 Efficiency curve based on intentional attack (edge No.104) in traditional model

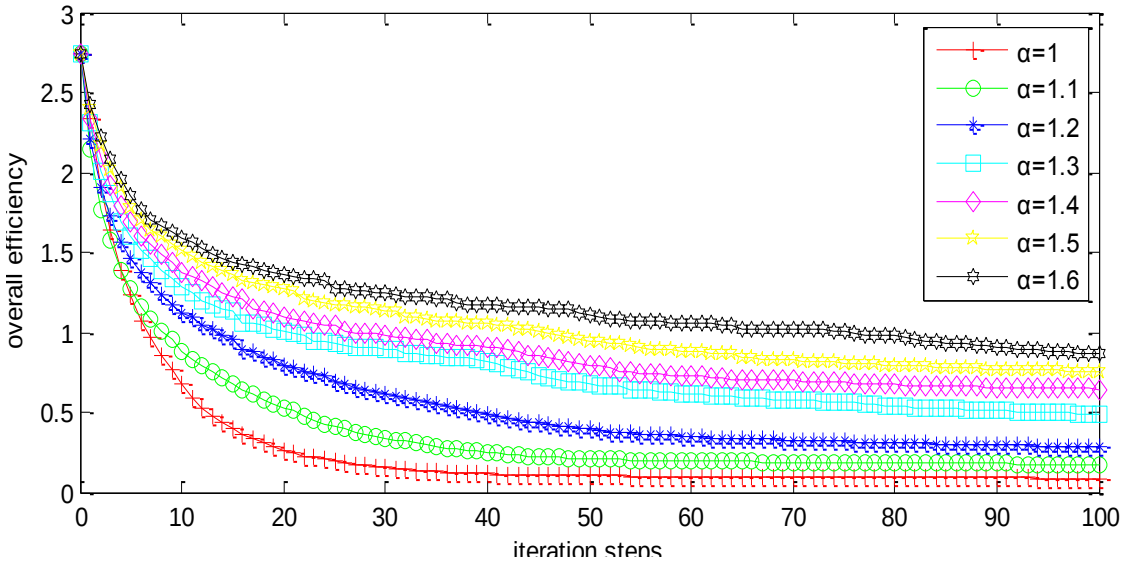

Fig 3.5 Efficiency curve based on intentional attack (edge No.104) in proposed model

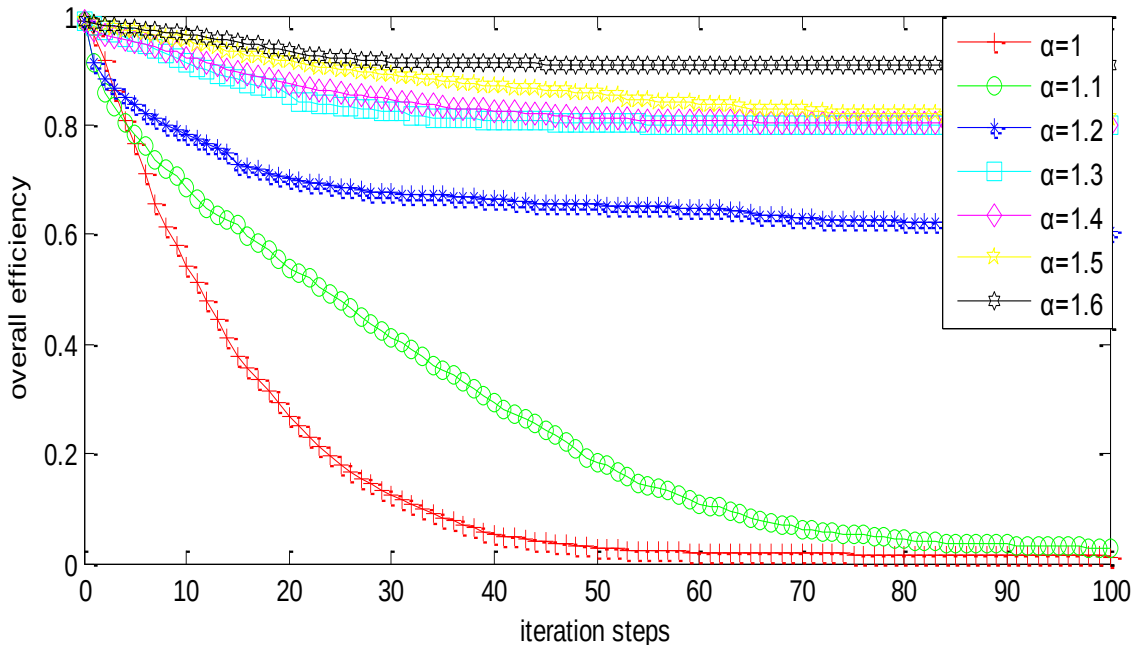

Fig 3.6 Efficiency curve based on random failure (edge No.97) in traditional model

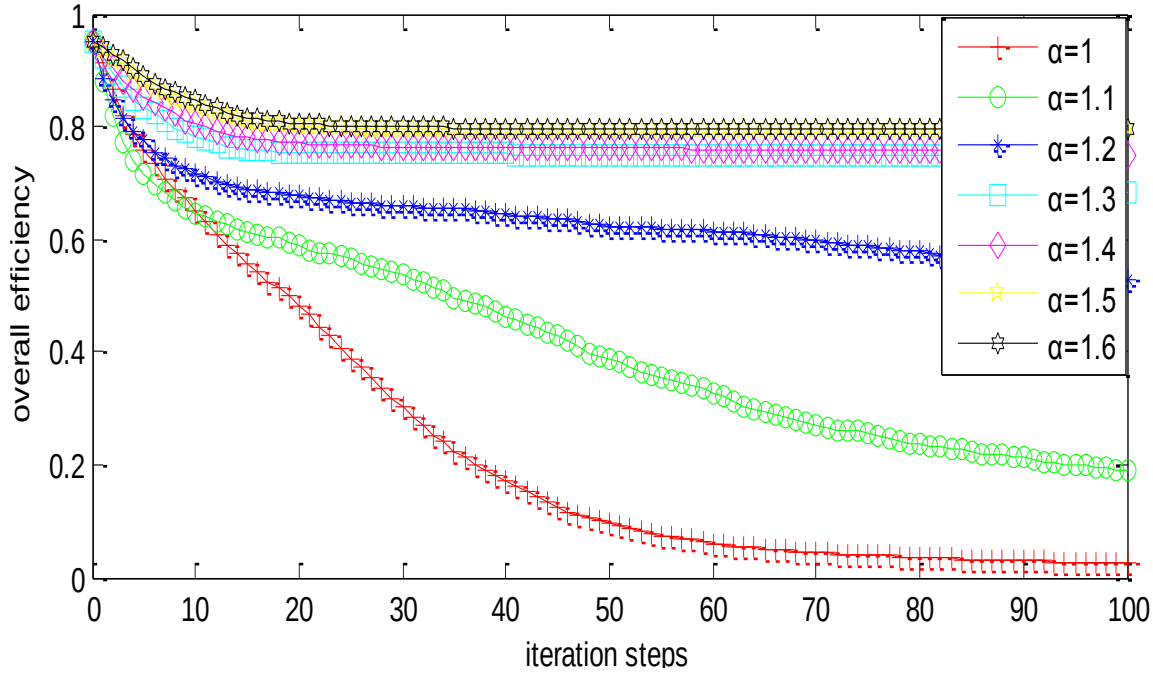

Fig 3.7 Efficiency curve based on random failure (edge No.97) in proposed model

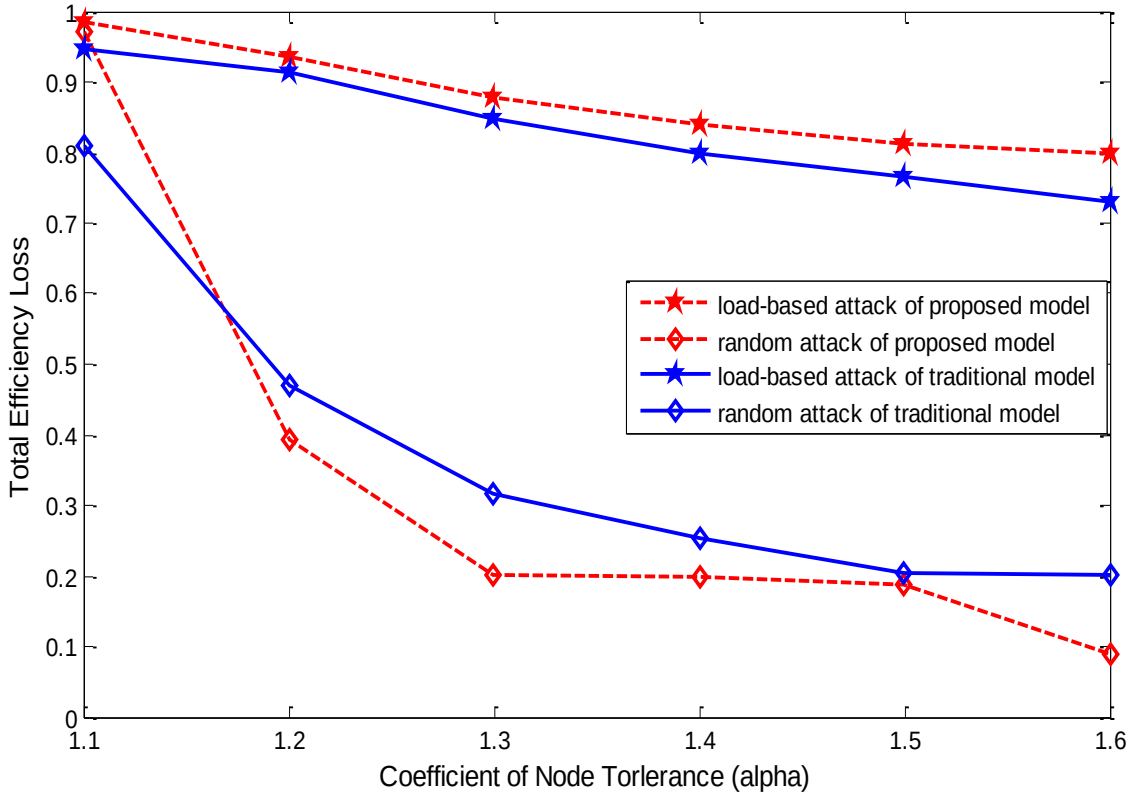

Fig 3.8 Total efficiency loss for both traditional and proposed models

To sum up, PAM is newly proposed in this section for structural vulnerability analysis. Its effectiveness has been demonstrated in a case study on IEEE 118-bus system. PAM is effective in capturing both topological information and load flow sensitivity of the whole network. For further application, PAM is also introduced in modeling PTN for identification of uncontrolled system separations, which will be discussed in details in Section 3.2.

3.2 Identification of Uncontrolled Separation in Power Transmission Network

3.2.1 Introduction

Power system operation is continuously subject to various internal or external disturbances such as time-varying load demands, malfunctions of electrical facilities (e.g. relay), incorrect manipulations of operators, accidents caused by human or animals, environmental disasters, etc. Such disturbances are most likely to cause transmission line outages in PTNs. In the worst cases, multiple line outages deteriorate the connectivity of the whole PTN and split it into isolated parts. Most frequently, the resultant uncontrolled separation can cause serious consequences, such as voltage collapse, frequency instability[90] and so forth. Therefore, fast identifying or even predicting the splitting situations is of key importance for system operators to procure preventive control strategies. However, due to the topological complexity of PTN, those situations are often “hidden” in the sense that they do not manifest at the early stage until some severe contingencies expose their existence.

Timely detecting the formation of islands in power system is of vital importance in two aspects. Firstly, it provides indispensable information needed to e.g. effectively dispatch the system according to simulation analysis. If network splits, all steady-state analysis programs (e.g. state estimation) utilizing Newton power flow method would suffer from the singularity of Jacobian matrix[93]. Effective modification of Jacobian

matrix by e.g. set more suitable slack buses in each island can resolve the problem. Secondly, effective forecast will allow suitable control strategies to be employed to prevent system faults/ contingencies from further spreading.

There are various methods to detect island formation in power systems. Based on different motivations, one may classify the existing methods into two categories. One is controlled system separation or intentionally islanding, which is to cope with different power system extremes, such as loss of synchrony, un-damped oscillations, voltage collapse, etc. Controlled islanding is usually conducted by protective units with a prior setting or guided by system control center. Such methods are mainly based on power system dynamic analysis in a fast time scale (e.g. slow coherency [84, 85]). Another one, which is also the main interest of this section, is uncontrolled system separation or islanding. In a large interconnected PTN, system stability, especially frequency stability reflecting the supply and demand balance, would be of concern following a severe system disturbance resulting in unexpected cascading trips then splitting the PTN into two or more islands. Most frequently, such unexpected splitting would lead the system to the escalation phase of cascading failures and eventually cause wide-spread blackout. Therefore, North American reliability standards now require that, “Each Transmission Operator shall operate to protect against instability, uncontrolled separation, or cascading outages resulting from multiple outages”. Motivated by this, the research work presented in this section aims to capture an insight of emerging topological

separation in PTNs so as to identify and even predict the potential islands at the early stage of disturbing events such as multiple transmission line outages.

Based on steady state analysis, the problem of islanding formation is widely studied in terms of numerical analysis and graph-theoretic methods. [94] and [95] present the pioneering works on islanding detections in power systems based on the monitoring data and linked list tables. In [90, 93, 96], some numerical approaches are reported based on network nodal connectivity matrix, LU decomposition and eigen-evaluation of susceptance matrix respectively. Graph-theoretic methods are stemmed from graph theory and focus on the relations of nodes and edges. In [97] node fusion is applied to outage analysis in the infrastructure network. Breadth first search algorithm utilized in electric network is developed in [98]. In [99], an effective approach based on path search is proposed. In general, numerical approaches are computationally efficient but fail to address topological properties of practical networks. In contrast, existing graph-theoretic methods based on global search take into account topological properties while entailing high computation costs.

In view of the weaknesses of existing approaches, the proposed work in this section is designed to seek the tradeoff between computational cost and detecting accuracy. A spectral clustering based method is proposed to identify uncontrolled system separation (i.e. existing or potential islands) caused by multiple line outages. It should be emphasized that real power imbalance and topological changes of PTN are main

concerns in this work. Although system dynamics, voltage stability, and other causal factors of system separation, e.g. environmental disasters, are interesting in their own right, they require much more complicated modeling and some analysis of them remain qualitative at this stage. So those issues are not discussed in this approach.

3.2.2 Proposed framework

A. Complex network based modeling of PTNs

As proposed in Section 3.1, PAM is introduced in this section for PTN modeling. According to the illustration of power flow sensitivity in Section 3.1, a formal definition is given below:

Definition 1: The set of real numbers is denoted by $\mathbb{R}$. $A_{power} \in \mathbb{R}^{|\mathrm{N}|\times|\mathrm{N}|}$ consists of off-diagonal elements of $\boldsymbol{H}$ obtained by power flow solution. Each entry of A_{power} is expressed as:

$$a_{i,j} = \begin{cases} h_{i,j} & i \neq j \\ 0 & i = j \end{cases} \tag{3-12}$$

Based on Definition 1, degree matrix $\boldsymbol{D}$ is redefined as:

$$D(\mathcal{G}) = diag\{d_1, d_2, ..., d_{|\mathrm{N}|}\}, d_i = \sum_{j=1}^{|N|} a_{i,j} \tag{3-13}$$

Based on graph theory, the Laplcian matrix is viewed as a matrix representation of a graph. In the sense of classic definition of Laplacian matrix and special features of PTNs,

the Electric-Laplacian matrix (denoted as L_e) is proposed, which contains topological and electrical information of PTNs.

Definition 2: Given a PTN, which consists of *n* buses and *m* transmission lines, Electric-Laplacian is defined as:

$$L_e = D - A_{power} \tag{3-14}$$

where diagonal element of L_e is given by the degree of associated vertex in the PTN, and off-diagonal element indicates the electrical attribute of each corresponding edge. According to the basic definition of Laplacian matrix[100], L_e is symmetric, singular and positive semi-definite.

B. Spectral properties of L_e

Various disturbing events (e.g. multiple transmission line outages) would deteriorate the connectivity of a PTN and lead the power system to an escalation phase of cascading failures, which would ultimately cause wide-spread blackout. Based on some global search algorithms, identifying network separation is an NP problem. In addition, such algorithms are less computationally efficient and hard to forecast the arisen islanding situations in terms of topological changes. In graph theory, spectral partitioning algorithms provide an efficient and systematic solution to study the connection patterns of a graph. Some previous studies on spectral properties of a graph are reported in Refs.[74, 101]. Inspired by these works, a useful method based on normalized spectral clustering is proposed with special extension to fit with specific case

of power system uncontrolled separation. In this sub-section, Spectral properties of electrical Laplacian are investigated in details. Some useful theorems and propositions are introduced in the following.

Notation: the first *k* eigenvectors of L_e are denoted by $v_1, v_2, \ldots, v_k$. The eigenvalues of L_e are denoted by λ_i, $i = 1, 2, ..., |\mathrm{N}|$. We write $\lambda_1 \le \lambda_2 \le \lambda_3 ... \le \lambda_n$ to be the ascending order of eigenvalues of L_e. $S \in \mathbb{R}^{|\mathrm{N}| \times k}$ containing the fist *k* eigenvectors. x_i is denoted as the *i-th* entry of a eigenvector v_i.

Theorem 1 [102-104]: If $\mathcal{G}$ is a given weighted graph with all weights non-negative, the following statements are true:

i) Laplacian matrix of $\mathcal{G}$ has only real eigenvalues.

ii) The smallest eigenvalue λ_1 is equal to 0 and its corresponding eigenvector is constant, i.e. $(1,1, ...,1)^{\mathrm{T}}$. The multiplicity of zero eigenvalues is determined by the number of splitting sub-graphs of $\mathcal{G}$.

iii) $\lambda_1 = 0$ and $\lambda_2 > 0$ iff $\mathcal{G}$ is connected.

This theorem is derived from Perron-Frobenius Theorem, and the proof can be found in [103-105].

In the application of PTN, the second smallest eigenvalue λ_2 reflects significant spectrum information of PTN. Based on Courant-Fischer's theorem, the second smallest eigenvalue (non-vanishing) can be formulated as:

$$\lambda_2 = \min v_i^T L_e v_i, \quad i = 1, 2, ..., |N| \tag{3-15}$$

λ_2 is termed as *algebraic connectivity* of $\mathcal{G}$.

When considering the situation of subjoining or subtracting a transmission line in PTN, one will reach the following theorem.

Theorem 2 (Courant-Weyl Inequality) [105]: Let $\mathcal{G}^* = \mathcal{G} + e$ be a graph altered by inserting a new edge e into $\mathcal{G}$. $\mathcal{G}^*$ and $\mathcal{G}$ have the same set of vertices. The following inequality is true:

$$0 = \lambda_1(\mathcal{G}) = \lambda_1(\mathcal{G}^*) \le \lambda_2(\mathcal{G}) \le \lambda_2(\mathcal{G}^*) \le \lambda_3(\mathcal{G}) \le ... \le \lambda_n(\mathcal{G}) \le \lambda_n(\mathcal{G}^*) \tag{3-16}$$

In order to investigate the detailed connection patterns of PTN and thereby detect the separation trends for different situations, spectral partitioning algorithm is adopted to study this problem. Proposition 1 is derived from [74, 100] and it well explains the rationale of spectral clustering.

Proposition 1: A connected graph $\mathcal{G}$, which is abstracted from a PTN, consists of *n* closely connected sub-graphs $\mathcal{G}_1, \mathcal{G}_2 ... \mathcal{G}_n$. For each sub-graph, its corresponding entries x_i of a non-vanishing eigenvector *v* of L_e are approximately identical.

Proof: this proposition can be proved through the following optimization problem. The objective is to minimize *f*.

$$f(x_1, x_2 ... x_{|N|}) = \sum_{i,j=1}^{|N|} (x_i - x_j)^2 \cdot a_{i,j} \tag{3-17}$$

$$\text{s.t.} \qquad \sum_{i,j=1}^{|N|} x_i \cdot x_j \cdot c_{i,j} = 1$$

where $c_{i,j}$ is the element of a given symmetric matrix C. The Lagrange dual function of (3-17) is given below, where γ is Lagrange multiplier:

$$\Lambda(x_1, x_2, ..., x_{|N|}, \gamma) = \sum_{i,j=1}^{|N|} (x_i - x_j)^2 \cdot a_{i,j} + \gamma(\sum_{i,j=1}^{|N|} x_i \cdot x_j \cdot c_{i,j} - 1) \tag{3-18}$$

Then:

$$\begin{cases} \dfrac{\partial \Lambda}{\partial x_i} = 2\sum_{j=1}^{|N|} (x_i - x_j) \cdot a_{i,j} + \gamma \sum_{j=1}^{|N|} x_j \cdot c_{i,j} = 0 \\ \dfrac{\partial \Lambda}{\partial \gamma} = \sum_{i,j=1}^{|N|} x_i \cdot x_j \cdot c_{i,j} - 1 = 0 \end{cases}$$

If $a_{i,j}$ is the entry of A_{power}, the solution of Eq. (3-18) can be expressed in a generalized matrix form:

$$(D - PA)X = \eta CX \Leftrightarrow C^{-1}(D - PA)X = \eta X$$

where $\eta = -0.5\gamma$. Thus, based on the above, the constrained optimization problem (3-17) is converted into an eigen-problem with different constraints associated with C. When C is identity matrix, $\boldsymbol{X}$ is the eigenvector v of L_e. Based on the spirit of the

optimization problem, elements x_i of eigenvector corresponding to close-connected vertices, which are with relatively large $a_{i,j}$, are approximately equal to each other. In this thesis, this numerical pattern is termed as *spectrum aggregation*.

Since the L_e changes due to transmission line outages in PTNs, spectrum aggregation will change accordingly at different levels. Clustering vertices into groups depends on the connectivity of the whole network. Any removal of edges in a cluster would globally weaken the connectivity of whole network and simultaneously make the vertices in this cluster more "dependent" to the rest of the network. On the other hand, outages of tie-lines connecting separate areas in PTNs would make vertices in a local cluster (or a specific control area in power system) more "independent". All of these conjectures can be reflected by the simulation results shown in the forthcoming sub-section 3.2.3.

According to Eq. (3-15), the quadratic form of λ_2 can be rewritten as:

$$\lambda_2 = \min \sum_{i,j=1}^{|N|} l_{i,j} x_i x_j = \min \sum_{i,j=1}^{|N|} (x_i - x_j)^2 \cdot l_{i,j} \tag{3-19}$$

where $l_{i,j}$ is the element of L_e. According to Theorem 2 and Eq. (3-19), algebraic connectivity is non-increasing for a given network subject to removals of any edges. In general, λ_2 globally reveals the connectivity of all vertices. Based on the analysis above, one can safely reach the following conclusion: In a PTN, if the connection of each

cluster is strong, the overall spectrum aggregation is unapparent. In addition, if the connection between a cluster and the rest of the network is weak, the spectrum aggregation of this cluster is hereby exposed. By proposing some specific metrics in the next sub-section, spectrum aggregation is well quantified to reflect the connectivity of the network.

C. An improved spectral clustering algorithm for PTNs

Two proposed metrics, i.e. *spectrum closeness* (SC) and *spectrum entropy* (SE) are incorporated into basic normalized spectral clustering algorithm, which play an essential role in detecting the topological changes. The two metrics can effectively quantify the transition process of PTN from integrated to separated status.

Basic algorithm of normalized spectral clustering includes six steps:[106]

i) Input power adjacency matrix A_{power} and the number of clusters *k*

ii) Compute the normalized electric-Laplacian matrix $L_e^* = D^{-1}L_e$

iii) Compute the first m eigenvectors $v_1,\ldots,v_m$ of L_e^*

iv) Construct $\boldsymbol{S} \in R^{|N|\times m}$ containing the fist *m* eigenvectors as columns

v) For i=1,2,..,|N|, let $t_i \in R^m$ be the vector corresponding to the *i-th* row of $\boldsymbol{S}$

vi) group the points $(t_i)_{i=1,..,|N|}$ with the k-means algorithm into clusters $\mathbf{C}_1,\ldots,\mathbf{C}_k$

The core of this application is step vi), a suitable clustering can well reveal the connection status of PTNs. In [74, 107], Euclidean or angular distance (i.e. the angle difference between two vectors stemming from the same origin in a *d*-dimensional space) has been introduced to quantitatively measure eye-inspected clusters (i.e. all points t_i mentioned in step vi). Some useful conclusions inspired by empirical observations indicate that the points associated with two closely connected nodes belonging to the same cluster may not be Euclideanly close while they are well aligned in similar direction[107]. Therefore, in the proposed method, angular distance is used in step vi as a metric for k-means algorithm.

With the classical k-means algorithm [108], the clustering results based on angular differences can be very much subject to the selected reference angle. Furthermore, the classical k-means also suffers from frequent algorithm failures due to random initialization of cluster centroids[108]. To overcome these drawbacks, an advanced k-means method is developed which has two important features: i) the original set of centroids is initialized by practical control areas in PTN; and ii) different angular references are selected in different cases. The main procedure of this algorithm is shown in Table 3.1.

Table 3.1 A tailor-made k-means algorithm based on angular distance

Inputs: *k* is the number of clusters.

orig_c is the original set of centroids obtained by the existing control areas in a PTN.

ang_dis1 is the set of angular distance of all points with reference vector(0,1).

ang_dis2 is the set of angular distance of all points with reference vector (-1,$\sqrt{3}$).

ang_dis3 is the set of angular distance of all points with reference vector (-1,$-\sqrt{3}$).

Output: all clusters and corresponding centroids

Function: Clustering

Initialization by *orig_c*;

For each *ang_dis*,

Solve ("kmeans"is a MATLAB function):

[*idx,centroid,sumd*]=kmeans(*ang_disn,k,'emptyaction','singleton','distance','sqEuclidean'*);

Repeat this process several times until stable solutions are reached;

End for

Select the solution obtained by *ang_disn* with minimum *sumd;*

Spectrum closeness is proposed to measure the degree of coupling of each cluster. *Spectrum entropy* is proposed to measure the uncertainty and complexity of Laplacian spectra and reveal the tendency of network evolution. Two definitions are given below:

Definition 3: Let $\boldsymbol{C_i}$ be the set of all vertices in a cluster i. ang_j^i is the angular distance associated with vertex j. c_i is the centroid of cluster i, which is obtained by k-means clustering algorithm. Denoted by σ_i spectrum closeness (SC) of a cluster i indicates the average deviation of all internal spectra points,

$$\sigma_i = \frac{1}{n_i} \sum_{j \in C_i} \| ang_j^i - c_i \|^2 \tag{3-20}$$

where n_i is the number of vertices in cluster i.

SC reflects the degree of independence of a cluster. If σ_i is getting smaller, it means that the connection between cluster i and the remaining parts of the graph is being weakened. Otherwise, the coupling of cluster i and the remaining network is being strengthened.

Definition 4: Assume that a graph G is partitioned into k sub-graphs (i.e. clusters). The two dimensional eigenvector space is equally divided into b angular intervals. Spectrum entropy (SE) is defined as:

$$En = \sum_i^k \sum_j^b \frac{z_i^j}{n_i} \ln \frac{z_j}{n_i} \tag{3-21}$$

where z_i^j is the number of points associated with cluster *i* lying in the interval *j*.

SE gives a useful indication of islanding formation. A higher SE reflects a more disordered spectrum point distribution, thus it is less likely to form islands in a PTN. Otherwise, it is very likely to form one or more islands when SE is significantly decreased.

Spectral analysis is an essential part of islanding detection. Table 3.2 illustrates the main procedure of spectral analysis in a given PTN. In the proposed approach, SC and SE play a very important role to evaluate the clustering performance. They have a direct bearing on the success of forecasting the vulnerable part that is on the edge of separation. With different inputs of *k*, SE reveals the global connection status under different partitioning scales. When comprehensively considering SC and SE, it is easy to find out the most critical partitioning results, which thereby indicate the most likely situations of network separation.

Table 3.2 Spectral analysis of PTN

Inputs: *casedata* is the basic network data of a PTN e.g. IEEE 39-bus system or 118-bus system

outage_line is the set of tripped transmission lines in all states (in each state, only one line is tripped)

num_areas is the number of control areas in this power system

areas is the set of all control areas

Output: spectrum plots of $\boldsymbol{L_e}$ in each state,

spectrum closeness,

spectrum entropy,

minimal cutsets,

Function: Spectral Analysis

Construct $\boldsymbol{L_e}$;

For each state

Remove a line from *outage_line*;

Upgrade $\boldsymbol{L_e}$;

Calculate the first two non-vanishing eigenvectors $\boldsymbol{v_1}$,$\boldsymbol{v_2}$;

Identify existing islands;

Conduct graph clustering based on the advanced k-means algorithm in Table 3.1;

Plot all spectrum points (i.e. t_i);

Calculate *spectrum closeness* according to Eq. (3-20);

Calculate *spectrum entropy* according to Eq. (3-21);

Produce the minimal cutset of each cluster;

If (*spectrum closeness* is sharply decreased) then

Return minimal cutsets of all potential islands;

Produce an islanding warning signal;

Break;

Else

Identify the potential islands with minimum spectrum closeness

End if

End for

3.2.3 Simulation results

In this section, simulations of islanding detection under two given scenarios are presented. The sequence of cascading failures is determined by the well established hidden failure model [32, 109], which is widely accepted in this field. By using the cascading chain caused by transmission line overload, the proposed approach can effectively reveal the process of the integrated PTN transiting to separated status.

Normally, an interconnected power system consists of some sub-systems, which are controlled by their respective control entities. Each sub-system is usually termed as a control area.

A. Case study using IEEE New England 39-bus system

There are three control areas in this test system, which are shown in Fig 3.9. Tie lines are $edge(1,2)$, $edge(3,4)$, $edge(14,15)$, and $edge(17,18)$ connecting different areas. A single line outage of $edge(14,15)$ connecting areas 1 and 3 is considered in this case.

As observed in Figs. 3.10 and 3.11, spectrum point distribution changes along with the outage of $edg(14,15)$, and the points of cluster 3 are getting closer, which is also reflected by the decrease of SC from 0.2141 to 0.0878 according to Table 3.3. Based on the topology in Fig 3.9, in the pre-contingency state, cluster 3 lost the significant connection to cluster 1. Accordingly, SE of the whole network is decreased from 0.3442 to 0.3375 in Table 3.3. On the other hand, SC of cluster 2 is accordingly increased from

0.4996 to 0.5961, which indicates that the coupling of cluster 2 to the whole network is strengthened. From Table 3.3, it is obvious that SC of a cluster is significantly decreased if the connection between this cluster and the remainder of the network is getting weak. In another word, such a cluster is highly vulnerable to be isolated and become a network island.

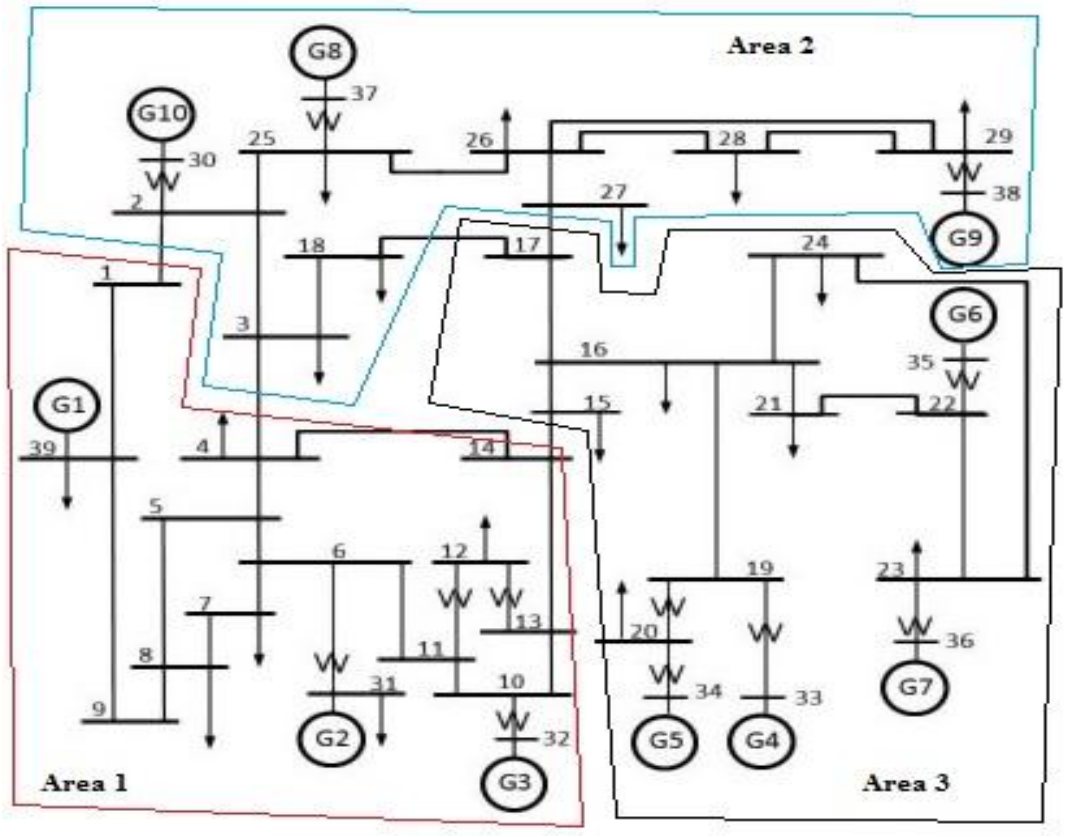

Fig 3.9 IEEE New England 39-bus system

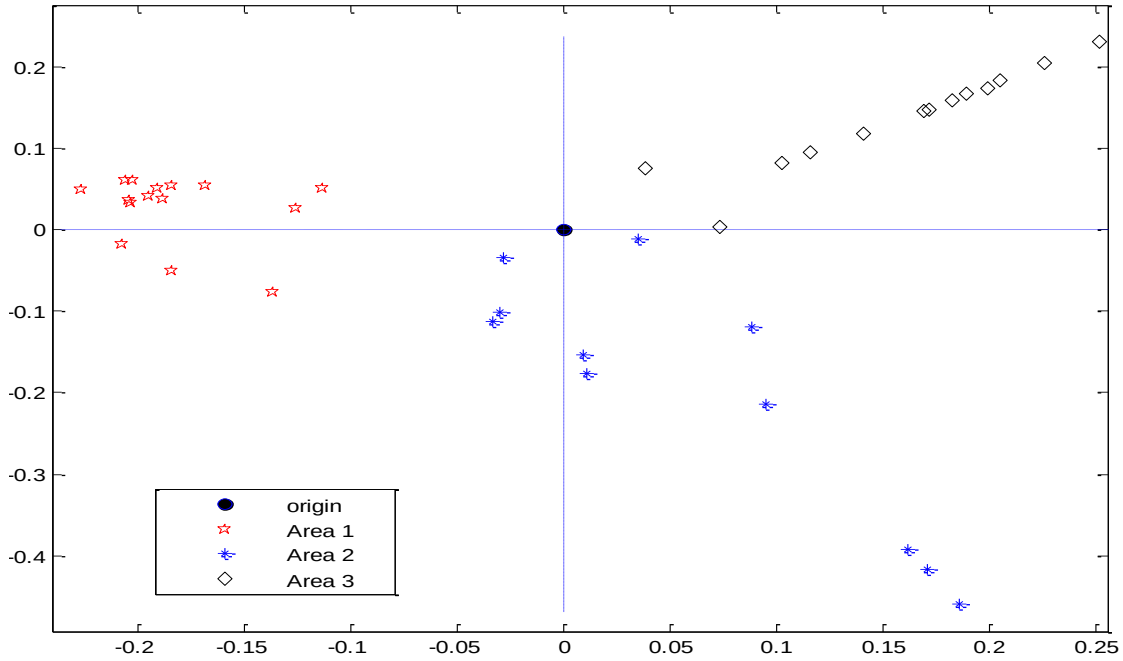

Fig 3.10 Spectrum plot of L_e in original state (IEEE New England 39-bus system)

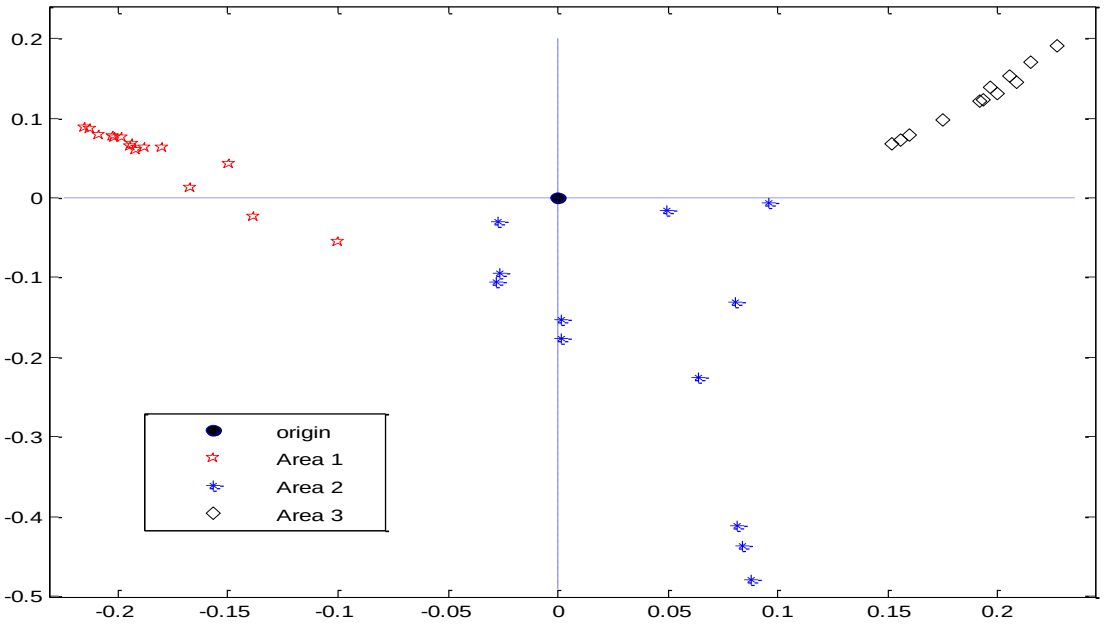

Fig 3.11 Spectrum plot of L_e in the post contingency state (IEEE New England 39-bus system)

Table 3.3 Comparison of spectrum at different states (IEEE New England 39-bus system)

state	Cluster No. and its Vertices		SC	SE
original	1	1 4 5 6 7 8 9 10 11 12 13 14 31 32 39	0.2379	0.3442
	2	2 3 18 25 26 27 28 29 30 37 38	0.4996	
	3	15 16 17 19 20 21 22 23 24 33 34 35 36	0.2141	
Post-contingency	1	1 4 5 6 7 8 9 10 11 12 13 14 31 32 39	0.2438	0.3375
	2	2 3 17 18 25 26 27 28 29 30 37 38	0.5961	
	3	15 16 19 20 21 22 23 24 33 34 35 36	0.0874	

B. Case study using IEEE 118-bus test system

This system operates in a normal condition at the original state. Basically, IEEE 118-bus system can be divided into 3 control areas according to Fig 3.12. In this case, the islanding detection scheme is to be tested for a cascading failure event consisting of 5 different states, which is based on the mechanism of hidden failure model [32]. In state 1, tie line $edge(37,40)$ connecting areas 1 and 3 fails due to some unexpected reasons. According to power flow results, this leads to overload of $edge(37,39)$ and the protection system trips $edge(37,39)$ in state 2, which is a tie line of clusters 1 and 3. Due

to the outages of $edge(37,40)$ and $edge(37,39)$, the rest tie lines connecting areas 1 and 3 including $edge(38,65)$, $edge(34,43)$ and $edge(24,70)$ are becoming stressful and eventually suffer from overloading. As such, these lines undergo cascading outages resulting in system states 3 to 5.

Figs 3.13-3.15 show the spectrum plots of the test system in different states. Due to transmission line outages, the connectivity of the whole network deteriorates progressively. As compared with the initial state, spectrum points of cluster 1 in state 2 is distributed closer under the outage of $edge(37,40)$ and $edge(37,39)$, which are shown in Figs. 3.13 and 3.14. After the outages of $edge(38,65)$, $edge(34,43)$ and $edge(24,70)$, spectrum points of cluster 1 are visually aligned into approximately one straight line in Fig 3.15, indicating islanding formation of cluster 1 is imminent and accordingly a warning signal can be issued. In the meantime, it is also observed in Fig 3.15 that the spectrum points of clusters 2 and 3 disperse significantly. From Table 3.4, SC of cluster 1 in state 2 as compared with original state is decreased from 0.3124 to 0.1418, which indicates that the independence of cluster 1 is notably increased, Along with further failures, SC of cluster 1 is consequently decreased to 0.0882 in state 5, which echoes the visual observation in Fig 3.15 and reflects imminent network splitting. In state 5, the minimal cutset of cluster 1 only consists of one edge i.e. $edge(71,72)$. Situation is being critical because the failure of $edge(71,72)$ will eventually cause power system islanding.

This analytical situation is consistent with the simulation results shown in Fig 3.15 and Table 3.4.

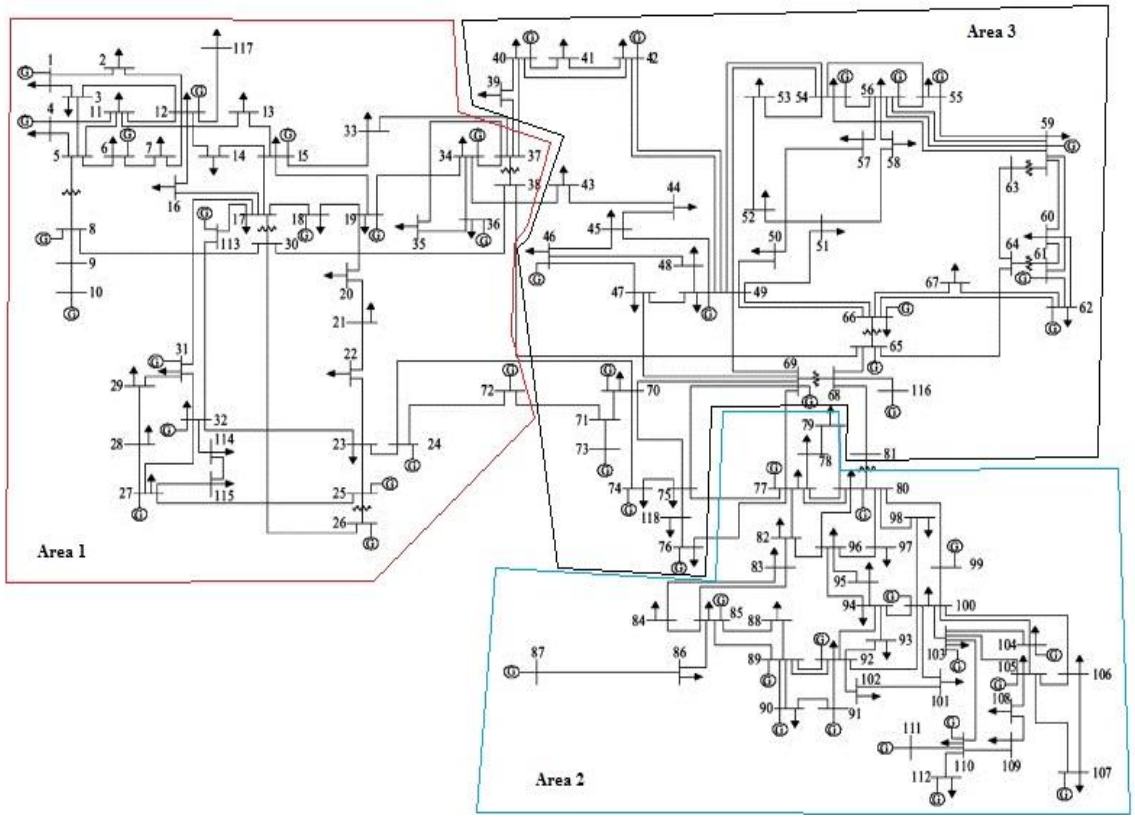

Fig 3.12 IEEE 118-bus test system

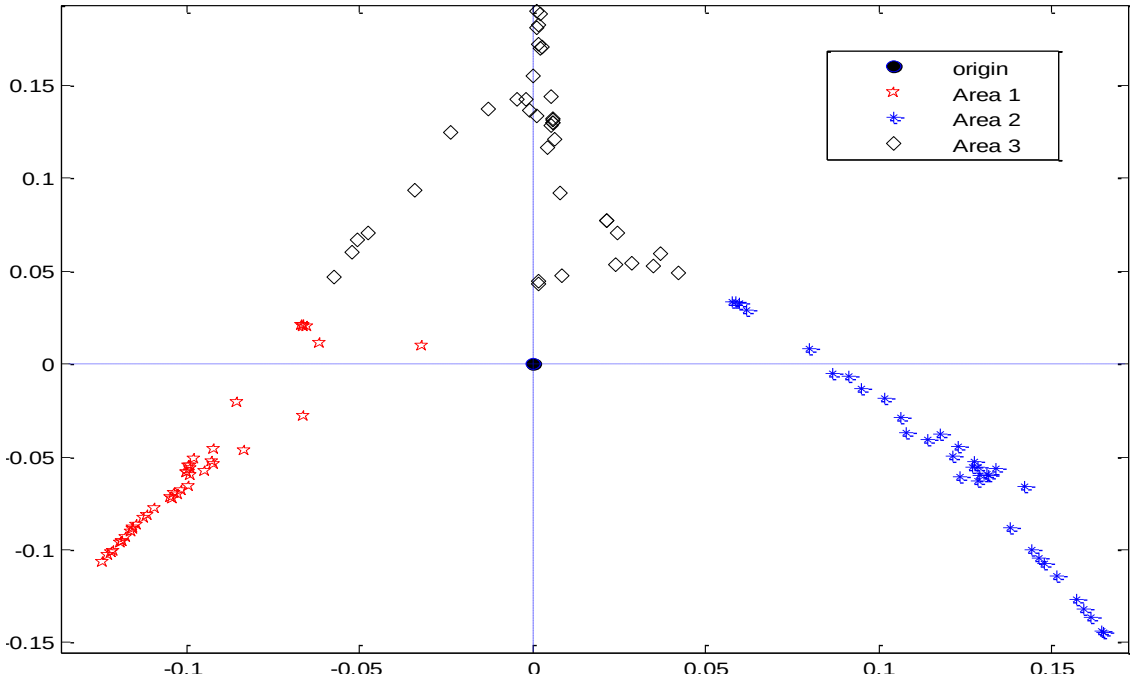

Fig 3.13 Spectrum plot of $\boldsymbol{L_e}$ at the original state (IEEE 118-bus system)

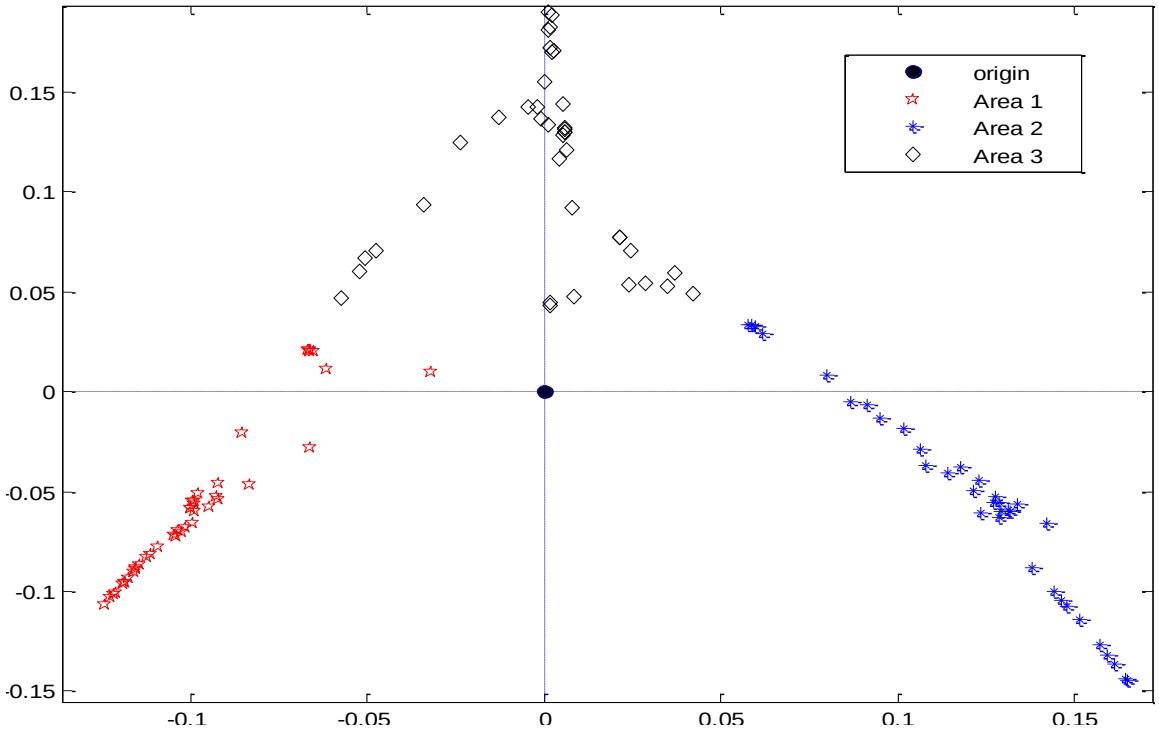

Fig 3.14 Spectrum plot of $\boldsymbol{L_e}$ in state 2 (IEEE 118-bus system)

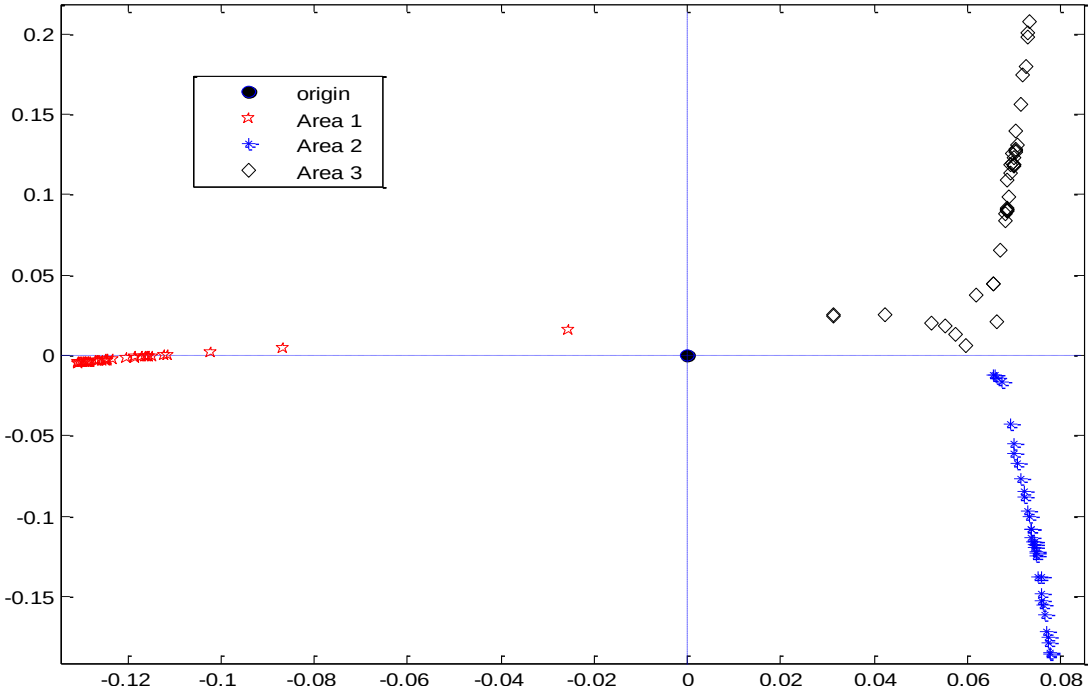

Fig 3.15 Spectrum plot of $\boldsymbol{L_e}$ in state 5 (IEEE 118-bus system)

Table 3.4 Comparison of spectrum at different states (IEEE 118-bus system)

state	Cluster No. and corresponding Vertices						SC	$\sum_j^b \frac{z_i^j}{n_i} \ln \frac{z_j}{n_i}$	SE
original	1	1	2	3	4	5	6	0.3124	0.1149	0.3592
			7	8	9	10	11			
			12	13	14	15	16			
			17	18	19	20	21			
			22	23	24	25	26			
			27	28	29	30	31			
			32	33	34	35	36			
			37	38	72	113	114			
					115	117				
	2	77	78	79	80	82	83	0.3520	0.1269	
			84	85	86	87	88			
			89	90	91	92	93			
			94	95	96	97	98			
			99	100	101	102	103			
			104	105	106	107	108			
				109	110	111	112			
	3	39	40	41	42	43	44	0.3203	0.1174	
			45	46	47	48	49			

			50	51	52	53	54				
			55	56	57	58	59				
			60	61	62	63	64				
			65	66	67	68	69				
			70	71	73	74	75				
			76	81	116	118					
	1	1	2	3	4	5	6	0.2936	0.1080		
			7	8	9	10	11				
			12	13	14	15	16				
			17	18	19	20	21				
			22	23	24	25	26				
			27	28	29	30	31				
			32	33	34	35	36				
			37	38	72	113	114				
					115	117					
1	2	82	83	84	85	86	87	0.1789	0.0623	0.3360	
			88	89	90	91	92				
			93	94	95	96	98				
			99	100	101	102	103				
			104	105	106	107	108				
			109	110	111	112					
	3	39	40	41	42	43	44	0.4508	0.1657		
			45	46	47	48	49				
			50	51	52	53	54				
			55	56	57	58	59				
			60	61	62	63	64				
			65	66	67	68	69				
			70	71	73	74	75				
			76	77	78	79	80				
			81	97	116	118					
	1	1	2	3	4	5	6	0.1418	0.0521		
			7	8	9	10	11				
			12	13	14	15	16				
			17	18	19	20	21				
			22	23	24	25	26				
			27	28	29	30	31				
			32	33	34	35	36				
			37	38	72	113	114				
					115	117					
2	2	77	78	79	80	82	83	0.2536	0.0914	0.2631	
			84	85	86	87	88				
			89	90	91	92	93				
			94	95	96	97	98				
			99	100	101	102	103				
			104	105	106	107	108				
			109	110	111	112					
	3	39	40	41	42	43	44	0.3261	0.1196		
			45	46	47	48	49				
			50	51	52	53	54				
			55	56	57	58	59				
			60	61	62	63	64				

		65	66	67	68	69			
		70	71	73	74	75			
		76	81	116	118				
3	1	1	2	3	4	5	6	0.1540	0.0567	0.2661
		7	8	9	10	11				
		12	13	14	15	16				
		17	18	19	20	21				
		22	23	24	25	26				
		27	28	29	30	31				
		32	33	34	35	36				
		37	38	43	72	113				
		114	115	117						
	2	77	78	79	80	82	83	0.3025	0.1090	
		84	85	86	87	88				
		89	90	91	92	93				
		94	95	96	97	98				
		99	100	101	102	103				
		104	105	106	107	108				
		109	110	111	112					
	3	39	40	41	42	44	45	0.2745	0.1004	
		46	47	48	49	50				
		51	52	53	54	55				
		56	57	58	59	60				
		61	62	63	64	65				
		66	67	68	69	70				
		71	73	74	75	76				
		81	116	118						
4	1	1	2	3	4	5	6	0.1027	0.0378	0.2414
		7	8	9	10	11				
		12	13	14	15	16				
		17	18	19	20	21				
		22	23	24	25	26				
		27	28	29	30	31				
		32	33	34	35	36				
		37	38	72	113	114				
		115	117							
	2	77	78	79	80	82	83	0.2799	0.1009	
		84	85	86	87	88				
		89	90	91	92	93				
		94	95	96	97	98				
		99	100	101	102	103				
		104	105	106	107	108				
		109	110	111	112					
	3	39	40	41	42	43	44	0.2801	0.1027	
		45	46	47	48	49				
		50	51	52	53	54				
		55	56	57	58	59				
		60	61	62	63	64				
		65	66	67	68	69				
		70	71	73	74	75				
		76	81	116	118					

5	1	1	2	3	4	5	6	0.0882	0.0325	0.2441
			7	8	9	10	11			
			12	13	14	15	16			
			17	18	19	20	21			
			22	23	24	25	26			
			27	28	29	30	31			
			32	33	34	35	36			
			37	38	72	113	114			
					115	117				
	2	77	78	79	80	82	83	0.2880	0.1038	
			84	85	86	87	88			
			89	90	91	92	93			
			94	95	96	97	98			
			99	100	101	102	103			
			104	105	106	107	108			
				109	110	111	112			
	3	39	40	41	42	43	44	0.2941	0.1079	
			45	46	47	48	49			
			50	51	52	53	54			
			55	56	57	58	59			
			60	61	62	63	64			
			65	66	67	68	69			
			70	71	73	74	75			
				76	81	116	118			

3.2.4 Summary

A useful spectral clustering based approach for identifying and predicting uncontrolled system separation is developed in this section. Distinguished from previous works in this field, the proposed approach can accurately identify and forecast the topological separation considering real power deliverability. Cases studies under single and multiple line outages in two different test systems are carried out and results demonstrate that the developed method is effective and reliable in detecting and predicting uncontrolled separation situations on a steady state basis.

Admittedly, there are many other factors (as stated above, system un-damped oscillations, voltage collapse, cascading outages and so forth) that can affect the uncontrolled system separation. To the author's best knowledge, it has been extremely difficult to come up with a comprehensive solution that can address all those factors. The proposed method provides a promising solution for system separation identification effectively taking real power deliverability of each branch into considerations. Nevertheless, this work is still extendable by considering more engineering factors. For large-scale PTNs which involve overwhelming amount of network data, more complicated operation conditions and uncertainties, it is imperative to further improve the developed method with respect to incorporation of power system steady-state analysis including specific power flow solution in each system state, as well as advanced data mining techniques to deal with massive data. In next section, network partitioning application in power systems will be further investigated.

3.3 K-way Network Partition

3.3.1 Introduction

Power system security is always a concern for electrical engineers due to the increasing complexities and uncertainties involved in large-scale system operation and control. The smart grid concept is aiming at developing a system that is well integrated with advanced metering, wide-area communication and flexible control. Its merits include fast-acting, intelligent controllability and high reliability when subjected to all

operating conditions [110]. In this sense, “self-healing” capability of smart grid becomes a focused area in power system security research, which is attracting more and more attentions in recent years.

Self-healing smart grid is defined as a power system equipped with advanced metering and control technologies, which can efficiently detect system faults and recover electrical functionality to a great extent when contingency events occur[111, 112]. Basically, a self healing process of smart grid should undergo three phases[112]: firstly, system faults are accurately located and control schemes are formed; secondly, specific control measures are promptly activated to alleviate the situation and prevent cascading failures, typically through network isolation; and thirdly, system reconfiguration is taking place to restore the whole power system to a stable and safe state. In the first step, sophisticated sensory and communication technologies are utilized to continuously monitor the system status, and the collected data are used for pre-contingency analysis, based on which proper control schemes can be well planned. In order to achieve self-healing effect, a suitable control strategy is adaptively formed by considering various operating conditions. This is of vital importance for the second and third steps to take fast reaction, recover the functionality of the whole system to guide it to a new and safe operating state. Hierarchical centralized supervisory control may provide the best solution for self-healing reaction of small-scale PTNs but can be less effective for large and highly interconnected systems [113]. In fact, several challenges caused by modern power grids (e.g. large amount of system data, complex network

structure, integration with renewable energies, etc) can be tackled by the reduction of system dimension. That is, the whole power system can be divided into some interacting but independent areas, and each area is self-sufficient and has its own decision-making framework for emergency conditions.

In recent year, many efforts have been made from de-centralized control perspective. Multi-agent control schemes are proposed and reported in many literatures (e.g. [114, 115]), which can somehow support self-healing smart grid. However, effective control actions are significantly dependent on an optimum network partitioning, which remains an open problem, especially for large inter-connected power systems. In view of the above, the work presented in this section mainly focuses on network partitioning problem under different operating conditions, thereby laying out a useful groundwork for smart grid planning and operation control with the self-healing capability enabled.

Network partitioning problem is not new and significant efforts have been made previously. However, not every partitioning algorithm is equally suitable for smart grid applications from a "self healing" perspective. This section mostly focuses on addressing topological connectivity, inter-area real power balance and voltage profile, which are of essential concerns in system planning and control. Considering all concerns above, a multi-objective optimization approach can then be formulated to solve the partitioning problem. Basically, existing works using the multi-objective formulation

can be classified into two categories—heuristic numeration and hierarchical/ multi-level partitioning (including recursive bisection). Heuristic numeration in e.g. [87, 90] formulates each consideration as a constraint and combines them into one or more objective functions. Partitioning solutions are obtained by solving an optimization problem. This type of methods is appropriate in handling different attributes simultaneously but may incur heavy computational cost when dealing with large scale networks. Multi-level partitioning approaches (e.g. [88, 116]) can well split the network into nearly equal-size clusters and are computationally efficient, but the quality of the solutions is significantly influenced by the predetermined number of clusters, which is an obscure parameter in most cases. Inspired by those methods, a hybrid partitioning approach that integrates spectral clustering algorithm and SOM, which is a classic artificial neural network algorithm and powerful for cluster extraction, is proposed. With the employment of SOM, several challenges involved in network partitioning e.g. the number of clusters, multi-objective partitioning, and big data in large-scale system are successfully tackled. Moreover, the simulation results illustrate that SOM based clustering outperforms a k-means algorithm based approach in terms of clustering accuracy.

3.3.2 Proposed approach of k-way partition for large-scale power transmission network

Echoed with Section 3.2, network partition is further investigated in this section based

on spectral properties of PTNs while addressing specific engineering considerations including particularly real and reactive power flows. Multi-objective partitioning problem is challenging and known to be NP-complete. Traditional spectral clustering fails to tackle multiple objectives. Some variations were proposed to handle multi-objectives (e.g.[117]) by adjusting each edge weight with different preference factors and integrate them into a combined-weight. However, this may incur excessive computational cost or results in unsatisfactory partitioning if the preference factors remain uncertain and unpredictable. The proposed approach in this section features two parts—automated clustering based on SOM and multi-objective optimization

A. Preliminaries of spectral representation for a PTN

The weighted adjacency matrix of $\mathcal{G}$ is denoted by $W = (\omega_{ij})_{i,j=1,\ldots,|N|}$. The value of each ω is determined by real and reactive power flow in the proposed study in order to ???. According to graph theory, the important information on the topological properties of a graph can be extracted from the eigenvalues and eigenvectors of Laplacian matrix. There are two forms of normalized Laplacian matrix [118]. Both are closely related to each other, which are formally defined as:

$$L_{sym} = D^{-1/2} L D^{-1/2} = I - D^{-1/2} W D^{-1/2} \tag{3-22}$$

$$L_{rw} = D^{-1} L = I - D^{-1} W \tag{3-23}$$

where L_{sym} is a symmetric matrix and L_{rw} is closely related to a random walk; $\boldsymbol{I}$ is identity matrix. In order to investigate the mechanism of spectral clustering being used in the

proposed study, the following important proposition and theorem are introduced.

Proposition: Given a non-directed graph $\mathcal{G}$ with non-negative weights. L_{sym} and L_{rw} are positive semi-definite and have $|N|$ non-negative real-valued eigenvalues, which are denoted as: $0 = \lambda_1 \leq ... \leq \lambda_{|N|}$. The multiplicity k of the eigenvalue 0 of L_{sym} and L_{rw} is equal to the number of disconnected components in the graph.

Proof of this proposition can be referred to [106]. This proposition describes the nature of the number of disconnected components. This is often considered as an ideal situation, where the similarity of all between-cluster is exactly zero. However, this is not always the case when applying the spectral clustering to a graph. In general, the similarities among different clusters are vanishing but not exactly zero.

The Davis-Kahan theorem [119] introduced below can well explain the relation between clustering performance and eigengap.

Theorem (Davis-Kahan): Given symmetrical matrices $J, H \in \mathbb{R}^{|N|\times|N|}$. Let $S \subset \mathbb{R}$ be an interval. The set of eigenvalues of J which fall into the interval S is denoted by $\Lambda_S(J)$. V is the corresponding eigen-space of $\Lambda_S(J)$. Consider perturbed $\tilde{J} = J + H$, and $\tilde{V}$ is the analogous quantity for $\tilde{J}$. The distance between S and the spectrum of J outside of S is:

$$\delta = \min\{|\lambda - s|; \lambda \notin S, s \in S\}$$

Then the distance $d(V,\tilde{V}) = \| \sin\Theta(V,\tilde{V}) \|$ is bounded by

$$d(V,\tilde{V}) \le \| H \| / \delta$$

where $\sin\Theta$ denotes a diagonal matrix with the canonical angles on the diagonal.

In explaining the relation between spectral clustering performance and eigengap, the Laplacian matrix L of an ideal case is considered as J, then the perturbed one is denoted as $\tilde{L}$. Given an interval S, if both $\Lambda_S(L)$ and $\Lambda_S(\tilde{L})$ are contained in it, then the eigen-space of the ideal case and perturbed case are approximately close to each other. Since their distance is bounded by $\| H \| / \delta$ according to the Davis-Kahan theory, hence the degree of the "approximation" is strongly related to the perturbation $\| H \|$. In the case that S is set by $[0, \lambda_k]$, then δ is consistent with the eigengap $| \lambda_{k+1} - \lambda_k |$.

Based on the Davis-Kahan theorem, one can safely draw the conclusion that the larger the eigengap $| \lambda_{k+1} - \lambda_k |$ is, the more clustering information is contained in the first *k* eigenvectors, and the better the spectral clustering performs. This conclusion lays out a theoretical foundation for the proposed partitioning approach, which will be described in details in the forthcoming sub-sections.

B. Spectral extraction of a PTN

The goal of partition mentioned in this approach is to find the optimal cut, which minimizes both real and reactive power exchange on the partitioning boundaries. It

makes reasonable sense that small real power exchange among different clusters (i.e. sub-networks) indicates a better "self-sufficient" condition, i.e. a small generation-load imbalance, for each cluster. However, the optimal partitions according to real power flows of PTNs may not fit with reactive power flows. Imbalanced reactive power supply can frequently lead to over or under voltage situations, which may result in voltage instability that can cause equipment outages and even blackouts. In this sense, an optimal partition should also minimize reactive power flow among different clusters if considering zero or very limited reactive compensation locally available at each bus.

The partitioning problem in the proposed study can be summarized as a minimal Ncut problem, which is to minimize the between-cluster similarity and maximize the within-cluster similarity. Ncut (firstly introduced in [120]) is defined as:

$$Ncut(C_1,...,C_k)=\sum_{i=1}^{k}\frac{cut(C_i,\overline{C_i})}{vol(C_i)} \tag{3-24}$$

where $\overline{C_i}$ is the complement of C_i

$$cut(C_i,\overline{C_i})=\sum_{i\in C_i,\, j\in\overline{C_i}}\omega_{ij}\ ,\ vol(C_i)=\sum_{i\in C_i}\sum_{j=1}^{|N|}\omega_{ij} \tag{3-25}$$

Min-Ncut problem is consistent with our partitioning objectives—to minimize the inter-cluster real and reactive power flow and maximize the intra-cluster self-contained rating. This type of partition effectively avoids "one-single-node cluster" situation. Therefore, normalized Laplacian matrix is selected as the topological representation of PTNs. This is because the normalized Laplacian matrix based spectral clustering can

well satisfy the min-Ncut objectives defined above [106]. Between L_{sym} and L_{rw}, the proposed application is in favor of L_{rw} due to its better experimental performance than that of L_{sym}. This may be because that eigenvectors of L_{sym} are additionally multiplied with $D^{1/2}$ that may undesirably influence its clustering performance. In addition, there is no computational advantage when using L_{sym}. Hence L_{rw} is selected in the proposed application.

When considering real and reactive power separately, one constructs the normalized Laplacian matrices L_{MW} and L_{MVar}, where the weights of their edges are given by the absolute value of real and reactive power flows, respectively. According to the discussion in 3.3.2-A, eigengaps exist in both L_{MW} and L_{MVar}, which reflect the clustering patterns of MW and MVar flows. If there is a large eigengap, it means that each cluster is well self-sufficient in real or reactive power supply. Otherwise, the clusters are overlapping and clustering boundaries are "blurry". If the eigengap is large enough, different clusters can be easily identified in their eigen-space by e.g. the traditional k-means algorithm [106].

In considering both real and reactive power in the proposed approach, a combined eigen-space comprising selective eigenvectors of L_{MW} and L_{MVar} is constructed and denoted as:

$$V_{comb} := [V_{MW} \vdots V_{MVar}] \tag{3-26}$$

where V_{MW} and V_{MVar} respectively consist of the first k eigenvectors of L_{MW} and L_{MVar}. This eigen-space can be adjusted in a heuristic way to contain clustering information regarding real and reactive power. In this section, k is referred as a *heuristic indicator*, and formulate as:

$$k_{MW} = art \max\{|\lambda_{k+1} - \lambda_k|; \lambda \in \Lambda_S(L_{MW})\} \tag{3-27}$$

$$k_{MVar} = art \max\{|\lambda_{k+1} - \lambda_k|; \lambda \in \Lambda_S(L_{MVar})\} \tag{3-28}$$

where $\boldsymbol{S}$ is a predefined interval. The following pseudo code illustrates how the combined eigen-space can be constructed.

Table 3.5 Construction of combined eigen-space

Inputs: *casedata* is the basic operating data of a power system for real and reactive power flow calculation. *S* is a predefined interval.
Output: Combined eigen-space
Function: Construction of combined eigen-space
Run Newton-Raphson power flow based on *casedata*
Construct weighted adjacency matrix.
ω = the absolute value of real or reactive power flow
Compute the normalized Laplacian matrices L_{MW} and L_{MVar} with Eq. (3-23)
Compute the heuristic indicators k_{MW} and k_{MVar} with Eqs. (3-27) and (3-28)
Compute the first k_{MW} and k_{MVar} eigenvectors of L_{MW} and L_{MVar} respectively
Construct combined eigen-space $V_{comb} \in R^{|N| \times (k_{MW} + k_{MVar})}$
For i=1:|N|
y_i = the i-th row of $\boldsymbol{V_{comb}}$
End for

Clustering the points $(y_i)_{i=1,...,|N|} := [x_1^i, ..., x_{k_{MW}+k_{MVar}}^i]$ obtained from the eigen-space is an essential procedure to identify the partitioning boundaries. It has been found that the conventional k-means algorithm may fail to find the optimal partitions in some cases. Therefore, the SOM algorithm, which can provide superior performance with respect to clustering accuracy and have capability of handling big data, is utilized in the proposed approach.

C. Automated clustering based on SOM

SOM (also called as Kohonen Map) [121-123] is an excellent and widely used tool for cluster extraction, visualization and data mining. SOM is an unsupervised, competitive artificial neural network that produces topology-preserving mappings of data spaces utilizing a self-organizing learning algorithm. This algorithm can project high-dimensional data $\mathcal{Y} \subset \mathbb{R}^d$ onto a low-dimensional (typically one- or two-dimensional) fixed lattice of weighted neurons denoted as $\mathcal{K}$. The classical SOM algorithm can be briefly explained as follows:

The weights (denoted as $W_i^{neu} := [w_1, ..., w_{|W^{neu}|}]$) of each neural unit in the Kohonen Map $\mathcal{K}$ is trained through a competitive learning process. The best matching unit (BMU) is determined by the minimal Euclidean norms for a given data sample $y \in \mathcal{Y}$, such that

$$|| y - W_{best}^{neu} || \leq || y - W_i^{neu} || \qquad \forall i \in \mathcal{K} \tag{3-29}$$

The weights of each neuron are updated based on a given rule:

$$W^{neu}(t+1) = W^{neu}(t) + \eta(t)\Theta[\sigma(t)](y - W^{neu}) \quad (3\text{-}30)$$

where $\eta(t)$ is learning rate which exponentially decreases with t. $\Theta(\cdot)$ is the neighborhood function and $\sigma(t)$ indicates the neighborhood size. The weight vector of each prototype is the centroid of its receptive field (*RF*).

SOM features high capability of extracting data structures under the condition of various density distributions and cluster-overlaps. Even though SOM has such advantageous property and has been successfully applied to power system studies in e.g. security assessment [124], load forecasting [125], and wide-area stability control [126], etc, further improvements with respect to the processing of clustering information contained in each individual prototype for better segmentation are still desired.

In the proposed study, a hierarchical agglomerative clustering algorithm based on SOM is applied to the multi-objective partitioning problem. Geometric representations (provided by Laplacian spectrum) of PTNs serve as the inputs for SOM training. In order to achieve automated clustering for large dataset and complex cluster sizes associated with large inter-connected power systems, this hierarchical partitioning algorithm is equipped with an effective visualization scheme (i.e. CONNvis [127]), which is advantageous over other visualization methods (e.g. Euclidean distance between quantization prototypes [128], neighborhood of SOM [129], etc) in the study to

capture a faithful data density distribution. This clustering algorithm is summarized in Table 3.6 and explained in details in the following.

Table 3.6 Automated clustering based on SOM

Inputs: V_{comb} is the combined Laplacian eigen-space

Output: Clustering results

Function: automated clustering

1) Construct V_{comb}
2) Train SOM with $t \times t$ prototypes
3) Construct connectivity matrix ***CONN***
4) Initialize similarity matrix ***S***
5) (Update similarity matrix iteratively)

    c=1

    while $c<t^2$

        c=c+1

        merge the most similar pair of clusters into one

        update similarity matrix ***S***

        compute *CONN linkage*

    end while
6) Determine the number of cluster based on *CONN linkage* and yield clustering results

1) Construct combined eigen-space V_{comb}. Each row of V_{comb} serves as an input for SOM training;

2) A t×t Kohonen map is constructed and trained through a competitive training process. Selection of the number of prototypes in Kohonen map follows the rule that t^2

should be significantly less than the number of data samples whilst being greater than the expected number of clusters [127];

3) Connectivity matrix contains two important clustering information, namely neighborhood relations in datasets and detailed data distribution [130]. It can be expressed as:

$$CONN(i, j) = \left|RF_{ij}\right| + \left|RF_{ji}\right| \tag{3-31}$$

where $RF_{ij} = \{y \in RF_i : \| y - W_j \| \leq \| y - W_l \| \quad \forall l \neq i\}$, and $|RF_{ij}|$ indicates the number of data vectors in RF_{ij}

4) Similarities between the prototypes are determined by the local data distribution. Mathematically, similarity matrix is initialized as connectivity matrix. ***S*=*CONN***;

5) In each iterative step, the most similar pair of clusters C_i and C_j (which may include one or more prototypes) is merged into a new one which is referred as cluster p. S(p, q) is formulated as:

$$S(p,q) = [|C_i| / (|C_i| + |C_j|)]S(i,q) + [|C_j| / (|C_i| + |C_j|)]S(j,q) \tag{3-32}$$

The corresponding rows and columns of the most similar pair in ***S*** are omitted accordingly. After t^2*-1* iterations, all prototypes are merged into one cluster. CONN linkage is calculated in each step, which is formulated as:

$$conn\_index = intra\_conn \times (1 - inter\_conn) \tag{3-33}$$

where

$$intra\_conn = \frac{1}{R}\sum_{r=1}^{R}\frac{\sum_{i,j\in C_r}|RF_{ij}|}{\sum_{i\in C_r}|RF_i|}$$

$$inter\_conn = \frac{1}{R}\sum_{r=1}^{R}\max\frac{\sum_{i\in C_r, j\in C_l}|RF_{ij}|}{\sum_{i\in B_{rl}}CONN(i,j)}$$

R is the number of clusters. B_{rl} is the set of prototypes in cluster r that are directly connecting to the prototypes in cluster l.

6) The maximum value of *conn_index* is 1, which indicates that all clusters are clearly separated. Based on the analysis in [127], higher *conn_index* value reflects better clustering results. In the proposed study, the number of clusters is determined according to the maximum *conn_index* value. Since R=1 is meaningless for the proposed partitioning problem, R is bounded within [2, $R_{\max}$], where $R_{\max}$ is the maximum number of acceptable clusters in a specific PTN.

The merit of the algorithm illustrated above is that it can perform large data clustering with no prior knowledge of the number of clusters. It also has been proven that SOM can well tackle the partitioning problem, where the clusters can be of unequal sizes [131]. Furthermore, the prototypes of SOM are trained by the controllable eigen-space (which can be adjusted by k_{MW} and k_{MVar}). This enables the algorithm to find a

tradeoff between real and reactive power considerations so as to yield a desired partitioning result automatically.

D. Pareto optimality

The weight vectors of SOM prototypes represent the eigen-structure of L_{MW} and L_{MVar}, which reflects the partitioning boundaries. Combined eigen-space constructed by different pairs of k_{MW} and k_{MVar} can significantly influence the clustering results. In general, clustering only based on real or reactive power flow alone can be fairly different. Therefore, in the combined eigen-space, k_{MW} and k_{MVar} respectively are used to guide the clustering results with respect to real and reactive power. For example, if more effective clustering information regarding reactive power flow is included in V_{comb}, this will "drag" the clustering boundaries towards optimal reactive power partitioning. In contrast, the case is the same for real power flow. As a result for k_{MW} and k_{MVar}, one enclosing more clustering information would "prevail" over another, while both real and reactive power flow are simultaneously taken into account.

Based on the analysis above, a heuristic method is proposed, by which various semi-optimal partitioning solutions can be obtained through effectual adjustment of k_{MW} and k_{MVar}. The pair-wise objectives of the partitioning problem are formulated as:

$$\min\{ f_1 : \sum_{r=1}^{R} | g_r - l_r |,\ \ f_2 : \sum_{r=1}^{R} | \Delta v_r | \} \tag{3-34}$$

where g_r and l_r are the total real power generation and load demand in cluster r. $\triangle v_r$ denotes the voltage violation in cluster r. In practice, voltage of each bus should be maintained within tolerance (i.e. $\pm$0.06 p.u.). The first objective is to minimize the total real power imbalance of the whole network, and the second one is to minimize the voltage violation from reactive power support perspective. In the thesis, the partitioning problem is simplified based on the assumption that only limited reactive power compensation is locally available on each bus.

The goal of the proposed approach is to firstly find out solutions that are close to its Pareto-optimal front and secondly, maintain a good spread of solutions on this front. Inspired by NSGA-II framework [132], a tailored algorithm for network partitioning is developed based on fast non-dominated sorting and crowding distance [132]. The whole procedure of this algorithm is as follows

Table 3.7 Heuristic partitioning algorithm

Inputs: L_{MW}, L_{MVar}

Output: Pareto front of partitioning solutions

Function: produce a Pareto front of multi-objective partitioning problem

1) Initialization. U(0) and U(1) are respectively including m pair-wise heuristic indicators.
   i=0
   Z(1)=U(0) $\cup$ U(1)
2) Calculate crowding distance and fast nondominated sorting: Z(1)$\rightarrow$F(1)
3) while (termination condition is not true)
   i=i+1
   split F(i-1)$\rightarrow$$F_{best}$($i$-1) $\cup$ F_{rest}(i-1)

4) update $F_{rest}(i\text{-}1) \rightarrow U(i)$

form $Z(i)= U(i) \cup F_{best}(i\text{-}1)$

calculate crowding distance and fast nondominated sorting:

$Z(i) \rightarrow F(i)$

End while

1) $U(\bullet)$ represents a string of m individuals. Each individual is a pair of heuristic indicators.

$$U(\bullet) = [u_1,\ u_2, \ldots u_m]$$

where

$$u = \begin{bmatrix} k_{MW} \\ k_{MVar} \end{bmatrix}$$

The heuristic indicator is randomly initialized in a given acceptable range [1, k_{max}], which is formulated as:

$$k = \lfloor 1 + k_{\max} \cdot \gamma \rfloor \tag{3-35}$$

where γ is a random number within [0,1).

U(0) and U(1) are randomly initialized without duplicate individuals. Z(1) is formed by combining U(0) and U(1).

2) In this step, all individuals in Z(1) are evaluated by the partitioning algorithm proposed in 3.3.2-C. Each partitioning solution corresponds to a pair of values—real power imbalance and voltage violation. Based on the fast non-dominated sorting method and crowding distance proposed in [132], Z(1) is sorted and rearranged as F(1).

3) The termination criterion adopted is $i \le (k_{MW} k_{MVar})_{\max} / 2m$, which indicates the maximum number of generations. F(i) is obtained by sorting Z(i). F(i) is divided into two parts with equal size. The first part is grouped as the best individuals, which is denoted as $F_{best}(i)$. The rest part is denoted as $F_{rest}(i)$.

4) The schematic diagram of updating process is shown in Fig . $F_{rest}(i)$ is updated referred to $F_{best}(i)$.

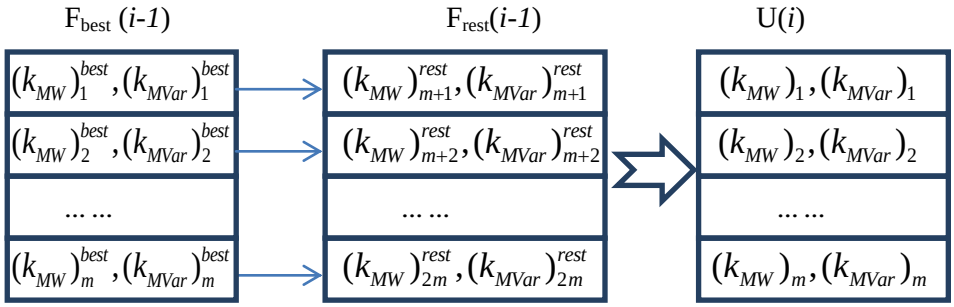

Fig 3.16 Schematic diagram of updating process

The updating operator is formulated as:

$$\begin{aligned} k_j &= \left\lfloor k_{m+j}^{rest} + (k_j^{best} - k_{m+j}^{rest} + 2) \cdot \gamma \right\rfloor, k_j^{best} \ge k_{m+j}^{rest} \\ k_j &= \left\lfloor k_{m+j}^{rest} + (k_j^{best} - k_{m+j}^{rest} - 2) \cdot \gamma \right\rfloor, k_j^{best} < k_{m+j}^{rest} \end{aligned} \tag{3-36}$$

where γ is a random number ranged within [0,1).

According to the updating operator, k_j is allowed to be assigned a random value ranged within $[k_{m+j}^{rest}, k_j^{best} + 1]$ or $[k_{m+j}^{rest} - 1, k_j^{best}]$. This enables the proposed algorithm to explore and exploit the search space in an effective way.

Z(i) is formed by incorporating U(i) and $F_{best}(i\text{-}1)$ to strengthen the elitism throughout the algorithm. F(i) is obtained by rearranging Z(i) based on the crowding distance and fast non-dominated sorting.

E. Fuzzy decision making

On the condition that there is no prior knowledge provided for the selection of candidate partitioning solutions in Pareto set, un-weighted fuzzy logic decision making strategy [133] is employed to select the best trade-off solution. It should be noted that other decision making criterions can also be considered under different conditions. In this proposed approach, one assumes that the preference of minimizing voltage violation or generation-load imbalance is unbiased. Fuzzy logic decision making is mathematically summarized as follows.

Given a Pareto set $\boldsymbol{S_{pareto}}$ for pair-wise objectives, the fuzzy membership is defined as:

$$\mu = \frac{f_i^{\max} - f_i}{f_i^{\max} - f_i^{\min}}, i = 1,2 \tag{3-37}$$

The normalized membership for each solution is expressed as:

$$\mu(j) = \frac{\sum_{i=1}^{2} \mu_i(j)}{\sum_{j=1}^{|S_{pareto}|} \sum_{i=1}^{2} \mu_i(j)} \tag{3-38}$$

According to the fuzzy logic principle [133], the best trade-off (most satisfactory) solution is selected by the maximum fuzzy membership value.

F. Computational efficiency

As compared with traditional clustering methods e.g. k-means[134], the proposed approach turns out to be more effective and efficient. Detailed experimental comparisons will be shown in Section 3.3.3. Generally, the number of evaluations in the proposed approach is nearly $(k_{MW} k_{MVar})_{\max} / 2$. In case that there is no prior knowledge about the dataset, a disadvantage for traditional k-means method is the need for a preset number of clusters. In order to find an optimal partitioning solution, the typical way is to repeat k-means algorithm a couple times and employ cluster validity indices (e.g. Davies-Bouldin Index (DBI) based on Davies-Bouldin Criterion [135]) to evaluate each solution. Normally, the *k* value is set from 2 to $\lfloor \sqrt{n} \rfloor$, where *n* is the number of samples in the clustering dataset. K-means favors clusters with nearly equal size, which makes the solutions less effective than the ones obtained by the proposed approach.

Furthermore, as compared with global search methods, the proposed partitioning algorithm is more computationally efficient since the search space is significantly decreased. This is because Laplacian spectrum naturally indicates semi-optimal partitioning solutions, which serves as a bridge for the proposed approach to explore Pareto solutions with less computational cost.

The major computational task of the hybrid approach includes construction of eigen-space, SOM based clustering and optimization. As for the first part, computing eigenvectors of L_{MW} and L_{MVar} normally takes O(|N|^3) time. The time complexity can still be reduced by employing sparse techniques for Laplacian matrix. Secondly, the total time complexity of training SOM is nearly O(*(T+1)I*), where *T* is the number of neurons and *I* is the number of iterations. In addition, automated clustering takes O(*T*) time. Thus, the time complexity for the second part is O((*T+2)I*). Lastly, optimization is an essential part, which only needs O($(k_{MW}k_{MVar})_{\max} / 2m$) time complexity. To sum up, such degree of time complexity makes the proposed partitioning method promising and competitive for practical application.

3.3.3 Case studies

The proposed approach is tested on three different test systems—two relatively small systems (i.e. IEEE New England 39-bus system and 118-bus test system) and a large one (i.e. 2383-bus transmission system in Poland). Comparative experiments are carried out based on traditional k-means algorithm. MATLAB SOM toolbox (developed by Helsinki University of Technology) is utilized for SOM training.

A. IEEE New England 39-bus system

This test system consists of 39 buses, 10 generators and 46 branches. In this case, two operating conditions are considered including normal operation and heavy loading.

1) Parameter setting

In normal operating condition, the total generation is 6297.87 MW and 1274.94MVar, and the total load is 6254.23 MW and 1387.1MVar. In heavy load operating condition, the system is operated under a total generation of 7044.46MW and 2020.11MVar, and a total load of 7004.23MW and 2136.10MVar. Power flow solution is calculated based on typical IEEE New England 39-bus system datasets [136].

In this case, one trains a 3×3 hexagonal Kohonen map by using MATLAB SOM toolbox (with a Gaussian neighborhood function). As a comparative experiment, k-means algorithm (in MATLAB Statistics Toolbox) is used to cluster combined eigen-space. The clustering performance is evaluated by DBI.

2) Network partitioning

According to the methodology presented in Section 3.2.2, different SOMs are firstly trained under two operating conditions. To demonstrate the automated clustering of SOM prototypes, two given SOMs, which are trained respectively by eigen-space with (k_{MW}=1, k_{MVar}=2) and (k_{MW}=3, k_{MVar}=2) in normal operating condition, are clustered based on CONN linkage. Comparative experiments have been carried out based on k-means algorithm. Clustering results are compared in Fig 3.17 and Table 3.8.

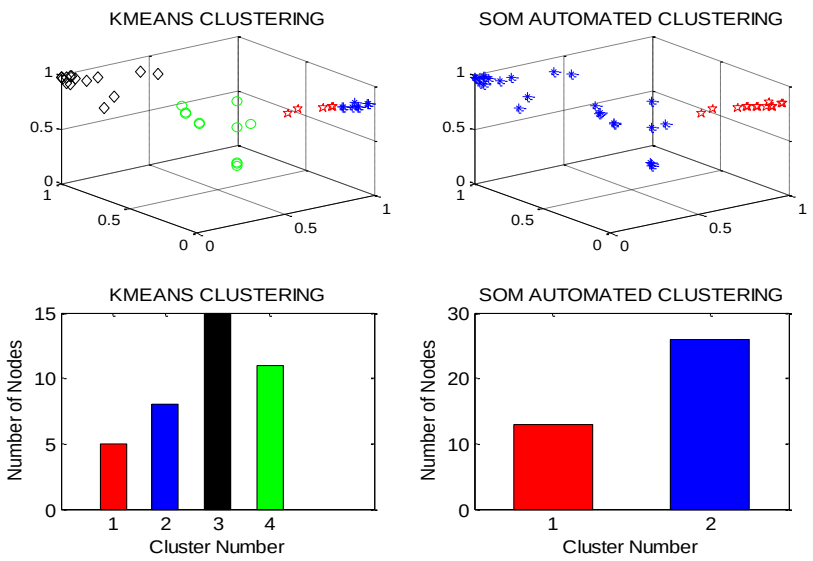

(a)

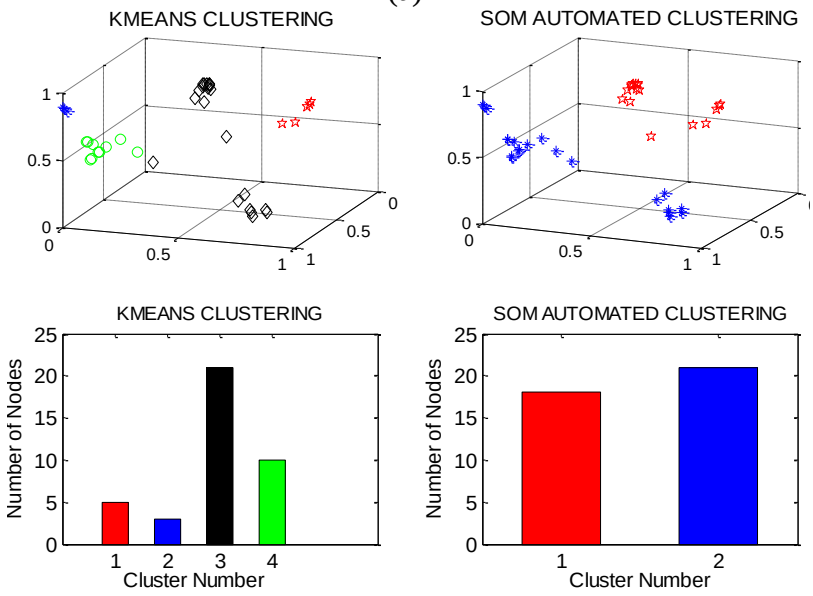

(b)

Fig 3.17 (a) clustering results based on SOM (k_{MW}=1, k_{MVar}=2) and kmeans in normal operating condition. (b) clustering results based on SOM (k_{MW}=3, k_{MVar}=2) and kmeans in normal operating condition

Table 3.8 Clustering performance based on SOM and k-means (IEEE New England 39-bus system)

		real power imblance (MW)	voltage violation (p.u)	Voltage violation (bus No.)
SOM	k_{MW}=1 k_{MVar}=2	147.259	0.0036	36
	k_{MW}=3 k_{MVar}=2	4.2	0.0212	4,7,8,36
k-means	k_{MW}=1 k_{MVar}=2	170.759	0.0288	4,15,24,36
	k_{MW}=3 k_{MVar}=2	195.1	0.0246	4,7,8,24,36

Each point plotted in Fig. 3.17 (a) and (b) corresponds to each bus in this system, whose coordinates are determined by the first three eigenvectors in the combined eigen-space. Apparently, under such a specific condition, clustering results of SOM and kmeans are fairly different. As for the k-means algorithm, the number of clusters is determined by Davies-Bouldin Criterion (in MATLAB statistics toolbox), which favors 4 in this case. In the proposed approach, 2 clusters with the highest *CONN_index* are found. The sizes of all clusters are shown in the histograms.

As shown by Table IV, clusters obtained by the proposed approach have less real power imbalance and total voltage violation. Moreover, when more clustering information of real power are considered (i.e. k_{MW}=3, k_{MVar}=2), the resultant clustering favors less real power imbalance based on the proposed approach. In contrast, the k-means based clustering fails to capture such data features since larger MW imbalance is undesirably obtained under the condition of k_{MW}=3, k_{MVar}=2. In the proposed study, SOM based clustering outperforms k-means because SOM can find an optimal

distribution of the prototype vectors in the combined eigen-space (which is an adaptive vector quantization process) such that the density distribution of the clustering information for real and reactive power can be best approximated. Therefore, SOM is more suitable for the proposed heuristic partitioning approach.

Based on the proposed heuristic method, SOM automated clustering and k-means are respectively incorporated and compared in Table 3.9. Partitioning alternatives are plotted in Fig. 3.18, where obtained Pareto fronts are marked by dash lines.

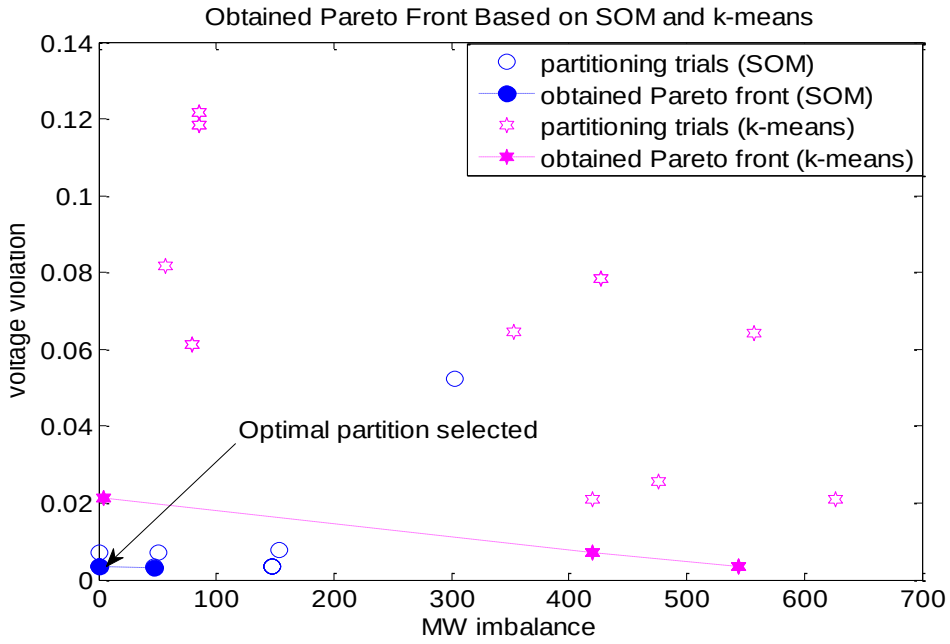

(a)

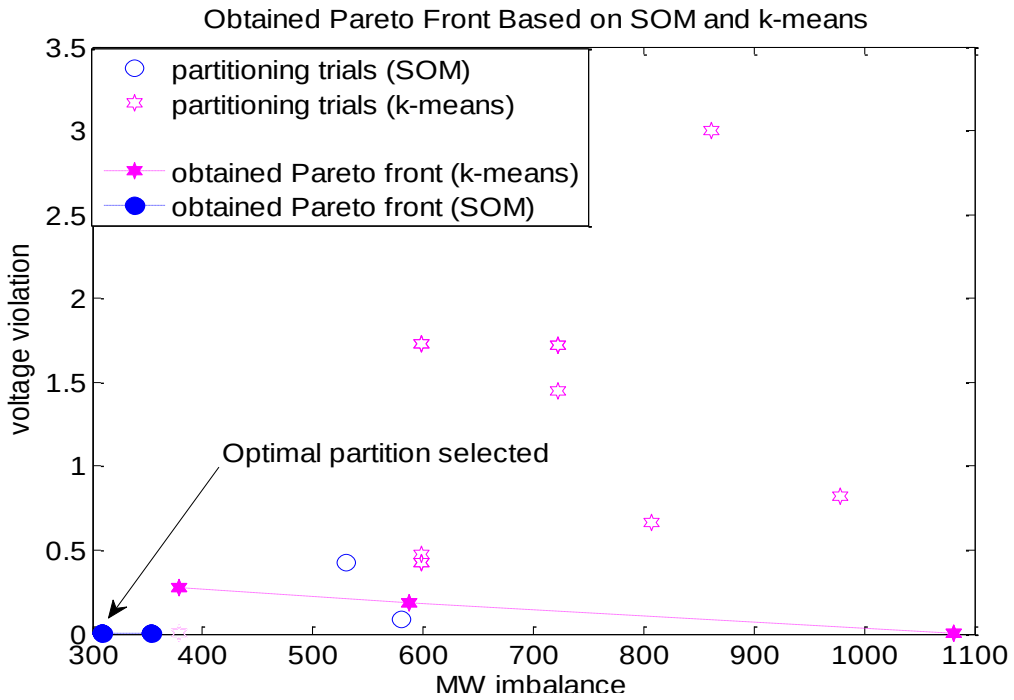

(b)

Fig 3.18 (a) Heuristic partitioning results based on SOM and k-means in normal operating condition. (b) Heuristic partitioning results based on SOM and k-means in heavy load operating condition.

Table 3.9 Partitioning results (IEEE New England 39-bus System)

Normal operating condition				
Heuristic partitioning	Partitioning alternatives (with cluster sizes)	MW imbalance (MW)	Voltage violation(p.u)	μ
SOM	Cluster1:14 Cluster2:25	0	0.0036	0.9241*
	Cluster1:7 Cluster2:32	46.6	0.003	0.0759
k-means	Cluster1:15 Cluser2:24	4.2	0.02117	0.5044
	Cluster1:6 Cluster2:13 Cluster3:14 Cluster4:6	420	0.007012	0.4063
	Cluster1:7 Cluster2:13	543.6	0.0036	0.0894

	Cluster3:14 Cluster4:5			
Heavy load operating condition				
SOM	Cluster1:13 Cluster2:26	309.5	0.0036	0.8926*
	Cluster1:12 Cluster2:27	353.5	0.0027	0.1074
k-means	Cluster1:19 Cluser2:20	378.3	0.2777	0.4195
	Cluster1:13 Cluster2:13 Cluster3:13	587.1	0.1877	0.3608
	Cluster1:9 Cluster2:16 Cluster3:14	1081	0.0036	0.2198

As shown in Fig 3.18 (a) and (b), SOM based heuristic partitioning is more effective than k-means because less partitioning trials are exploited and the obtained Pareto front is better than the one obtained by k-means. This is reasonable since k-means based clustering fails to capture the data topology which combines information of real and reactive power, while SOM based automated clustering is performing well (This has been proven through the whole experiment study and an example is shown in Table 3.8). Among all partitioning alternatives (reported in Table 3.9), optimal partitions are respectively selected with maximum fuzzy membership values, which are marked by asterisks. Partitioning boundaries are depicted in Fig 3.19.

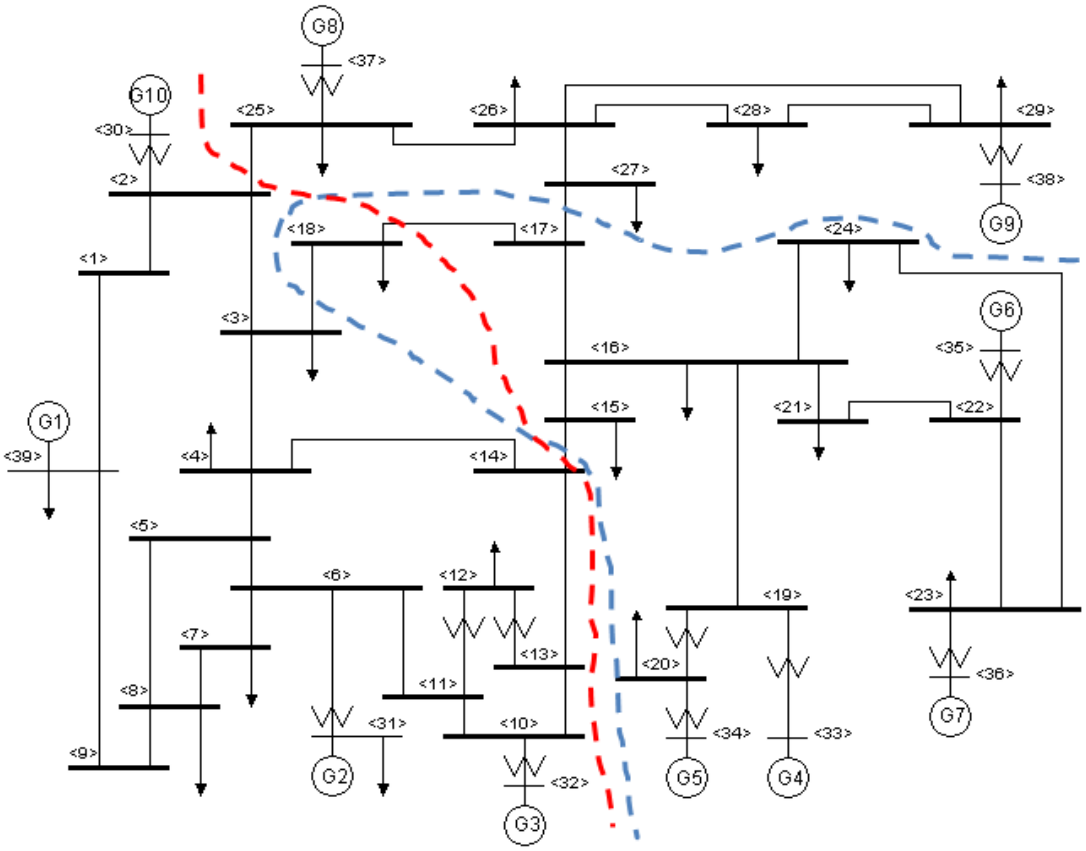

Fig 3.19 IEEE New England 39-bus system partitioning boundaries in normal (blue dash line) and heavy load (red dash line) operating conditions

B. IEEE 118-bus test system

The IEEE 118-bus test system is extracted from Midwestern US power grid in 1962, which consists of 54 generators and 186 branches. In this case, three operating conditions with different load levels are being considered.

1) Parameter setting

Three operating conditions with total load (4242MW, 1438MVar), (5302.5MW, 1840.6MVar), and (6151MW, 2157MVar) are taken into account. Power flow solutions are produced based on typical IEEE 118-bus system datasets [137].

In this case, a 4×4 hexagonal Kohonen map is trained by using MATLAB SOM toolbox (with a Gaussian neighborhood function), k-means algorithm (in MATLAB Statistics Toolbox) is applied to compare the clustering results with the proposed approach.

2) Network partitioning

In this case, along with the increasing of network size, the complexity of data topology (i.e. combined eigen-space) is increased accordingly. In order to illustrate how the proposed hybrid approach produces optimal partitioning solutions, one partitions the IEEE 118-bus system under different operating conditions, and compares the MW imbalance and voltage violation with the ones obtained by k-means. Comparative results are shown in Fig. 3.20 and Table 3.10. In Fig. 3.21, cluster sizes of all Pareto optimal partitioning alternatives are shown by histograms.

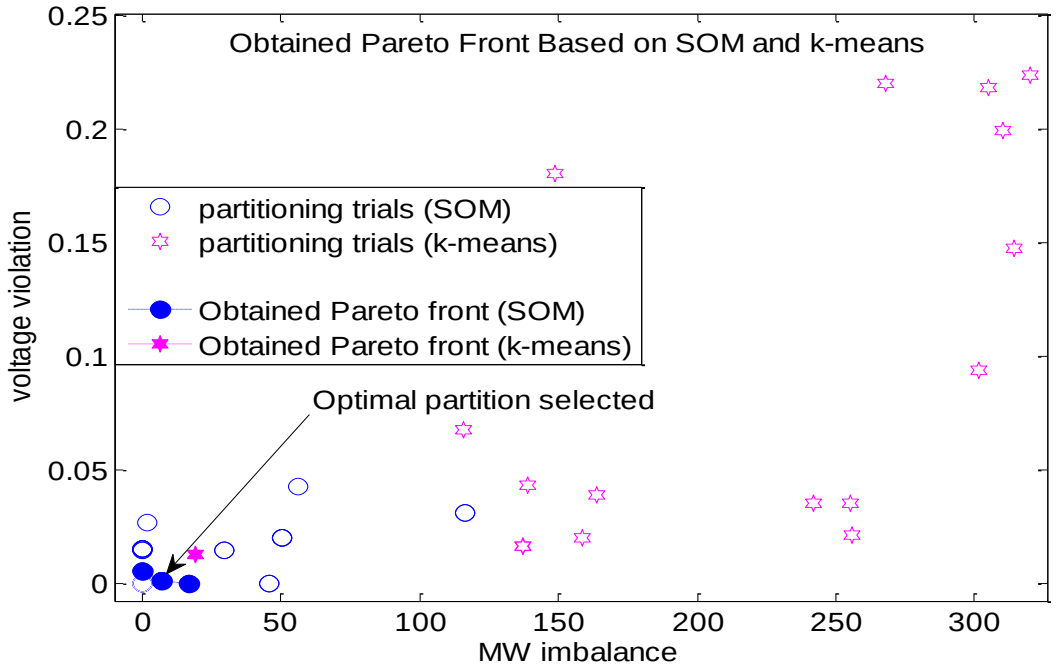
Obtained Pareto Front Based on SOM and k-means
partitioning trials (SOM)
partitioning trials (k-means)
Obtained Pareto front (SOM)
Obtained Pareto front (k-means)
Optimal partition selected
voltage violation
MW imbalance
0.25
0.2
0.15
0.1
0.05
0
0
50
100
150
200
250
300

(a)

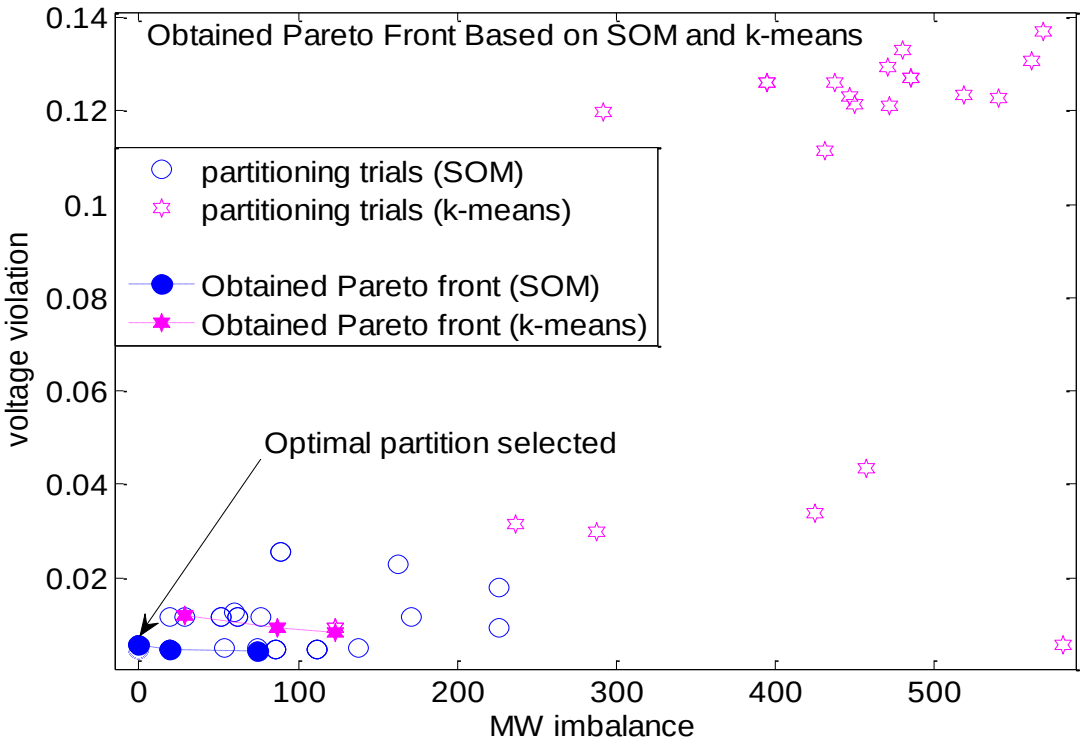
Obtained Pareto Front Based on SOM and k-means
partitioning trials (SOM)
partitioning trials (k-means)
Obtained Pareto front (SOM)
Obtained Pareto front (k-means)
Optimal partition selected
voltage violation
MW imbalance
0.14
0.12
0.1
0.08
0.06
0.04
0.02
0
100
200
300
400
500

(b)

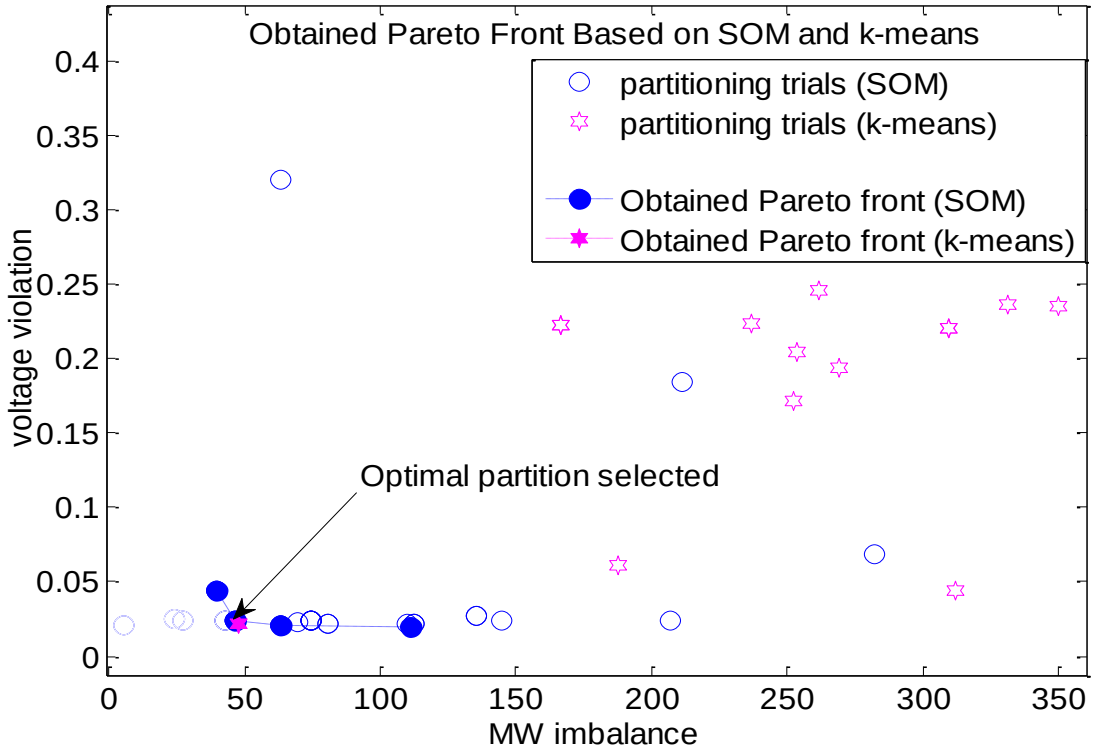

(c)

Fig 3.20 Heuristic partitioning results based on SOM and k-means with total load (a) 4242MW, 1438MVar (b) 5302.5MW, 1840.6MVar, and (c) 6151MW, 2157MVar

Table 3.10 Partition results (IEEE 118-bus system)

Total load (4242MW, 1438MVar)				
Heuristic partitioning	Partitioning alternatives (with cluster sizes)	MW imbalance (MW)	Voltage violation(p.u)	μ
SOM	Cluster1:62 Cluster2:56	0	0.005653	0.3312
	Cluster1:65 Cluster2:53	7	0.001025	0.3399*
	Cluster1:29 Cluster2:89	17	0	0.3290

k-means	Cluster1:35 Cluster2:36 Cluster3:18 Cluster4:29	19	0.01284	1
Total load (5302.5MW, 1840.6MVar)				
SOM	Cluster1:15 Cluster2:46 Cluster3:57	0	0.005658	0.3522*
	Cluster1:12 Cluster2:46 Cluster3:60	19.85	0.004657	0.3449
	Cluster1:12 Cluster2:37 Cluster3:69	74.02	0.004478	0.3029
k-means	Cluster1:45 Cluster2:40 Cluster3:33	28.46	0.0118	0.3443
	Cluster1:27 Cluster2:38 Cluster3:43 Cluster4:10	87.43	0.009168	0.3320
	Cluster1:47 Cluster2:33 Cluster3:15 Cluster4:23	122.9	0.008321	0.3236
Total load (6151MW, 2157MVar)				
SOM	Cluster1:27 Cluster2:15 Cluster3:46 Cluster4:30	39.76	0.04368	0.2598
	Cluster1:34 Cluster2:47 Cluster3:37	46.2	0.02394	0.2675*
	Cluster1:35 Cluster2:46 Cluster3:37	63.31	0.0206	0.2557
	Cluster1:5 Cluster2:33 Cluster3:43 Cluster4:37	111.2	0.01978	0.2170
k-means	Cluster1:40 Cluster2:45 Cluster3:33	47.73	0.02142	1

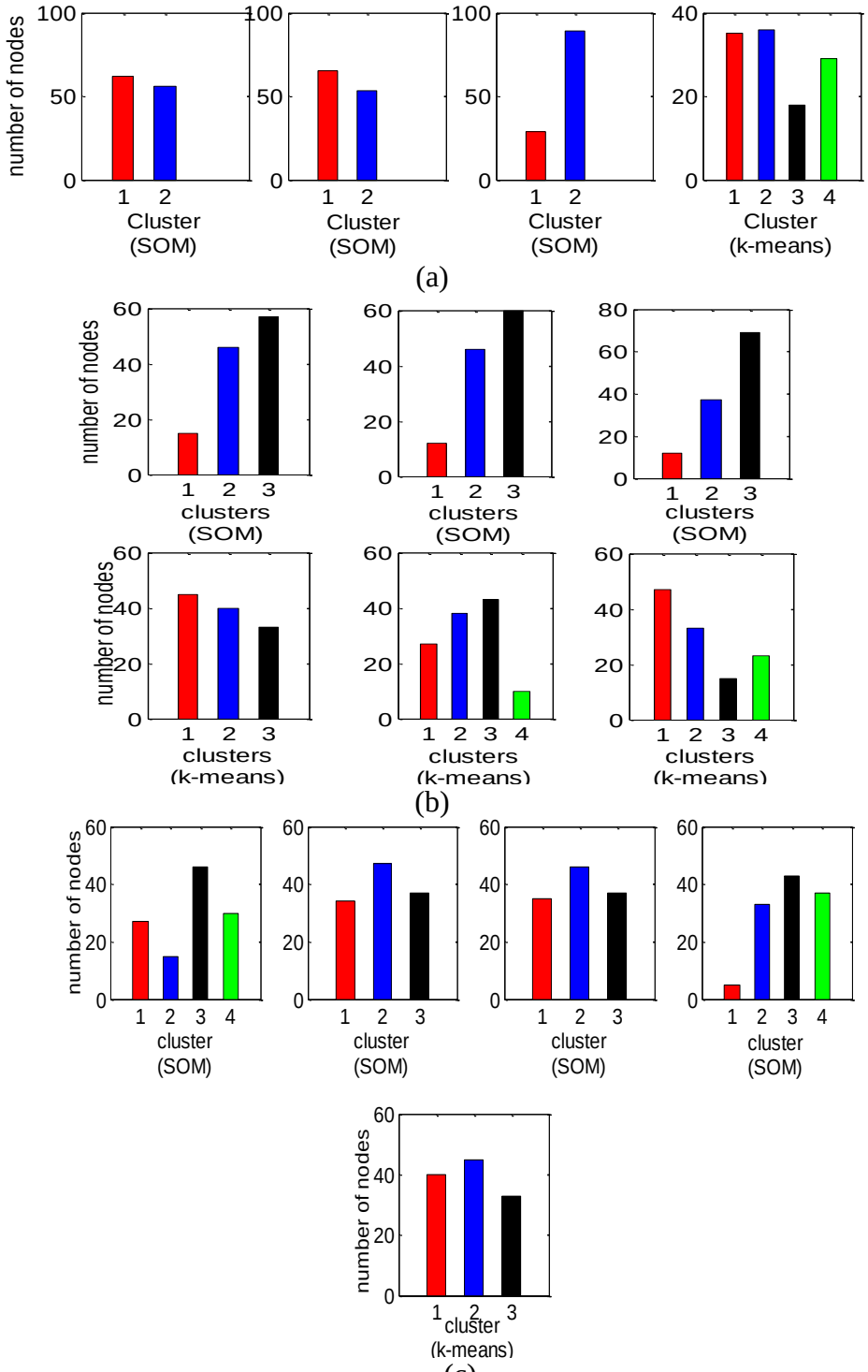

Fig 3.21 Cluster sizes of each Pareto partitioning solution under conditions of total load (a) 4242MW, 1438MVar (b) 5302.5MW, 1840.6MVar, and (c) 6151MW, 2157MVar

The results shown in Fig 3.20 and Table 3.10 indicate that the proposed hybrid approach outperforms k-means based clustering. Obviously, more partitioning trials are in need for k-means based clustering. This indicates that it is less effective for k-means algorithm to find out an appropriate density distribution of clustering information for this test case. With the size of PN becoming larger, the proposed approach still performs well with less partitioning trials and better obtained Pareto front. This provides evidence that using SOM based automated clustering can well capture the data topology of real and reactive power under different operating conditions.

C. Polish 2383-bus transmission system

To further test the proposed approach on a realistic and relatively large transmission system, the 2383-bus transmission network data from Poland grid is used and two realistic load profiles are considered in this case. This transmission network consists of 327 generators and 2896 branches.

1) Parameter setting

Two operating conditions with different load profiles are considered, i.e. i) total generation of 25280.97 MW, 8810.45 MVar, and total load of 24558.38MW, 8143.92MVar; and ii) total generation of 18961 MW, 6607.8 MVar, and total load of 18419MW, 6108MVar.

A 6×6 hexagonal Kohonen map is trained by using MATLAB SOM toolbox (with a Gaussian neighborhood function), k-means algorithm (in MATLAB Statistics Toolbox) is also applied on this transmission network to compare the clustering results.

2) Network partitioning

As one can see in Fig 3.22, with the complexity of data topology considerably increased, the proposed approach incorporating SOM based automated clustering is substantially more effective than k-means. As reported in Table 3.11, it is worth noting that k-means based clustering with employment of DBI is incapable of favoring the satisfactory clusters that fit the objectives of minimizing real power imbalance and voltage violation. As shown in Fig. 3.22 (a) and (b), also reported in Table 3.11, the Pareto optimal partitioning solutions produced by the proposed approach is much better than the ones obtained by k-means. The cluster sizes for each partition are reported via histograms in Fig 3.23.

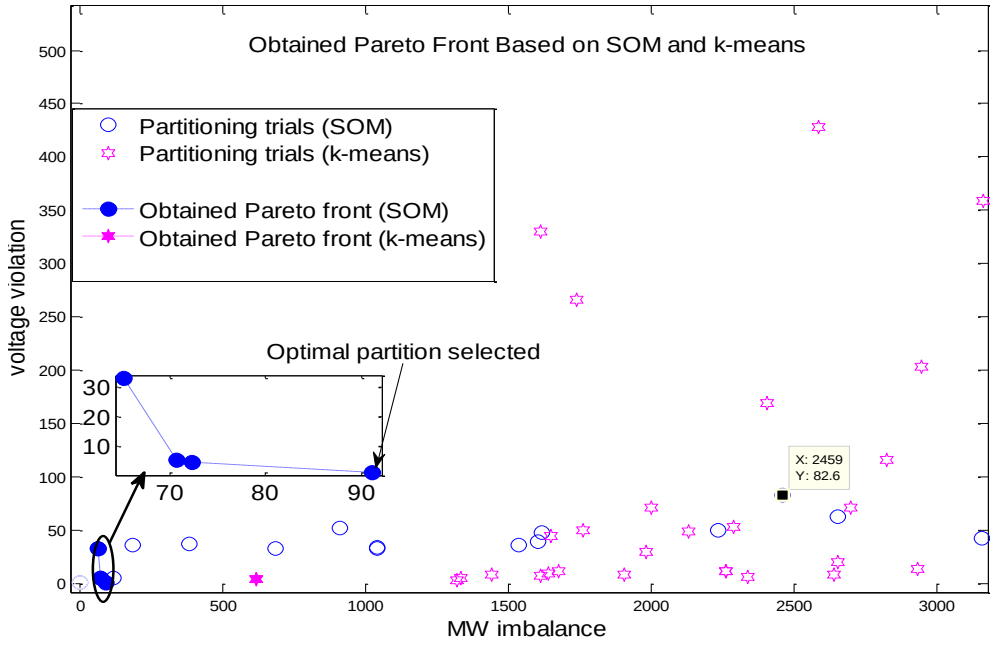

(a)

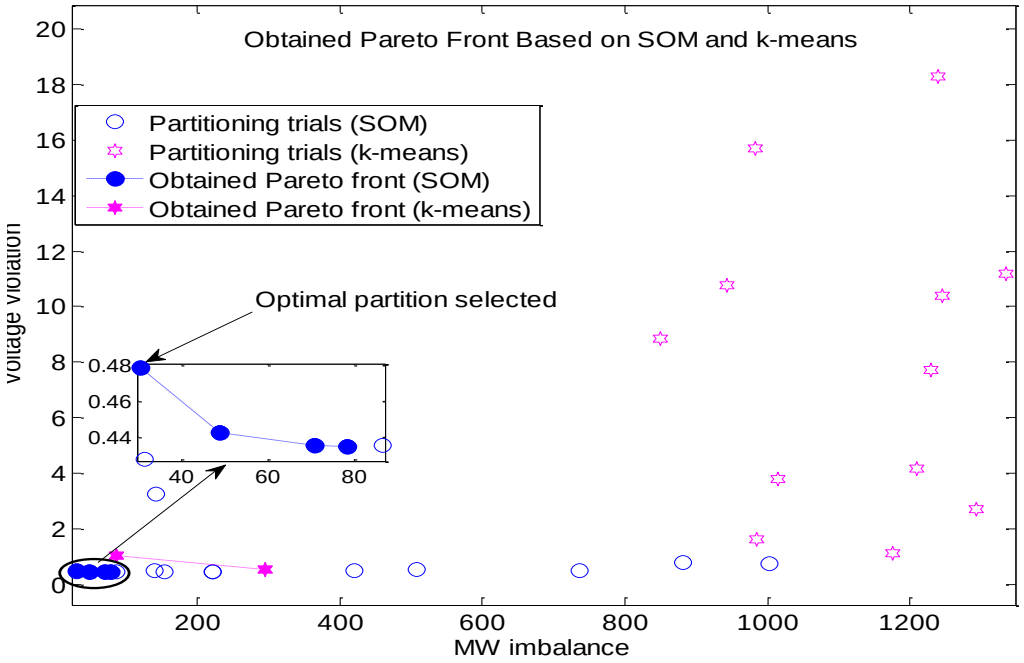

(b)

Fig 3.22 Heuristic partitioning results based on SOM and k-means with total load (a) 24558.38MW, 8143.92MVar, and (b) 18419MW, 6108MVar

Table 3.11 Partitioning Results (Polish 2383-bus system)

Heuristic partitioning	Partitioning alternatives (with cluster sizes)	MW imbalance (MW)	Voltage violation(p.u)	μ
Total load (24558.38MW, 8143.92MVar)				
SOM	Cluster1:24 Cluster2:1894 Cluster3:465	65.21	32.89	0.2146
	Cluster1:82 Cluster2:464 Cluster3:1153 Cluster4:684	70.73	5.315	0.2595
	Cluster1:465 Cluster2:1153 Cluster3:765	72.31	4.56	0.2607
	Cluster1:466 Cluster2:1917	91.09	1.237	0.2653*
k-means	Cluster1:521 Cluster2:70 Cluster3:723 Cluster4:1069	619	3.795	1
Total load (18419MW, 6108MVar)				
SOM	Cluster1:58 Cluster2:2325	30.62	0.479	0.2521*
	Cluster1:347 Cluster2:2036	48.72	0.4427	0.2513
	Cluster1:350 Cluster2:2033	70.94	0.4352	0.2488
	Cluster1:429 Cluster2:1944	78.37	0.4348	0.2478
k-means	Cluster1:852 Cluster2:1277 Cluster3:254	86.11	1.032	0.5183

	Cluster1:395 Cluster2:960 Cluster3:1028	295.9	0.5156	0.4817

From all the observations and comparisons above, one can safely conclude that the proposed hybrid approach based on SOM is highly effective and robust for the partitioning problem with the concerned pair-wise objectives in power systems.

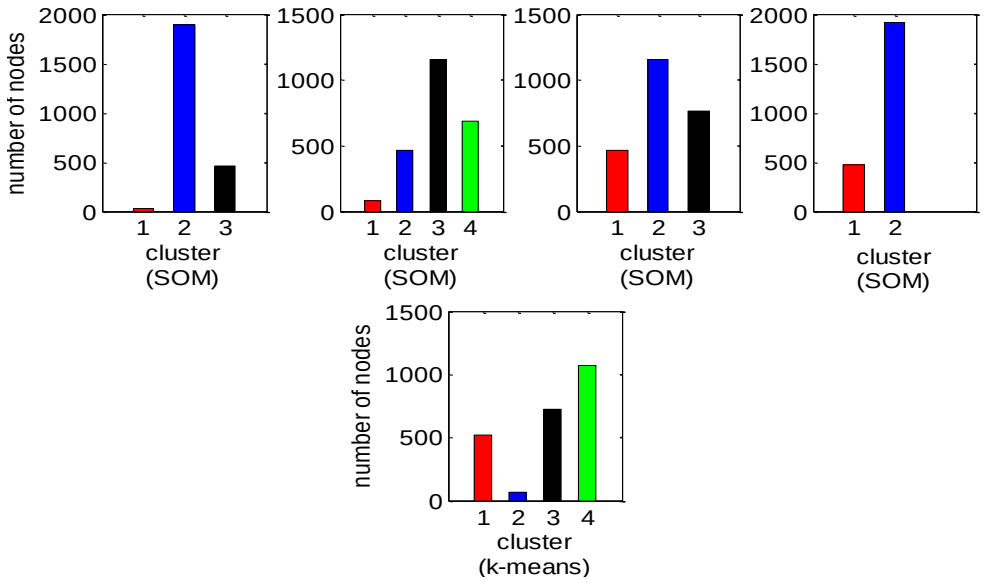

(a)

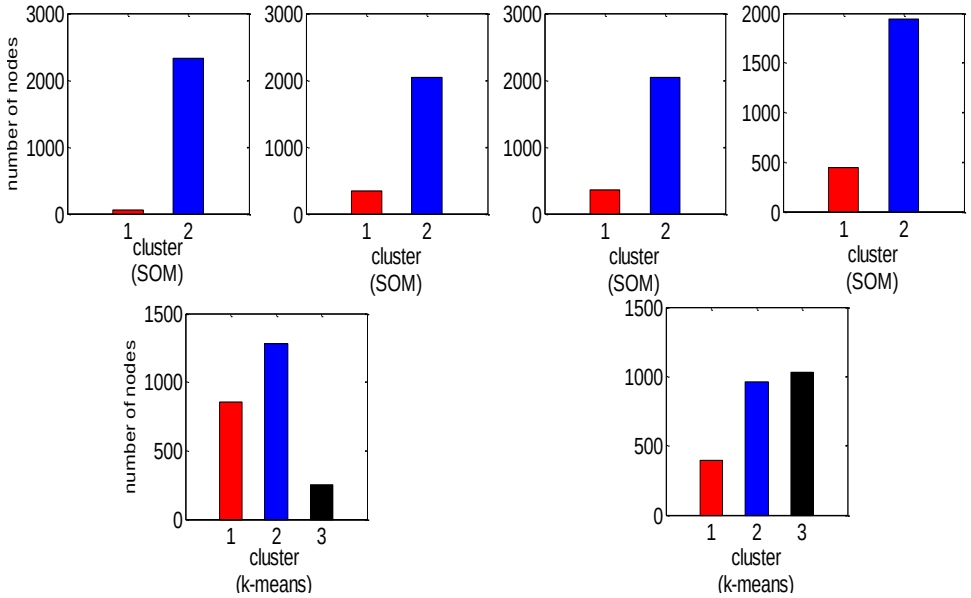

(b)

Fig 3.23 Cluster sizes of each Pareto partitioning solution under conditions of total load (a) 24558.38MW, 8143.92MVar, and (b) 18419MW, 6108MVar

D. Elapsed time

All case studies are carried out 10 times on workstation (Dell Precision T7600, Intel Xeon CPU E5-2667 0 @2.90GHz, 2 processors). The average computing time for each test case is reported in Table 3.12. Such level of elapsed time is competitive, which shows high potential for practical application.

Table 3.12 Elapsed time in different cases

Test case	Load profiles	Averaging elapsed time (s)
IEEE 39-bus system	6254.23MW 1387.1MVar	6.241
	7044.46MW 2020.11MVar	6.140
IEEE 118-bus system	4242MW, 1438MVar	8.126
	5302.5MW, 1840.6MVar	8.233
	6151MW, 2157MVar	8.569
Polish 2383-bus system	24558.38MW, 8143.92MVar	89.324
	18419MW, 6108MVar	93.605

3.3.4 Summary

A hybrid k-way partitioning approach is proposed in this section, which combines Laplacian spectrum of PNs and SOM automated clustering. A tailored heuristic optimization algorithm is also proposed to solve multi-objective partitioning problems in power systems. Case studies based on IEEE 39-, 118-bus systems and Polish 2383-bus transmission system demonstrate that the proposed approach can effectively produce optimal partitioning solutions to ensure the self-sufficient capability (i.e. less real power imbalance) and high-quality voltage profiles in each cluster. Experimental results illustrate that the proposed approach is much more effective than the k-means based algorithm. Furthermore, this hybrid approach is computationally efficient, which indicates a high potential for practical application in smart grid.

3.4 Topological Resilience Against Electrical Component Outages

3.4.1 Investigation of "small-world" properties in power transmission network

"Small-world effect" was firstly discovered by Milgram in 1967 [138], which indicates that any two of several billion human beings can be directly connected by a short chain of typical length about 6. A large number of studies have been conducted subsequently to confirm this conclusion, although the number "6" remains questionable for an accurate estimation. Such "small-world effect" inaugurated a new way of understanding the topological structural of networks. In 1998, Watts and Strogatz proposed a new model of "small-world" networks in *Nature*, which are characterized by characteristic path length and clustering coefficient [139]. This model can reflect the "small-world effect" at different levels, which serves as an essential groundwork to further study the structural properties of "small-world" networks. Meanwhile, power grids of the western United States are also proven to be small-world networks in [139].

In order to have a deep insight of underlying network structures of power grids, small-world properties, i.e. characteristic path length and clustering coefficient, are firstly investigated on New England 39-bus system, IEEE 118-bus system and Polish 2383-bus transmission system. Based on the following results, a bond percolation model on small-world PTN is proposed in the sub-section 3.4.2.

The abstract graphs of New England 39-bus, IEEE 118-bus, and Polish 2383-bus systems are shown in Figs 3.24-3.26. Characteristic path length $Len(\mathcal{G})$ and clustering coefficient $Coeff(\mathcal{G})$ are defined as Eqs (3-39) and (3-40), respectively.

$$Len(\mathcal{G}) = \frac{|\mathcal{N}| \times (|\mathcal{N}| - 1)}{2} \sum_{i,j \in \mathcal{N}} l_{i,j}^{shortest} \tag{3-39}$$

$$Coeff(\mathcal{G}) = \frac{1}{|\mathcal{N}|} \sum_{i=1}^{|\mathcal{N}|} \frac{2 |\{edge_{jk} : n_j, n_k \in Neighbor_i, edge_{jk} \in \mathcal{E}\}|}{d_i (d_i - 1)} \tag{3-40}$$

where $l_{i,j}^{shortest}$ is the number of edges through the shortest path between vertices *i* and *j*. d_i is the degree of vertex *i*. The neighborhood set of vertex *i* is defined as:

$$Neighbor_i = \{n_j : edge_{ij} \in \mathcal{E}\}$$

$Len(\mathcal{G})$ reflects a global property of a graph, which measures the typical length between two vertices in the graph. $Coeff(\mathcal{G})$ reflects a local property that measures the cliquishness of a typical neighborhood [139]. [139] indicates that a small-world network has the following features:

$$Len_{actual} \gtrsim Len_{random}, \text{ but } Coeff_{actual} \gg Coeff_{random}$$

where Len_{random} and $Coeff_{random}$ are respectively the characteristic path length and clustering coefficient of a random network with the same number of vertices and average number of edges per vertex.

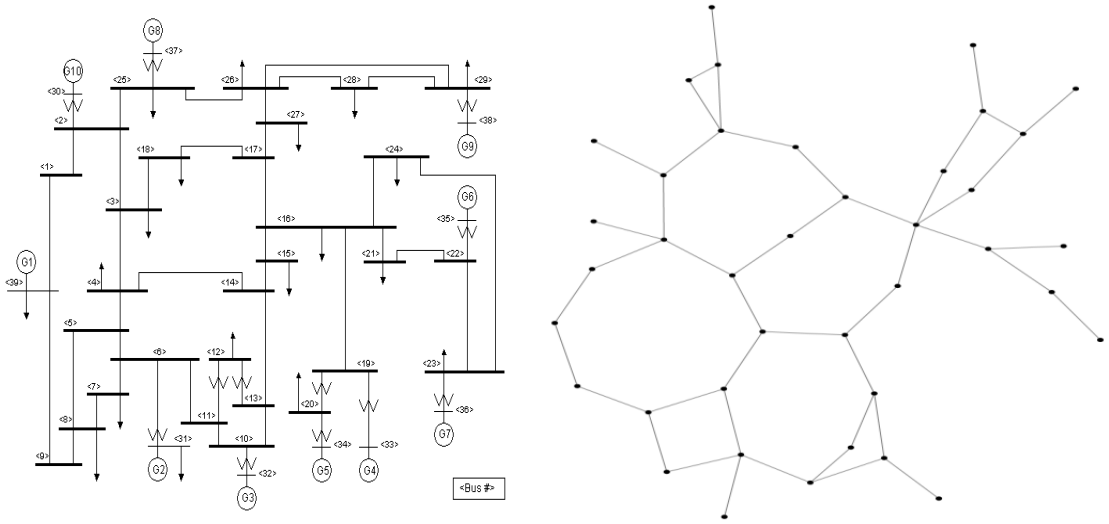

Fig 3.24 Abstract graph of New England 39-bus system

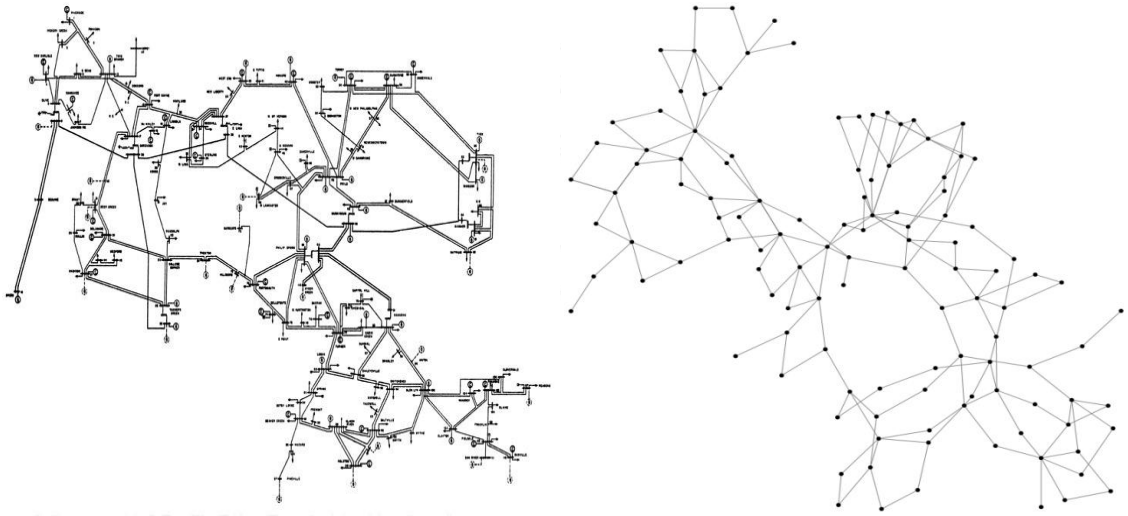

Fig 3.25 Abstract graph of IEEE 118-bus system

Fig 3.26 Abstract graph of Polish 2383-bus transmission system

According to Eqs (3-39) and (3-40), characteristic path length and clustering coefficient of actual testing PTNs and their corresponding random graphs are respectively reported in Table 3.13, which demonstrates that all three PTNs show the small-world phenomenon.

Table 3.13 Small-world phenomenon of three testing PTNs

	Len_{actual}	Len_{random}	$Coeff_{actual}$	$Coeff_{random}$
New England 39-bus system	4.7490	3.8340	0.0385	0.0072
IEEE 118-bus system	6.3087	4.3562	0.1651	0.0113
Polish 2383-bus system	12.7590	14.3577	0.0093	6.994e-4

3.4.2 Percolation phenomena as critical phase transitions in power transmission network

The initial incentive of constructing power transmission networks is to transfer bulk power from power stations to demand sides over long distances. Basically, a simple transmission unite consists of a source node (i.e. generation node), a sink node (i.e. load node), several connecting nodes (i.e. sub-stations) and transmission lines. A bunch of such units are interconnected together and form a complete PTN. Inspired by the work presented in [140], a bond percolation model for small-world PTN is proposed in order to study the resilience of PTN against multiple transmission line outages. A schematic diagram is shown in Fig 3.27.

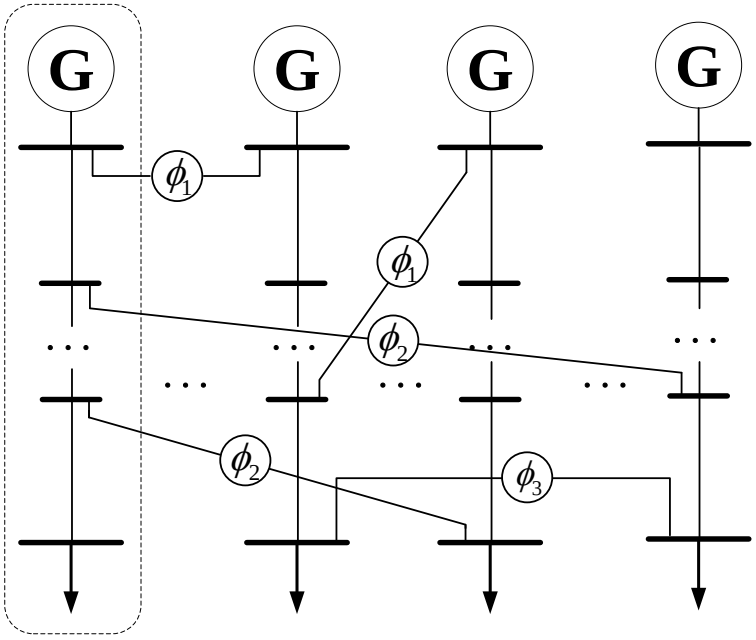

Fig 3.27 A PTN with small-world property

In this model, sites representing all nodes in a PTN are placed on a one-dimensional lattice of size $N_{lattice}$. Each site is connected to its nearest neighbors up to a fixed range d. Based on the small-world features of PTNs, additional links, also termed as "shortcuts", are placed between specific pairs of sites. Those links are stemmed from generation node, connecting node and load node with probabilities ϕ_1, ϕ_2, and ϕ_3 per link, respectively. That is, there exists an average of $(\phi_1 + \phi_2 + \phi_3)dN_{lattice}$ shortcuts in total. In this bond percolation model, a fraction p of bonds in the lattice are chosen to be "occupied", which represents that physical links (i.e. transmission lines) exist and are practically functional in the PTN. Based on the illustration above, a solution of bond percolation on small-world PTN is given as follows:

Similar to the method proposed in [140], the basic idea is to find out the largest local cluster that consists of occupied sites, bonds and shortcuts. The probability that a site belongs to a connected local cluster of size n is denoted as $P(n)$. Generating function method is adopted to evaluate $P(n)$. One defines that:

$$H(z) = \sum_{n=0}^{\infty} P(n) z^n \tag{3-41}$$

According to the discussion in [140], $H(z)$ satisfies the Dyson-equation-like iterative condition. Thus, Eq (3-41) can be rewritten in it self-consistent form as Eq (3-42).

$$H(z)=\sum_{n=0}^{\infty}P_0(n)z^n(\sum_{m=0}^{\infty}[P_1(m\mid n)+P_2(m\mid n)+P_3(m\mid n)]\cdot[H(z)^m]) \tag{3-42}$$

where $P_0(n)=np^{n-1}(1-p)^2$ for d=1. $P_1(m\mid n)$, $P_2(m\mid n)$ and $P_3(m\mid n)$ are probabilities of there being m shortcuts emerging from generation nodes, connecting nodes and load nodes respectively in a local cluster of size n. In this model, a local cluster represents a transmission unit. Thus, $P(m\mid n)$ is defined as follows:

$$P_1(m\mid n)=\binom{2\phi_1 pd\theta N_{lattice}}{m}\left[\frac{1}{N_{lattice}}\right]^m\left[1-\frac{1}{L}\right]^{2\phi_1 pd\theta N_{lattice}-m} \tag{3-43}$$

$$P_2(m\mid n)=\binom{2\phi_2 pd\gamma N_{lattice}}{m}\left[\frac{n-2}{N_{lattice}}\right]^m\left[1-\frac{n-2}{L}\right]^{2\phi_2 pd\gamma N_{lattice}-m} \tag{3-44}$$

$$P_3(m\mid n)=\binom{2\phi_3 pd\mu N_{lattice}}{m}\left[\frac{1}{N_{lattice}}\right]^m\left[1-\frac{1}{L}\right]^{2\phi_3 pd\mu N_{lattice}-m} \tag{3-45}$$

where θ, γ, and μ are fractions of generation nodes, connecting nodes and load nodes in a PTN, respectively.

Substitute Eqs (3-43)-(3-45) to Eq (3-42),

$$\begin{aligned}H(z)=\sum_{n=0}^{\infty}P_0(n)z^n\Bigg\{&\left[\frac{1}{N_{lattice}}(H(z)-1)+1\right]^{2\phi_1 pd\theta N_{lattice}}+\left[\frac{n-2}{N_{lattice}}(H(z)-1)+1\right]^{2\phi_2 pd\gamma N_{lattice}}\\&+\left[\frac{1}{N_{lattice}}(H(z)-1)+1\right]^{2\phi_3 pd\mu N_{lattice}}\Bigg\}\end{aligned} \tag{3-46}$$

For $N_{lattice}$ large,

$$H(z)=\sum_{n=0}^{\infty}P_0(n)z^n\left[e^{2d\phi_1\theta(H(z)-1)p}+e^{2d\phi_2\gamma(H(z)-1)(n-2)p}+e^{2d\phi_3\mu(H(z)-1)p}\right] \tag{3-47}$$

One defines:

$$H_0(z)=\sum_{n=0}^{\infty}P_0(n)z^n=\sum_{n=0}^{\infty}np^{n-1}(1-p)^2z^n=\frac{(1-p)^2}{p}\sum_{n=0}^{\infty}n(pz)^n=z\frac{(1-p)^2}{(1-pz)^2} \quad (3\text{-}48)$$

Substitute Eq (3-48) to Eq (3-46),

$$H(z)=e^{2d\phi_1\theta(H(z)-1)p}\cdot H_0(z)+e^{2d\phi_2\gamma(H(z)-1)(n-2)p}\cdot H_0(z)+e^{2d\phi_3\mu(H(z)-1)p}\cdot H_0(z) \quad (3\text{-}49)$$

Theoretically, the mean size of local cluster is given by the first derivative of $H(\bullet)$,

$$\begin{aligned}\langle n\rangle = H'(1) &= 2d\phi_1\theta p\cdot H'(1)\cdot H_0'(1)+H_0'(1)-4d\phi_2\gamma p\cdot H'(1)\cdot H_0(1)\\ &\quad +H_0'(1)[1+2d\phi_2\gamma pH'(1)]+2d\phi_3\mu p\cdot H'(1)\cdot H_0(1)+H_0'(1) \quad (3\text{-}50)\\ &=\frac{3(1+p)}{(1-p)\{1-2dpH_0(1)[\phi_1\theta-2\phi_2\gamma+\phi_3\mu]-2d\phi_2\gamma pH_0'(1)\}}\end{aligned}$$

It is straight forward that,

$$H_1(1)=1$$

Thus, giant component exists at the point that the mean size of local cluster diverges. i.e. the denominator of Eq (3-50) is equal to zero. The percolation threshold p_c indicates this critical point of phase transition, which is expressed as follows:

$$p_c=\frac{(2\phi_1\theta-2\phi_2\gamma+2\phi_3\mu+1)+\sqrt{(2\phi_1\theta-2\phi_2\gamma+2\phi_3\mu+1)^2-8(\phi_1\theta-3\phi_2\gamma+\phi_3\mu)}}{4(\phi_1\theta-3\phi_2\gamma+\phi_3\mu)} \quad (3\text{-}51)$$

In a PTN, contingency induced loss of system integrity is mostly caused by transmission line outages, which can be considered as an inverse bond percolation process in an interconnected PTN. In power systems, the integrity of underlying network has a significant impact on operation stability. If the percolation threshold p_c is small, the network is more resilient to keep the overall integrity under several trips of

transmission lines. On the contrary, if p_c is large or even close to 1, the network is vulnerable to any line outages. In this section, the resilience of a PTN under a number of transmission line outages is defined as:

$$Resilience(\mathcal{G}) = \frac{1 - p_c^*}{p_c} \tag{3-52}$$

where p_c^* is the initial percolation threshold of a PTN; p_c is the percolation threshold of the PTN in the post-contingency phase (i.e. under one or more transmission line outages).

Based on the macroscopic behaviors of the underlying network in power systems, the proposed metric is used to quantitatively measure the resilience of PTN to bear with contingencies that might deteriorate the integrity of the whole system. This metric is further utilized in Chapter 4 (Section 4.2) to evaluate the contingency risk in different system operating scenarios.

3.4.3 Case studies

In this sub-section, the proposed bond percolation model is tested on New England 39-bus, IEEE 118-bus and Polish 2383-bus systems, which have been verified as small-world PTNs in Section 3.4.2. With different probability *p* of occupied bonds, the mean size of local cluster is shown in Figs 3.28-3.30. According to Eq (3-51), the percolation thresholds of three testing systems are reported in Table 3.14

Table 3.14 Percolation thresholds of testing power systems

Testing Power Systems	Percolation Threshold p_c	Resilience
New England 39-bus System	0.7184	0.3920
IEEE 118-bus System	0.8149	0.2271
Polish 2383-bus Transmission System	0.7452	0.3419

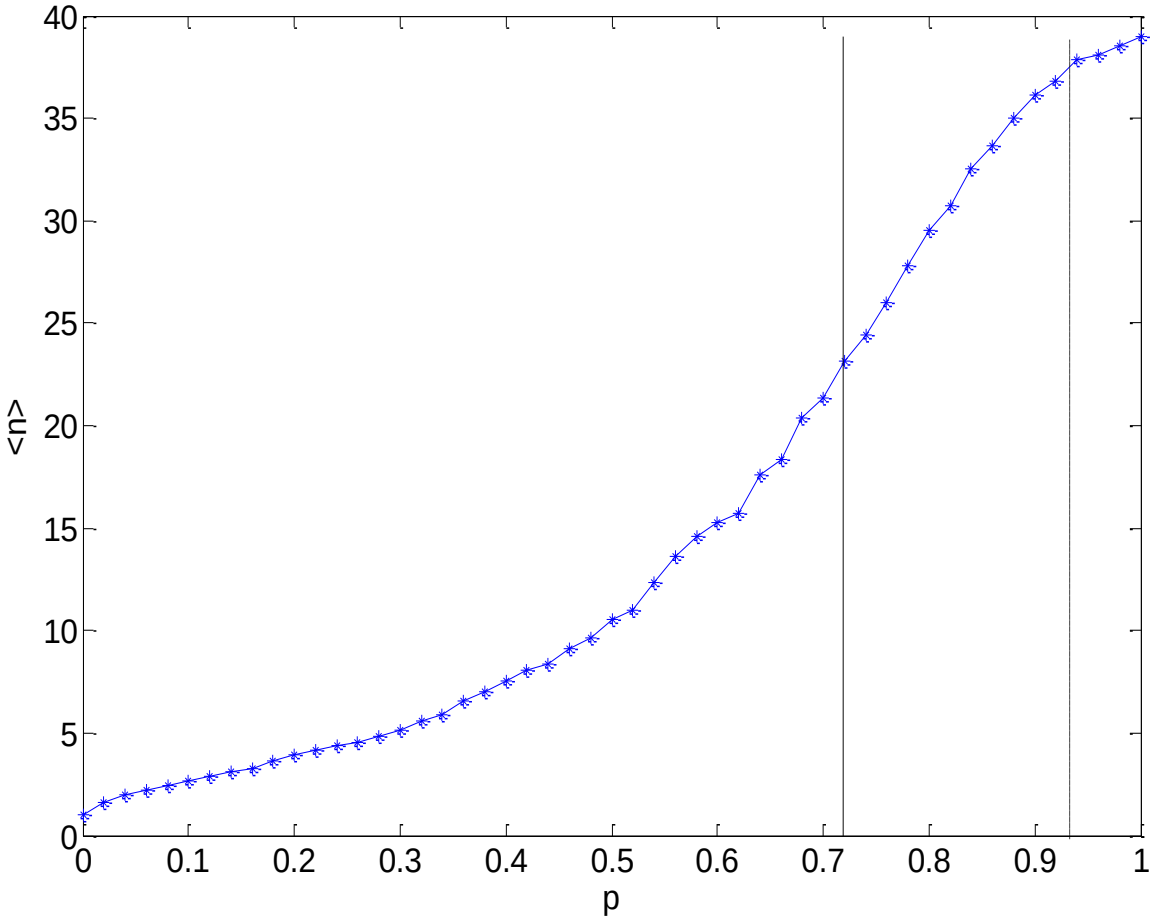

Fig 3.28 Mean size of local cluster under different occupied probabilities (New England 39-bus system). Solid line indicates p_c obtained by Eq (3-51); dash line indicates the actual critical point of phase transition.

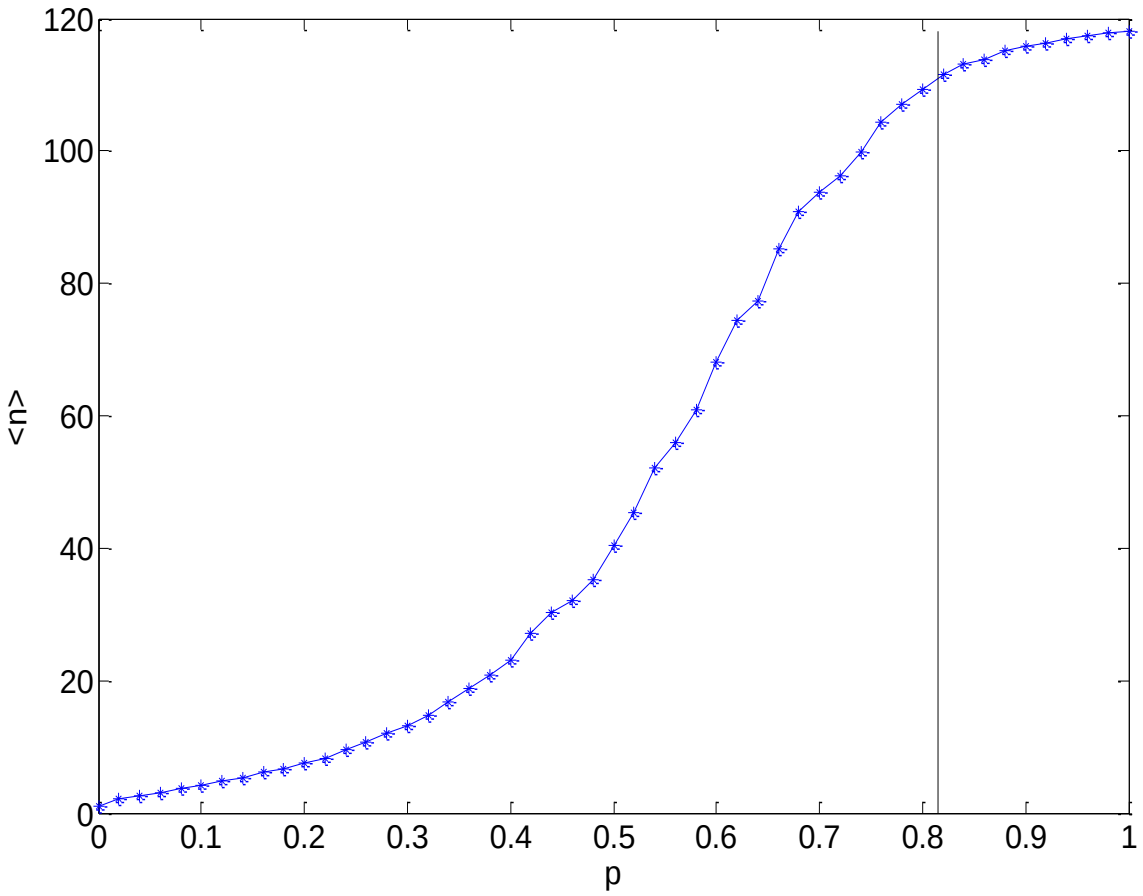

Fig 3.29 Mean size of local cluster under different occupied probabilities (IEEE 118-bus system). Solid line indicates p_c obtained by Eq (3-51).

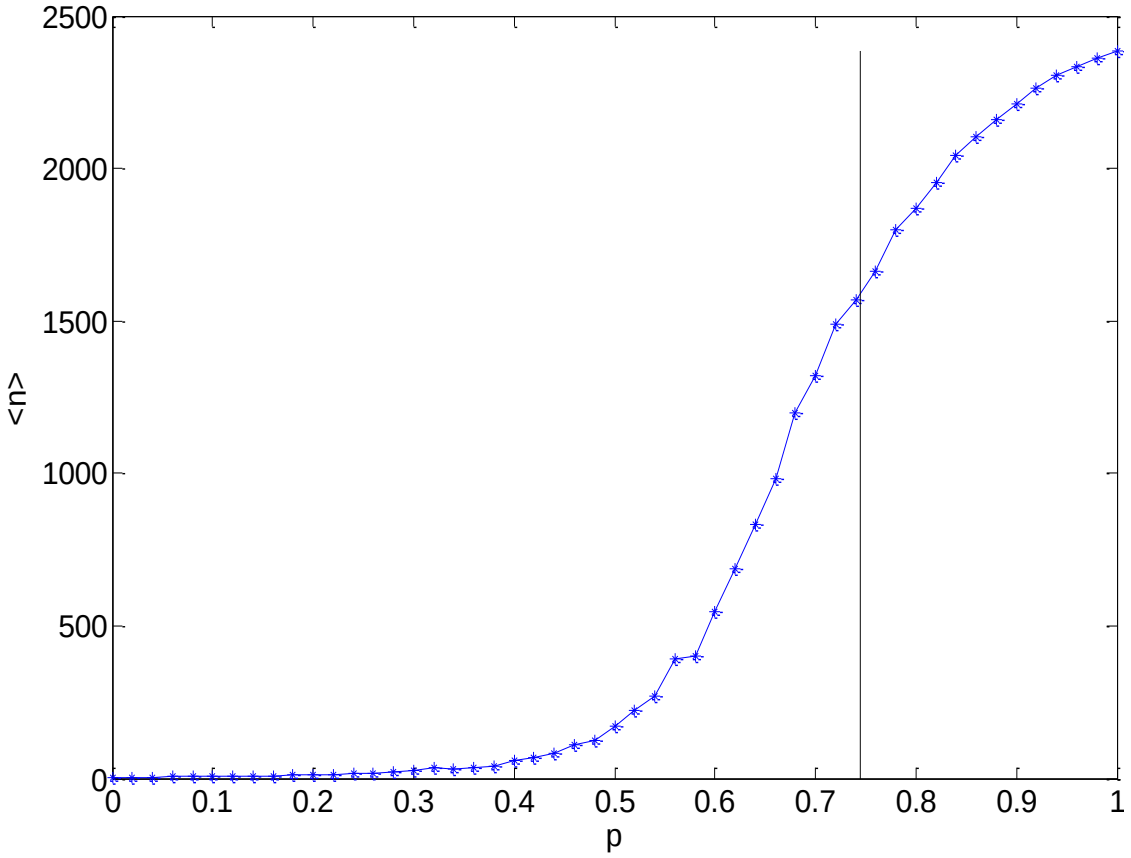

Fig 3.30 Mean size of local cluster under different occupied probabilities (Polish 2383-bus transmission system). Solid line indicates p_c obtained by Eq (3-51).

From Figs 3.28-3.30, it is obvious that p_c obtained by Eq (3-51) on case of IEEE 118-bus system best fit the critical phase transition. It is worth noting that the bond percolation solution expressed by Eq (3-51) indicates critical phase transition on the assumption that $N_{lattice}$ is large. For a small-scale PTN, this solution might be inaccurate, for example, the one shown in Fig 3.27. As reported in Table 3.13, the case of IEEE 118-bus system best matches small-world features. Therefore, it is reasonable that p_c

obtained by Eq (3-51) on case of IEEE 118-bus system has a better indication of critical phase transition than that of Polish 2383-bus system.

3.5 Conclusion

This Chapter mainly focuses on topological properties of power systems. In Section 3.1, a model based on complex network theory is proposed, which is effective for structural vulnerability analysis by embedding power sensitivity into adjacency matrix. In events of system component outages occur, an efficient approach is proposed in Section 3.2 to accurately identify and predict the topological separation by considering real power deliverability. Furthermore, a more advanced network partitioning approach based on Laplacian spectrum and SOM is reported in Section 3.3. Case studies have demonstrated the effectiveness of this approach and shown high potential of practical application in smart grid environment. Lastly, a bond percolation model on small-world PTN is newly proposed in Section 3.4. This model effectively reflects the percolation behaviors of PTNs. Meanwhile, an exact solution of critical phase transition is obtained, which is essentially useful for risk evaluation of cascading contingencies in Chapter 4.

Chapter 4 *N-k* Contingency Screening

4.1 Introduction

As introduced in Chapter 1, *N-k* contingency analysis is always challenging due to i) high computational cost; ii) high complexity of PTN topological structure and operation conditions. In this Chapter, a comprehensive framework of *N-k* contingency analysis is proposed, which mainly consists of three modules—CFSM (for cascading failure simulation in post-contingency phase), REM (for risk evaluation based on machine learning techniques), and CSM (for efficiently screening out high risk *N-k* contingencies). It is highlighted in the thesis that three major contributions have been made in this field through the proposed framework including— i) potential cascading risk is effectively considered when conducting *N-k* screening; ii) topological resilience is incorporated for a more comprehensive cascading risk evaluation; and iii) different levels of Pareto fronts containing high-risk *N-k* contingencies can be generated simultaneously.

4.2 Risk Evaluation of *N-k* Induced Cascading Contingencies

4.2.1 Proposed methodology

The proposed approach comprises a CFSM to simulate and collect sufficient amount of *N-k* induced cascading risk data, and an advanced DNNE based REM to fast

extract the hidden knowledge and evaluate an overall risk for a specific combination of multiple contingencies. Similar to most existing works, steady state analysis of the PNIP is focused in this work. That is, initial multiple contingencies are regarded as a combination of outages occurring within a short period of time. Even though the sequence of such multiple contingencies really matter in a fast time scale (as discussed in [141], dynamic analysis is needed), the scope of this Chapter is limited to a relatively long-term time period considering post-contingency phase based on steady state analysis. Further, various cascades of different paths are probable following an initial *N-k* contingency, of which the severity is evaluated by an average risk over a number of such possibilities.

The schematic diagram of Fig 4.1 shows the structure of the proposed approach. CFSM is constructed based on a powerful computing platform, where parallel processing is allowed to efficiently execute Monte Carlo simulations and collect corresponding risk data. REM is responsible for fast learning and prediction, and can be easily implemented using a normal PC. Details of these two modules will be discussed in Sections 4.2.2 and 4.2.3, respectively.

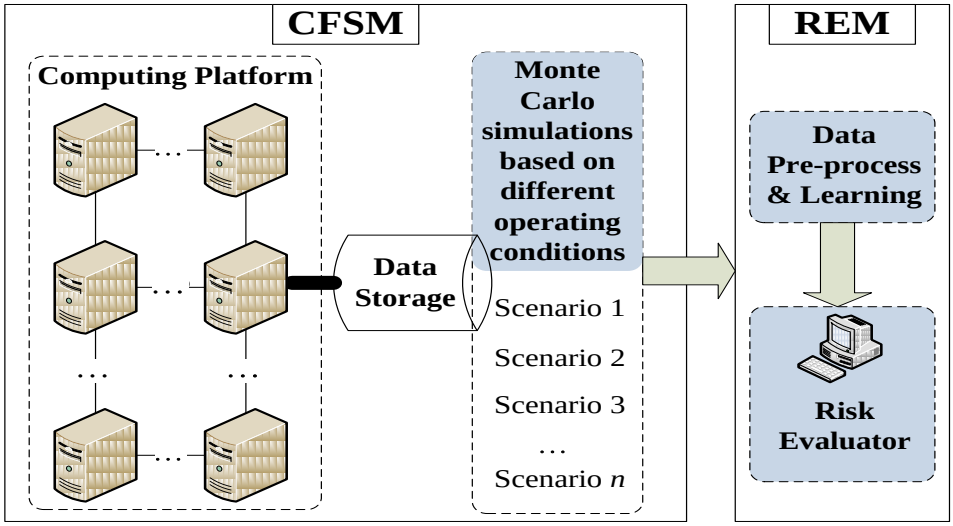

Fig 4.1 Structure of the proposed approach for *N-k* induced cascading contingency analysis

4.2.2 *N-k* Induced cascading failure simulation

An initial *N-k* contingency can trigger various cascades with different probabilities. Without loss of generality, CFSM aims to simulate the post-contingency phase using probabilistic model and generate an overall risk caused by a specific *N-k* contingency through Monte Carlo simulations. The cascading risk data collected by this module will input into REM later on.

A. Cascading failure simulation model

Triggered by an initial disturbance, the propagation of cascading failures can be attributed to quite a few mechanisms such as thermal overloads, voltage collapse, relay failure, etc. Thus far, modeling the cascading process in great detail remains challenging

and perhaps infeasible. The existing models differ substantially due to their own particular emphases on a subset of those mechanisms. A comprehensive review of cascading failure models can be referred to Chapter 2 (Section 2.2.2).

In assessing the risk of cascading failures, considerable research efforts have been devoted and a number of commercial tools are used in the current electrical industries [31]. For example, CAT (Cascade Analysis Tool) based on AC power flow is adopted in the US; and ASSESS based on DC or AC steady state plus dynamic simulations is adopted in the UK. Several research-grade models also exist, such as hidden failure model considering the incorrect or inappropriate actions of relay systems under thermal overloads [32, 33], Manchester model considering interactions of outage components and post-contingency re-dispatch [45, 46], OPA model based on DC load flow and random line outages [142], etc. Among others, hidden failures due to malfunction of relay are regarded as an important reason for cascading development. Therefore, hidden failures of protection system caused by thermal overload are assumed to be the main inducement of fault propagation in this thesis. This assumption is reasonable to a certain extent based on the historical data analysis of major blackouts in the U.S, which has been reported by NERC that more than 70% relay system failures contribute to cascading events in power systems [143].

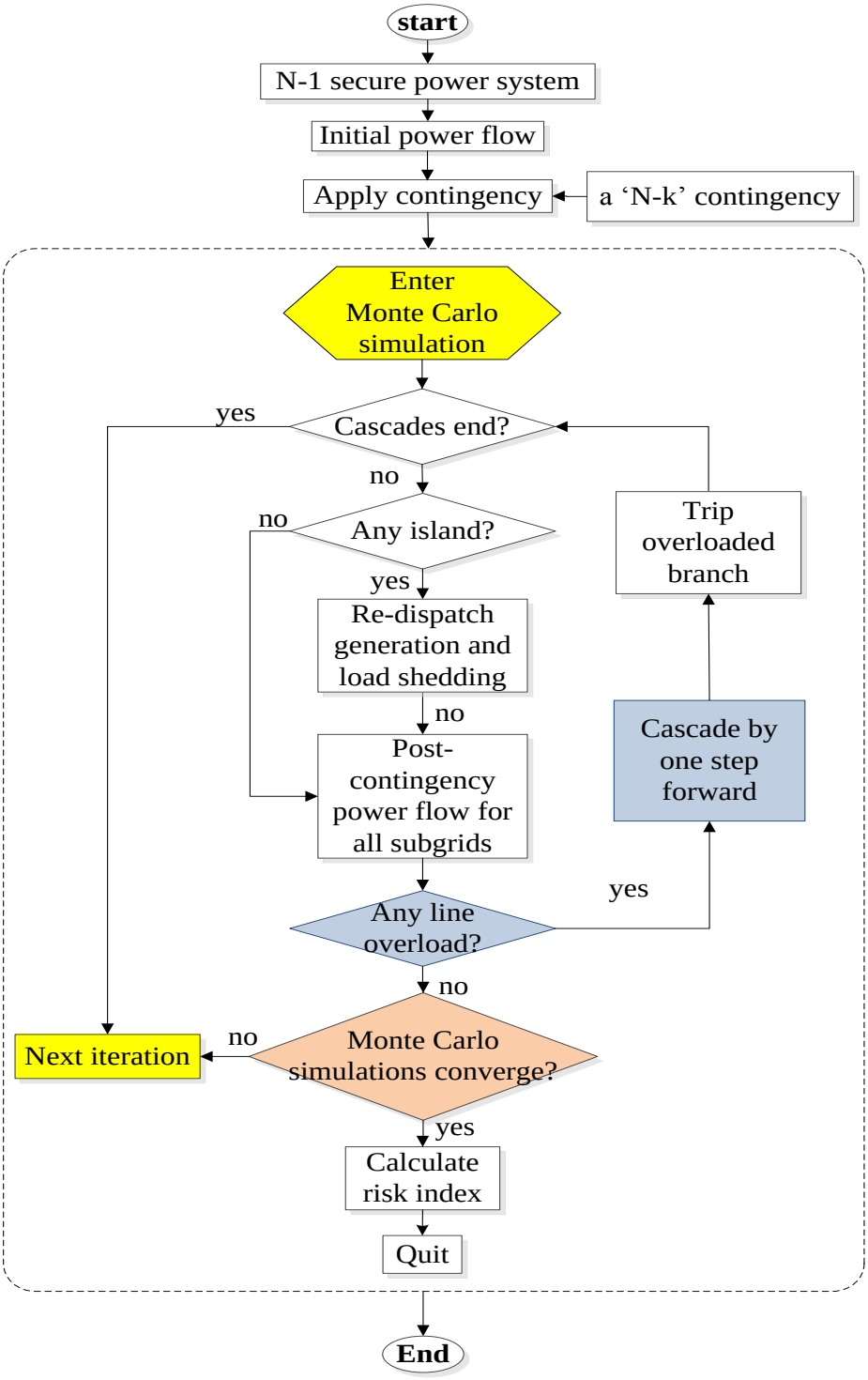

Fig 4.2 Flowchart of N-k induced cascading failure simulation

The main procedures of cascading failure simulation are shown in the flowchart of Fig. 4.2. Specifically, each step is illustrated as follows:

1) **Initialization**. In this study, the power system is initialized to be *N-1* secure. Pre-contingency AC load flow is calculated based on Newton-Raphson method under a specific operating scenario. A set comprising various *N-k* contingencies is also initialized in this step, which can be determined by random selection or an expert system.

2) **Apply an *N-k* contingency**. One of the *N-k* contingencies in the set is applied to the testing system. *k* indicates the number of electric components that fail to function properly in the transmission network. In this work, such contingency is particularly referred to branch outages.

3) **System security estimation**. Once initial *N-k* contingency occurs, the power system may operate in an insecure status due to transmission line overload, voltage collapse, existence of uncontrolled system islands where real power is significantly imbalanced, etc. In particular, according to hidden failure model [32], a branch *i* will unexpectedly trip with a probability *p* if the load flow f_i exceeds the capacity c_i. If the load flow is greater than the thermal limit $(c_i)_{max}$ of a branch, corresponding relays will react at a short time and trip this branch promptly. The probability p_i is formulated as Eq. (4-1).

$$p_i = \begin{cases} 1, & f_i \geq (c_i)_{\max} \\ \dfrac{f_i - c_i}{(c_i)_{\max} - c_i}, & c_i < f_i < (c_i)_{\max} \end{cases} \quad (4\text{-}1)$$

In practice, the bus voltage is required to be maintained in a certain range, e.g. 0.95~1.05 p.u. Voltage violation may considerably drive the whole system into a critical stage. Furthermore, uncontrolled system separations are not allowed. If an initial contingency gives rise to system separations and real power imbalance, generation re-dispatch or specific load shedding strategies should be taken accordingly. Without the aforementioned conditions, in this study the testing system is considered secure under the specific operating condition and *N-k* contingency.

4) **Start Monte Carlo simulations**. Cascades can be notably different through different tripping lines with different probabilities. Monte Carlo simulations are utilized hereby to consider a series of potential cascading chains.

5) **Cascades ending criterions**. To end an iteration of Monte Carlo simulations, two termination criterions can be used for different cases. **Criterion 1**: the following conditions should be simultaneously satisfied: i) no more transmission line overload; ii) no bus voltage violation; and iii) no real power imbalance in each separated islands. Besides them, if a pre-defined fraction of power system is out of service (e.g. 40% in our study), a severe system failure has occurred and the current iteration terminates.

Criterion 2: a certain number of transmission line outages occur. This criterion could be used for large-scale PTNs, which can make the simulation more efficient.

6) **Islanding detection** (uncontrolled system separation). In this step, the integrity of the whole transmission network is checked. If there exist two or more isolated islands, simulation moves to step 7. Otherwise, go to step 9.

7) **Re-dispatch generation and load shedding**. In a sub-grid G_j, the real power imbalance is expressed as:

$$P_{imb} = P_g - P_d - P_{loss} \tag{4-2}$$

where P_g and P_d are total generation and load in the sub-grid, respectively. P_{loss} is the power loss on the transmission lines. If $P_{imb}>0$, each generator is ramping down until $P_{imb}=0$. If the automatic control of all generators have reacted at full capacity while $P_{imb}>0$, a generator with the smallest generation is tripped. This process will not stop until $P_{imb}\leq 0$. A specific load shedding strategy needs to be taken subsequently to achieve a balance between generation and load demand. For simplicity, homogeneous load shedding is adopted.

8) **Calculate load flow for all sub-grids**. In each sub-grid, the bus contributing the greatest generation is selected as the reference (slack bus) to perform load flow calculation.

9) **Check thermal overload of each branch**. Roulette-wheel algorithm [144] is utilized to select a branch to be tripped according to the hidden failure probability (formulated in Eq. 4-1) in each cascading stage.

10) **Repeat step 5 to 9 until Monte Carlo simulation converges**. In the *m-th* iteration, the total load shedding and voltage violation are denoted by ΔD_m and ΔV_m, respectively. Both of them are per-unit values and expressed as follows:

$$\Delta D_m = \frac{\Delta D_m^{loss}}{D_{base}} \tag{4-3}$$

$$\Delta V_m = \frac{\Delta V_m^{violate}}{V_{base}} \tag{4-4}$$

where D_{base} and V_{base} are predefined by a severe post-contingency state (e.g. a state in which 40% of load demand fails to be supplied and 30% of buses suffering voltage collapse). Monte Carlo simulation terminates when the mean value of total load shedding and voltage violation converge.

11) **Calculate risk index**. Risk is defined as the product of probability and cascading consequence, where the probability is determined by hidden failure model and consequence is measured by average load shedding and voltage violation. An overall risk metric is proposed in this Chapter to comprehensively consider the impacts of load

shedding and voltage violation, as well as the topological resilience, which is formulated in Eq. (4-5).

$$R_{\{N-k\}} = \frac{p_c}{1-p_c^*}(\omega_D \hat{R}_D + \omega_V \hat{R}_V) \tag{4-5}$$

where

$$\hat{R}_D = \frac{1}{M}\sum_{m=1}^{M} \Delta D_m \cdot p_m \tag{4-6}$$

$$\hat{R}_V = \frac{1}{M}\sum_{m=1}^{M} \Delta V_m \cdot p_m \tag{4-7}$$

$\hat{R}_D$ and $\hat{R}_V$ denote the average risk in terms of load shedding and voltage violation, respectively; M is the number of iterations; ω_D and ω_V are entropy weights; p_c^* and p_c reflect the original and post-contingency topological resilience (i.e. percolation transition threshold), respectively.

Information entropy is employed in data analysis of cascading severity[49], and the entropy weights are formulated as follows:

$$H_D = -\frac{1}{\ln M}\sum_{m=1}^{M} \frac{\Delta D_m \cdot p_m}{\sum_{m=1}^{M} \Delta D_m \cdot p_m} \ln \frac{\Delta D_m \cdot p_m}{\sum_{m=1}^{M} \Delta D_m \cdot p_m} \tag{4-8}$$

$$H_V = -\frac{1}{\ln M}\sum_{m=1}^{M} \frac{\Delta V_m \cdot p_m}{\sum_{m=1}^{M} \Delta V_m \cdot p_m} \ln \frac{\Delta V_m \cdot p_m}{\sum_{m=1}^{M} \Delta V_m \cdot p_m} \tag{4-9}$$

$$\omega_D = \frac{H_D}{H_D + H_V} \tag{4-10}$$

$$\omega_V = \frac{H_V}{H_D + H_V} \tag{4-11}$$

Entropy weights are employed here to deal with information / data uncertainties by quantitatively measuring the disorder of existing data. High entropy exposed from the data reveals high resilience to information loss, which awards greater weights.

B. Data collection for REM

As shown in Fig 4.1, a number of representative *N-k* contingencies under different scenarios are identified based on random selection or expert system to collectively reflect possible extreme events. A dataset is constructed in this module comprising a contingency-feature vector and its corresponding risk vector. A specific *N-k* contingency *i* is characterized by vector $\mathcal{F}_i=[f_1/c_1, f_2/c_2,..., f_N/c_N]$, where *f* denotes the post-contingency load flow on each branch. Regarding to all simulated contingencies with $\mathcal{F}=[F_1, F_2,..., F_{|F|}]$, the corresponding risk data are stored in $\mathcal{T}=[R_1, R_2,..., R_{|F|}]$

4.2.3 Big data analysis of *N-k* contingencies

In order to effectively learn from massive data collected in CFSM, an advanced DNNE is newly developed in this module to perform risk evaluation. Subsequently, an overall cascading risk of an *N-k* contingency can be predicted efficiently by the trained DNNE.

A. Advanced decorrelated neural network ensembles with random weights

In considering the complex nature of PNIP, ensemble learning using DNNE is utilized to model the underlying data distribution with sufficiently large space of hypotheses. Such learning method is advantageous over single neural network based regression especially for e.g. the PNIP problem of high complexities and nonlinearities. Inspired by [145], an advanced DNNE is developed in this Chapter, which has the following advantages.

Firstly, negative correlation learning scheme is employed to effectively maintain the ensemble diversity, which achieves better learning performance as compared to simply averaging all independent base model outputs.

Secondly, the training objective is to obtain a well-balanced trade-off between bias and variance for every single base learner. This is achieved by bias-variance-covariance decomposition.

Thirdly, Random vector functional-link (RVFL) networks [146] are selected as ensemble component models. In most cases, gradient-based learning algorithms for training single-layer feed-forward networks (SLFN) have several disadvantages i.e. local minima, slow convergence and poor sensitivity to learning rate setting [145]. RVFL networks successfully overcome those drawbacks with randomly assigned weights between the input and hidden layers, which also feature extremely fast learning

speed. It should be pointed out that a single RVFL learner (also known as extreme learning machine [147]) fails to perform stably due to the random initialization in the learning process. It has been proved that the error of RVFL approximator converges to zero with order $O(1/\sqrt{n})$ only for a large n [148], where n denotes the number of neurons in hidden layer. Nevertheless, this shortcoming can be abstained to a great extent by combining a cluster of RVFL networks.

Lastly, a coordinated strategy is proposed to assign weight to each component network (i.e. RVFL network). Promising approximating results reported in Section 4.2.4 demonstrate the effectiveness of this ensemble strategy in universally approximating complex non-linear problems.

The proposed DNNE is illustrated as follows, which is also shown in Fig 4.3:

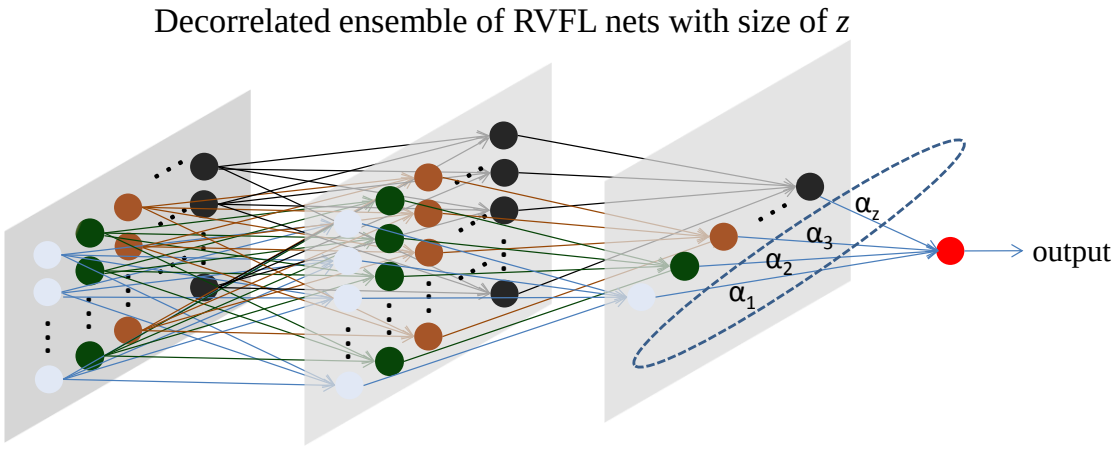

Fig 4.3 Decorrelated ensembles of RVFL nets

Given a training dataset $\mathcal{D}(\boldsymbol{x}, \boldsymbol{y})$ contains *s* instances. The ensemble output and decorrelated error of *i*-th individual learner $b_i(\cdot)$ are formulated below.

$$\bar{b}(x_n) = \sum_{i=1}^{z} \alpha_i \cdot b_i(x_n) \tag{4-12}$$

$$e_i = \sum_{v=1}^{s} [\frac{1}{2}(b_i(x_v) - y_v)^2 - \lambda(b_i(x_v) - b(x_v)^2)] \tag{4-13}$$

where α_i is the weight of *i*-th base network; b_i is the output of *i*-th base network; *z* is the ensemble size; $b(\cdot)$ is the ensemble collective function; and $\lambda \in [0,1]$ is a regularizing factor.

For each individual learner, the output of *i*-th base network is expressed as:

$$b_i(x_v) = \sum_{j=1}^{n} \beta_{ij} g_{ij}(x_v) \tag{4-14}$$

where $g(\cdot)$ is any squashing basis function, and β_{ij} is the output weight of the *j*-th hidden neuron in the *i*-th base learner; is the number of hidden neurons in a base learner.

All base learners are assumed to have homogeneous hidden layers and combine together with ensemble size of *z*. When the gradient of error expressed in Eq. (4-13) vanishes, DNNE will achieve an optimal performance. That is,

$$\nabla e_i = 0 \text{, for } i=1,2,..., z$$

which leads to:

$$\frac{\partial e_i}{\partial \beta_{ij}} = \sum_{v=1}^{s} \frac{\partial e_i(x_v)}{\partial \beta_{ij}} = 0 \tag{4-15}$$

$$\begin{aligned}\frac{\partial e_i(x_v)}{\partial \beta_{ij}} &= g_{ij}(x_v)[b_i(x_v)-y_v]+\lambda[g_{ij}(x_v)-\alpha_i g_{ij}(x_v)]\sum_{j\neq i}[b_j(x_v)-\bar{b}(x_v)] \\ &\quad -\lambda(z-1)\alpha_i[b_i(x_v)-\bar{b}(x_v)]g_{ij}(x_v) \\ &= g_{ij}(x_v)\{[1-\lambda(z-1)\alpha_i]b_i(x_v)-\lambda(z-1)(1-2\alpha_i)\bar{b}(x_v) \\ &\quad +\lambda(1-\alpha_i)\sum_{j\neq i}b_i(x_v)\}-g_{ij}(x_v)y_v\end{aligned} \tag{4-16}$$

Substitute Eqs (4-12) and (4-14) into Eq (4-16),

$$\frac{\partial e_i(x_v)}{\partial \beta_{ij}} = g_{ij}(x_v)[\gamma_i\sum_{k=1}^{n}\beta_{ik}g_{ik}(x_v)+\tau_i\sum_{l=1}^{z}\sum_{k=1}^{n}\alpha_l\beta_{lk}g_{lk}(x_v)+\vartheta_i\sum_{l=1}^{z}\sum_{k=1}^{n}\beta_{lk}g_{lk}(x_v)]-g_{ij}(x_v)y_v \tag{4-17}$$

where

$$\gamma_i = 1-\lambda(z\alpha_i-2\alpha_i+1)$$

$$\tau_i = -\lambda(z-1)(1-2\alpha_i)$$

$$\vartheta_i = \lambda(1-\alpha_i)$$

According to Eq (4-15), one can obtain:

$$\frac{\partial e_i}{\partial \beta_{ij}} = \sum_{v=1}^{s}\frac{\partial e_i(x_v)}{\partial \beta_{ij}} = 0 \tag{4-18}$$

Thus:

$$\begin{aligned}\frac{\partial e_i}{\partial \beta_{ij}} &= \sum_{k=1}^{n}\beta_{ik}\sum_{v=1}^{s}\gamma_i g_{ik}(x_v)g_{ij}(x_v)+\sum_{l=1}^{z}\sum_{k=1}^{n}\beta_{lk}\sum_{v=1}^{s}\tau_i\alpha_l g_{lk}(x_v)g_{ij}(x_v) \\ &\quad +\sum_{l=1}^{z}\sum_{k=1}^{n}\beta_{lk}\sum_{v=1}^{s}\vartheta_i g_{lk}(x_v)g_{ij}(x_v)-\sum_{v=1}^{s}g_{ij}(x_v)y_v = 0\end{aligned} \tag{4-19}$$

For (i, j, l, k), i=1, 2,..., z; j=1, 2,..., n; l=1, 2,..., z; k=1, 2,..., n, define:

$$\varphi_1 = \varphi_1(i, j, i, k) = \gamma_i \sum_{v=1}^{s} g_{ik}(x_v) g_{ij}(x_v) \tag{4-20}$$

$$\varphi_2 = \varphi_2(i, j, l, k) = \tau_i \sum_{v=1}^{s} \alpha_l g_{lk}(x_v) g_{ij}(x_v) \tag{4-21}$$

$$\varphi_3 = \varphi_3(i, j, l, k) = \vartheta_i \sum_{v=1}^{s} g_{lk}(x_v) g_{ij}(x_v) \tag{4-22}$$

$$\varepsilon(i, j) = \sum_{v=1}^{s} g_{ij}(x_v) y_v \tag{4-23}$$

Using Eqs (4-20)~(4-23), Eq (4-19) is rewritten as:

$$\sum_{k=1}^{n} \beta_{ik} \varphi_1(i, j, i, k) + \sum_{l=1}^{z} \sum_{k=1}^{n} \beta_{lk} \varphi_2(i, j, l, k) + \sum_{l=1}^{z} \sum_{k=1}^{n} \beta_{lk} \varphi_3(i, j, l, k) = \varepsilon(i, j) \tag{4-24}$$

Thus:

$$\begin{aligned} &\sum_{i=1}^{z} \sum_{j=1}^{n} \sum_{k=1}^{n} \beta_{ik} \varphi_1(i, j, i, k) + \sum_{i=1}^{z} \sum_{j=1}^{n} \sum_{l=1}^{z} \sum_{k=1}^{n} \beta_{lk} \varphi_2(i, j, l, k) + \sum_{i=1}^{z} \sum_{j=1}^{n} \sum_{l=1}^{z} \sum_{k=1}^{n} \beta_{lk} \varphi_3(i, j, l, k) \\ &= \sum_{i=1}^{z} \sum_{j=1}^{n} \varepsilon(i, j) \end{aligned} \tag{4-25}$$

This linear system can be rewritten in a matrix form as follows:

$$H_{corr} B_{ens} = T_h \tag{4-26}$$

where

$$H_{corr}(x_H, y_H) = \begin{cases} \varphi_1(i, j, i, k) + \varphi_2(i, j, l, k) + \varphi_3(i, j, l, k), & \text{if } i = l \\ \varphi_2(i, j, l, k) + \varphi_3(i, j, l, k), & \text{otherwise} \end{cases} \tag{4-27}$$

$x_H, y_H = 1, \ldots, z \times n$, $i = \left\lceil \frac{x_H}{n} \right\rceil$, $j = ((x_H - 1) \bmod n) + 1$, $l = \left\lceil \frac{y_H}{n} \right\rceil$,

$k = ((y_H - 1) \bmod n) + 1$ .Modulo operation is denoted by mod.

$$B_{ens} = [\beta_{11}, \beta_{12}, ...\beta_{1n}, \beta_{21}, \beta_{22}, ...\beta_{2n}, ..., \beta_{z1,}\beta_{z2}, ..., \beta_{zn}]^T_{zn\times 1}$$

$$T_h = [\varepsilon(1,1), \varepsilon(1,2), ..., \varepsilon(1,n), \varepsilon(2,1), \varepsilon(2,2), ..., \varepsilon(2,n), ..., \varepsilon(z,1), \varepsilon(z,2), ..., \varepsilon(z,n)]^T_{zn\times 1}$$

Therefore,

$$B_{ens} = H^{\dagger}_{corr} T_h \tag{4-28}$$

To be consistent with [145], the same terminology is utilized in this thesis. $\boldsymbol{H_{corr}}$ is termed as the hidden correlation matrix; $\boldsymbol{B_{ens}}$ is termed as the global output weights matrix; and $\boldsymbol{T_h}$ is termed as the hidden-target matrix. Without iteratively tuning output weights, $\boldsymbol{B_{ens}}$ can be simply and timely calculated by Eq (4-28). $H^{\dagger}_{corr}$ is the Moor-Penrose generalized pseudo-inverse [149] of correlation $\boldsymbol{H_{corr}}$.

In order to achieve a reliable and accurate ensemble output, the weight of each base leaner is determined by the learning performance of each individual RVFL network.

Given a training dataset $\mathcal{D}$ ($\boldsymbol{x}$; $\boldsymbol{y}$), regression results obtained by *i*-th RVFL network is ($\boldsymbol{x}$; $\boldsymbol{y}^*$). Two sets (i.e. $\boldsymbol{S_{good}}$ and $\boldsymbol{S_{weak}}$) are respectively defined in the following to quantitatively reflect the overall performance of a RVFL network.

$$S_{good} : \{(x_v, y_v) \mid \left| \frac{y_v^* - y_v}{y_v} \right| \le \delta\}$$

$$S_{weak} : \{(x_v, y_v) \mid \left| \frac{y_v^* - y_v}{y_v} \right| > \delta\}$$

Based on $\boldsymbol{S_{good}}$ and $\boldsymbol{S_{weak}}$, one defines:

$$p_i^{good} = \frac{|S_{good}|}{|\mathcal{D}|} \tag{4-29}$$

$$p_i^{weak} = \frac{|S_{weak}|}{|\mathcal{D}|} \tag{4-30}$$

Globally, roof mean square error (RMSE) is selected as a metric to assess the performance of an individual learner other than mean absolute error (MAE), which is defined as follows:

$$\sigma_i = \sqrt{\frac{1}{|\mathcal{D}|}\sum_{v=1}^{|\mathcal{D}|}(y_v - y_v^*)^2} \tag{4-31}$$

Thus, the weights of individual base learners can be expressed as:

$$\alpha_i = \frac{\sqrt{\frac{1}{|\mathcal{D}|}\sum_{v=1}^{|\mathcal{D}|} y_v{}^2} - H_i^{RVFL}\sigma_i}{2\sqrt{\frac{1}{|\mathcal{D}|}\sum_{v=1}^{|\mathcal{D}|} y_v{}^2} - \sum_{i=1}^{z} H_i^{RVFL}\sigma_i} \tag{4-32}$$

where

$$H_i^{RVFL} = -\frac{1}{\ln 2}(p_i^{good}\ln p_i^{good} + p_i^{weak}\ln p_i^{weak})$$

B. Data learning and prediction for risk evaluation

In the study of cascading risk evaluation, simulation data $\mathcal{D}_{\text{risk}}$:$[\mathcal{F},\mathcal{T}]$ obtained in CFSM is used to train a DNNE. The feature vector $\mathcal{F}_i$ characterizes a specific contingency under a given operating scenario, which serves as the input of DNNE. $\mathcal{T}$

represents all risk values obtained by cascading failure simulations for all investigated contingencies under different operating conditions, which serves as a target vector for DNNE.

Before the training process, three parameters, i.e. number of hidden neurons in each RVFL network *n*, ensemble size *z*, and regularizing factor λ, need to be set in an optimal way to ensure the performance of DNNE. In this study, exhaustive search method is used to select the best *n*, *z* and λ.

Prediction errors, i.e. mean absolute percentage error (MAPE) and root mean square error (RMSE), are adopted to evaluate the performance of RVFL based DNNE, which are defined as:

$$MAPE = \frac{1}{s'}\sum_{v=1}^{s'}\left|\frac{R_v - \tilde{y}_v}{R_v}\right| \tag{4-33}$$

$$RMSE = \sqrt{\frac{1}{s'}\sum_{v=1}^{s'}(R_v - \tilde{y}_v)^2} \tag{4-34}$$

where s' is the number of instances in validation dataset; $\boldsymbol{R_v}$ is the real risk value generated by CFSM; and $\tilde{y}_v$ is the prediction value obtained by DNNE, expressed as: $\tilde{y}_v = h(\mathcal{F}_v)$.

For the application of *N-k* contingency screening, as reported in [150], the effectiveness of risk evaluation can also be demonstrated by a series of worst-case selections. For example, given an experiment with several *N-k* instances, DNNE based

risk evaluation is effective, if and only if the worst instance selected from DNNE evaluation is consistent with the one obtained by Monte Carlo simulations. Correctness index (CI) is defined below. Larger CI indicates better performance of DNNE.

$$CI = \frac{1}{n_s}\sum_{i=1}^{n_s} Co_i \tag{4-35}$$

where Co_i=1 if the worst case is correctly selected based on DNNE, otherwise, Co_i=0. n_s is the total number of experiments.

4.2.4 Case studies

In this section, the proposed approach for *N-k* cascading contingency analysis is applied to two IEEE test systems with different network sizes, i.e. 39 and 118 buses. Case data in MATPOWER [151] (i.e. case39 and case118) are used to calculate power flow solution.

A. Risk evaluation of cascading contingency on New England 39-bus system

1) Simulation setup

This test system consists of 39 buses, 10 generators and 46 branches. Case data in MATPOWER case39 is used to represent a normal operating condition. The thermal capacity is assumed to be 1.35 times power flow on each branch in normal condition, and thermal limit is 1.4 times thermal capacity. In normal operating condition, the total generation is 6297.87MW and 1274.94MVar, and the total load is 6254.23 MW and

1387.1 MVar. Ten operating scenarios are generated through randomly increasing or decreasing the load on each bus by 5 percent of normal condition. For a test without the loss of generality, seven scenarios are randomly sampled to construct the training dataset $\mathcal{D}_{train}$, and the rest ones are collected to be validation dataset $\mathcal{D}_{validate}$.

In CFSM, *N-k* contingency set is firstly constructed, where $k \in [2,10]$. For each *k*, 400 instances of line outages are randomly sampled. **Criterion 1** is utilized to terminate cascading failure simulation. Simulations are executed on a workstation of 2 processors (with 24 cores, 2.90GHz frequency) and 64.0 GB of RAM. Monte Carlo simulations converge if the variances of the averaging risk values in terms of load shedding and voltage violation are less than 0.0015 p.u. In REM, exhaustive linear search applies to $n \in [50,90]$, $z \in [4,15]$, and $\lambda \in [0,1]$ to find out an optimal DNNE.

2) Simulation results

As an example, a Monte Carlo simulation process is shown in Fig 4.4, where the system is operated under normal condition and branches (4-14), (16-21), and (17-18) are initially tripped. It can be seen that the simulation converges near 950 iteration steps.

In REM, risk evaluation of cascading contingency is carried out through a well-trained DNNE. Simulation results are listed in Table 4.1. In order to demonstrate the effectiveness of REM, some prediction results from DNNE are randomly sampled and

shown in Fig 4.5. Worst-case selection experiments (1000 times) are also conducted. For each experiment, two *N-k* instances are randomly chosen from validation dataset.

According to the simulation results in Table 4.1, it can be seen that cascading failure simulations are time consuming while DNNE based evaluation is efficient. Prediction accuracy is satisfactory based on MAPE and RMSE. It is worth noting that CI obtained in this case is quite high up to 97.8%. In Fig 4.5, some predictions deviate from the real risk values significantly, this may be because 1) the training dataset is randomly sampled, which may not sufficiently represent all operating patterns; and 2) CFSM itself does not model the cascading process in a comprehensive way (which is also unpractical to do so).

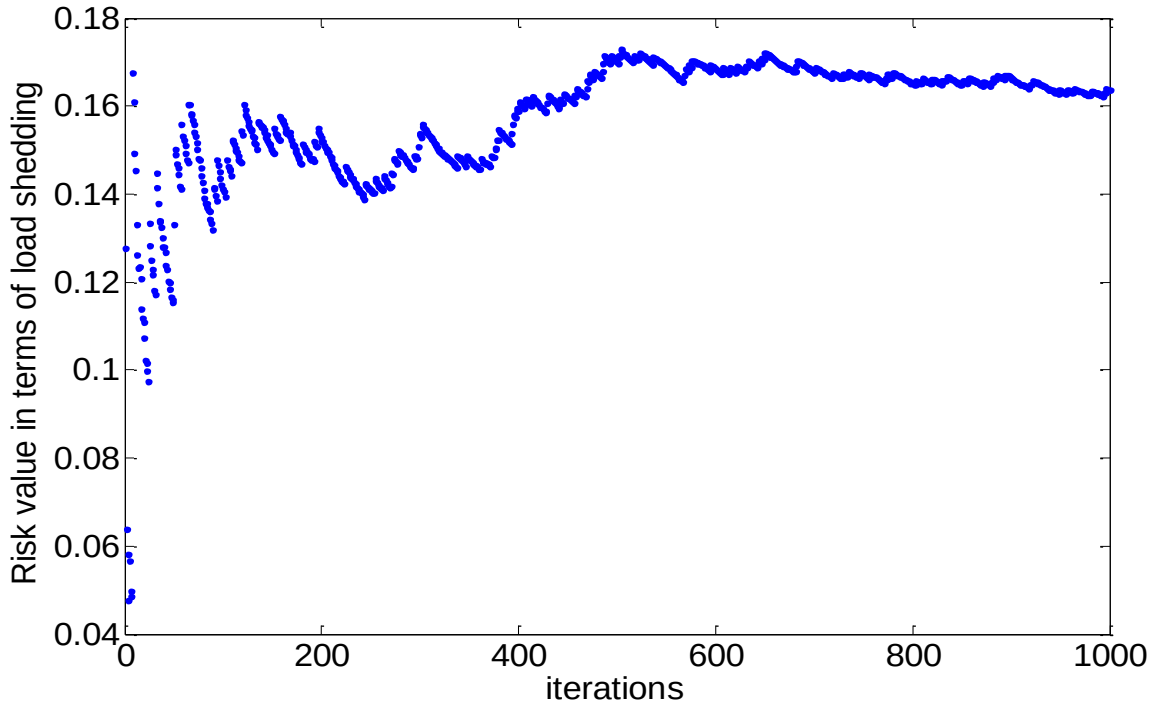

(a)

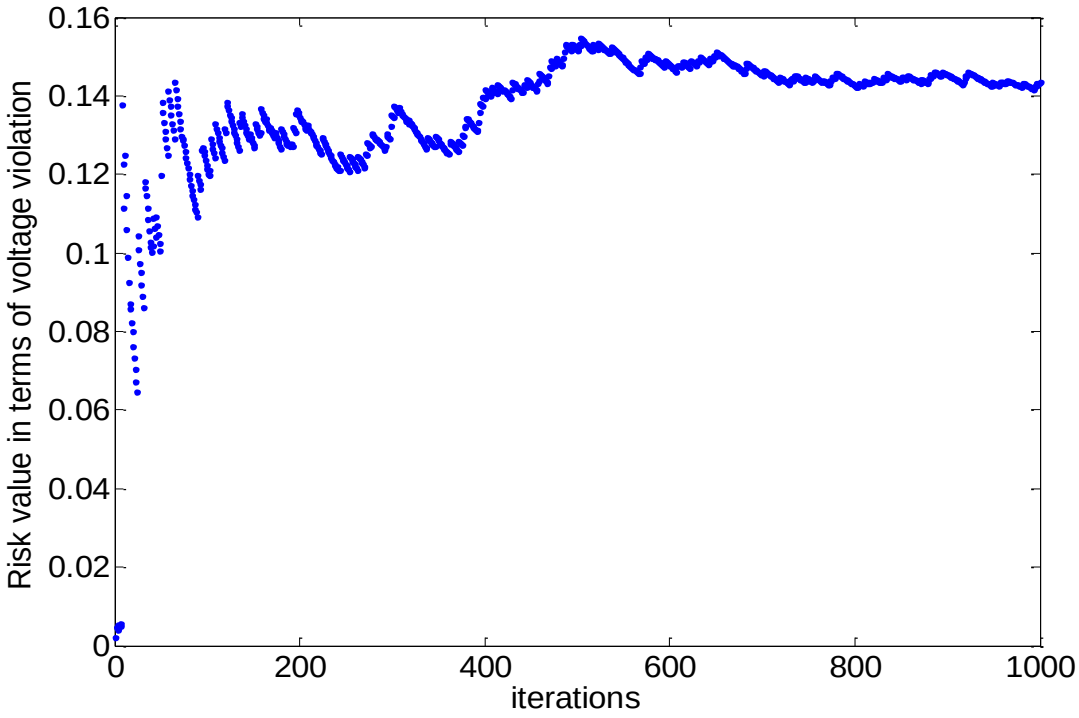

(b)

Fig 4.4 An example of Monte Carlo simulation results under normal operating condition (New England 39-bus system)

Table 4.1 Simulation results (New England 39-bus system)

	Overall elapsed time			
CFSM	31412s			
	MAPE	RMSE	CI	Elapsed time in training
REM	8.432%	2.934%	97.8%	1.034s

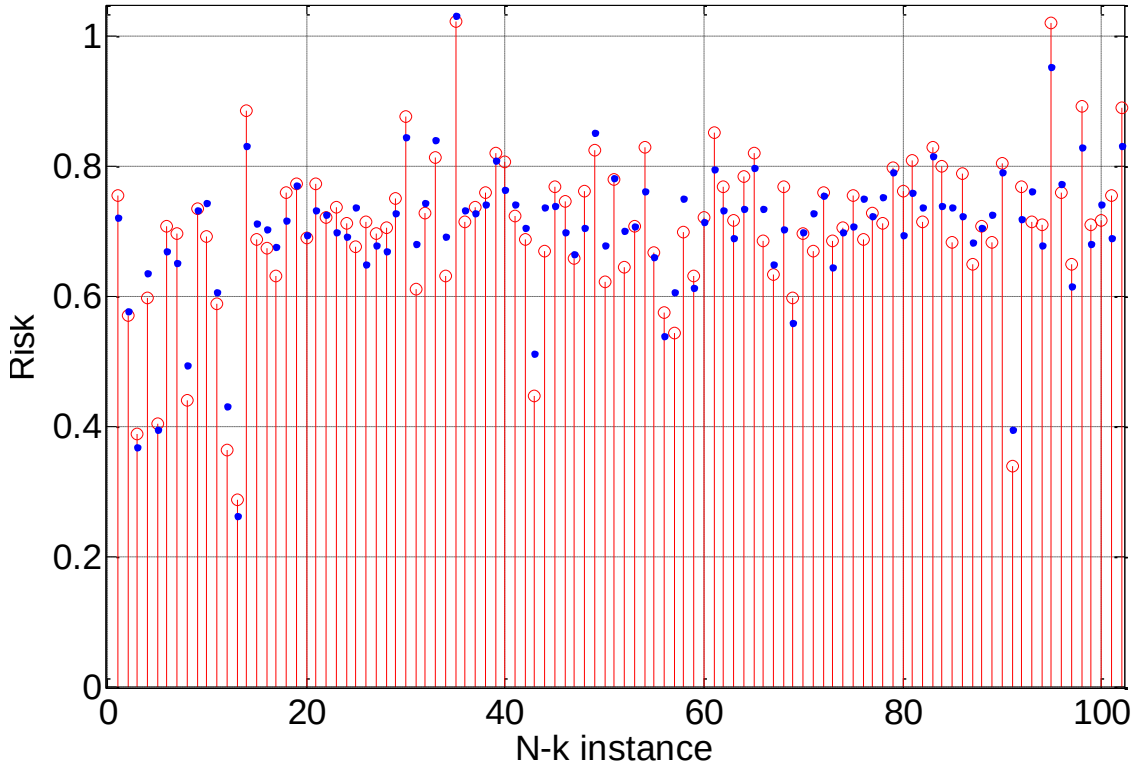

Fig 4.5 DNNE prediction results based on New England 39-bus system (Red stems represent the real risk values; blue dots represent predicting values)

B. Risk evaluation of cascading contingency on IEEE 118-bus system

1) Simulation setup

The IEEE 118-bus system is extracted from mid-western US power grid in 1962, which consists of 54 generators and 186 branches. Similar to the initialization of New England 39-bus system, the transmission line capacity, thermal limit, and operating scenarios are initialized in the same way.

In CFSM, *N-k* contingencies are firstly sampled with maximum *k*=10, where 500 instances for each *k*. Simulations are executed on the same computation platform. Due to the larger search space in this case, the convergence criterion of Monte Carlo simulations is relaxed to variance less than 0.003 p.u. Meanwhile, for each cascading failure simulation, **Criterion 2** is utilized, where up to three cascading stages are considered. In REM, similarly, exhaustive linear search applies to $n \in [70,130]$, $z \in [5,20]$, and $\lambda \in [0,1]$.

2) Simulation results

In Fig 4.6, a Monte Carlo simulation process is shown under normal condition with branch (30-38), (49-69), and (23-24) initially tripped. In this case, simulation converges near 1700 steps, which is much slower than previous case.

Simulation results are shown in Table 4.2, as well as some randomly selected instances shown in Fig 4.7. Worst-case selection experiments are also conducted with 2000 times.

According to the simulation results shown in Table 4.2 and Fig 4.7, the overall performance of the proposed approach is satisfactory with MAPE of 10.76% and RMSE of 9.92%. As compared with 39-bus case, MAPE and RMSE obtained in this experiment are bit worse. This is reasonable because the search space is enlarged significantly and

limited *N-k* instances are difficult to represent various operating patterns. Furthermore, in order to accelerate the cascading simulation in this case, the convergence criterion is relaxed, which may cause some slight inaccuracies on the simulation results. Nevertheless, CI obtained in this case is still high with 95.1%. This demonstrates that the proposed approach is quite promising and attains high potential in practical application of *N-k* contingency screening.

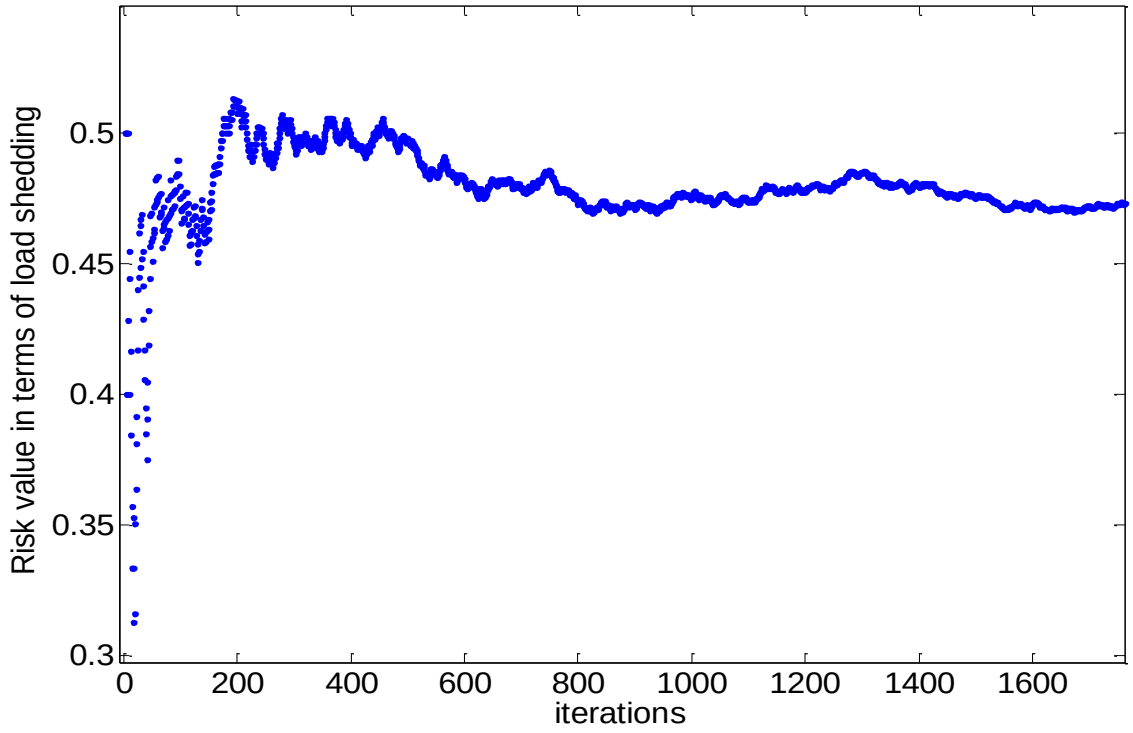

(a)

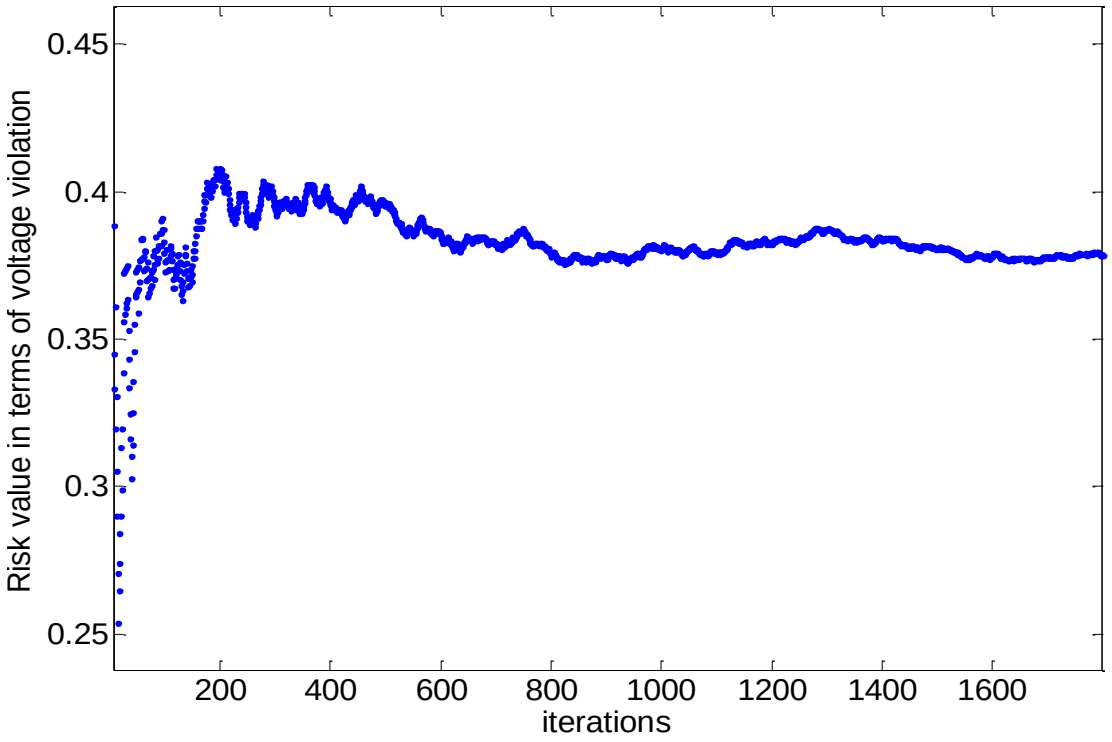

(b)

Fig 4.6 An example of Monte Carlo simulation results under normal operating condition (IEEE 118-bus system)

Table 4.2 Simulation results (IEEE 118-bus system)

	Overall elapsed time			
CFSM	172323s			
	MAPE	RMSE	CI	Elapsed time in training
REM	10.76%	9.92%	95.1%	3.294s

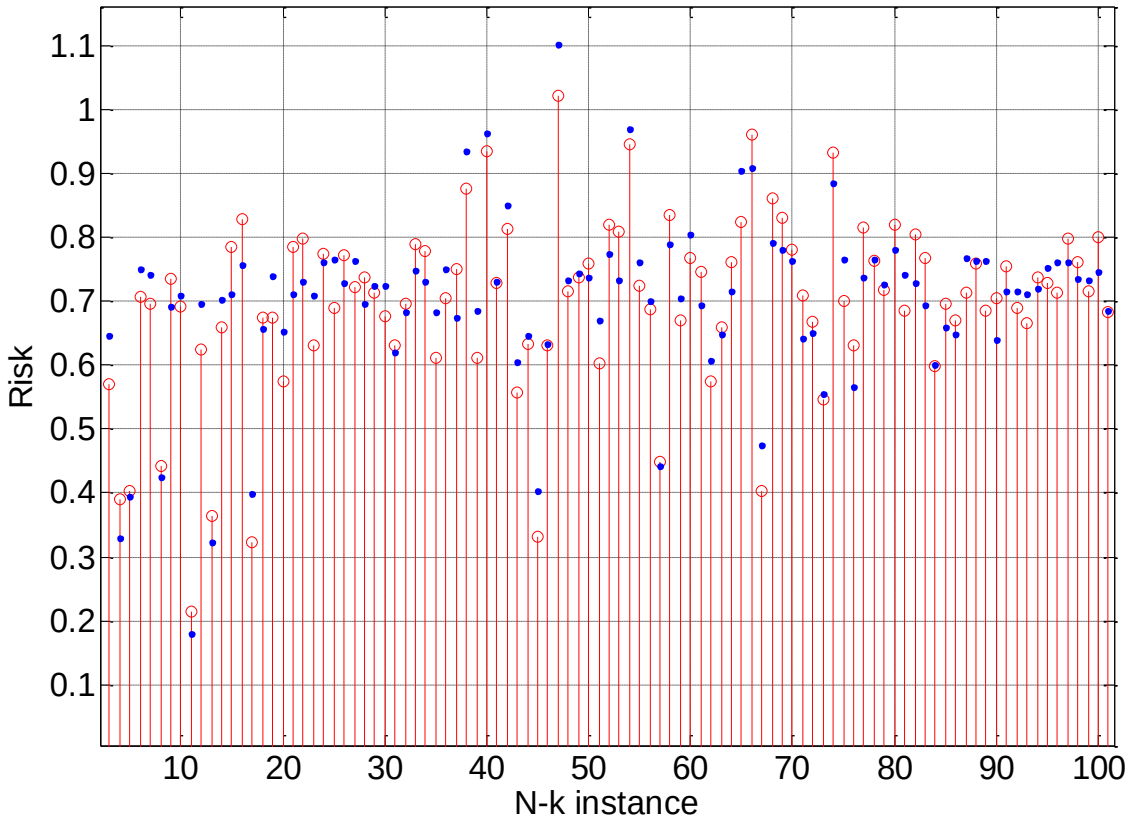

Fig 4.7 DNNE prediction results on IEEE 118-bus system (Red stems represent the real risk values, and blue dots represent predicting values)

4.3 *N-k* Contingency Screening based on Quantum Inspired Multi-objective Evolutionary Algorithm

4.3.1 Proposed methodology

In order to obtain a credible list of *N-k* contingencies in a large search space, optimization method is widely studied in the existing literature (e.g. [25, 27, 152]) to screen out highest risk / severity multiple contingencies. However, the solutions

achieved by those methods might be overly pessimistic and incomprehensive for system planning. In this thesis, the objective for contingency analysis is to identify a bunch of Pareto fronts containing multiple contingencies with different risk rankings in a large search space.

In this study, a multi-objective optimization problem is formulated as follows:

$$\begin{cases} \max & R_{\{N-k\}} \\ \min & k \end{cases} \quad (4\text{-}36)$$

$$s.t.$$

$$k \le k^*$$

where k^* is the upper limit of transmission line outages. $R_{\{N-k\}}$ can be easily generated by a trained DNNE.

The status of a transmission line is formulated as a *0/1* variable (*0* indicates line outage). To achieve non-dominated sets with good quality and ensure the diversity of population in this optimization problem, NSGA-II based Quantum-inspired evolutionary algorithm is adopted, which is introduced in details in Section 4.3.2.

4.3.2 Quantum inspired multi-objective evolutionary algorithm

QEA is inspired by the concept of quantum computing, which features effective exploration and exploitation capability in search space for a global optimal solution [153, 154]. In QEA, a 0/1 variable is represented by a Q-bit, which is a probabilistic representation based on the concept of qubits [153]. A Q-bit individual is defined as Eq

(4-37), which consists of *m* Q-bits. $Q(t)$ consists of *n* Q-bit individuals, where *t* is the number of generation, and *n* is the population size.

$$q_i^t = \begin{bmatrix} \alpha_{i1}^t & \alpha_{i2}^t & \cdots & \alpha_{im}^t \\ \beta_{i1}^t & \beta_{i2}^t & \cdots & \beta_{im}^t \end{bmatrix} \tag{4-37}$$

$$Q(t) = \{q_1^t, q_2^t, ..., q_n^t\} \tag{4-38}$$

where $|\alpha_{ij}^t|^2 + |\beta_{ij}^t|^2 = 1$.

The procedure of QEA is summarized in Table 4.3. [153]

Table 4.3 Main procedures of QEA

1) $t \leftarrow 0$
2) Initialization

   $Q(0) = \{q_1^0, q_2^0, ..., q_n^0\}$, where $\alpha_{ij}^0 = \beta_{ij}^0 = 1/\sqrt{2}$
3) Observation

   $P(0)$ is obtained by observing $Q(0)$. The state of a Q-bits is either 0 or 1, which is determined with the probability of either $|\alpha_i|^2$ or $|\beta_i|^2$, respectively.
4) Evaluate $P(0)$

   Each binary solution in $P(0)$ is evaluated and a corresponding fitness value is obtained.
5) Store the best solutions among $P(0)$ to $B(0)$

   In the initial generation, the best solutions are the same as the binary ones in $P(0)$, i.e. $B(0)=P(0)$
6) **While** (non-termination condition) **do**

   $t \leftarrow t+1$
7) Obtain $P(t)$ by observing the states of Q(t-1)
8) Evaluate $P(t)$

9) Update $Q(t)$

10) Store the best solutions among $B(t-1)$ and $P(t)$ into $B(t)$

11) Store the best solution **b** in $B(t)$

12) **If** (migration condition)

Migrate **b** to $B(t)$ locally or globally

End if

End While

In Step 9), Q-bit individuals are updated by Q-gate, which is defined as:

$$Q\text{-gate}(\Delta\theta)=\begin{bmatrix}\cos(\Delta\theta) & -\sin(\Delta\theta)\\ \sin(\Delta\theta) & \cos(\Delta\theta)\end{bmatrix} \tag{4-39}$$

where $\Delta\theta$ is a rotation angle of each Q-bit. $\Delta\theta$ is pre-defined in compliance with different optimization problems.

In single objective problem, migration is useful to balance the exploration and exploitation of QEA. However, migration operation can have a negative impact on the diversity of solutions in multi-objective optimization problems [155]. Therefore, Step 12) is not utilized in the proposed optimization problem.

There are two goals of the proposed optimization problem for contingency screening. Firstly, obtained solutions should be close to the Pareto-optimal front. Secondly, diversity of population should be effectively preserved so as to achieve as many solutions as possible. In this case, NSGA-II [132], which outperforms other multi-objective strategies in terms of elite conservation and diversity preservation, is utilized

in this thesis to solve the proposed multi-objective optimization problems. Furthermore, through NSGA-II, different levels of Pareto front can be obtained in the process of searching Pareto-optimal front. This is useful in contingency screening since not only the highest-risk contingencies are considered.

The main procedure of QMEA is summarized in Table 4.4.

Table 4.4 Main procedure of QMEA

1) $t \leftarrow 0$
2) Initialize $Q(0)$
3) Obtain $P(0)$ by observing $Q(0)$
4) Evaluate $P(0)$
5) **While** (non-termination condition) do
   $t \leftarrow t+1$
6) Obtain $P(t)$ by observing $Q(t)$
7) Evaluate $P(t)$
8) Fast non-dominated sorting for $P(t) \bigcup P(t-1)$
9) Calculate crowding distance and sort
10) $P(t)$ is constructed by the first n elements in the sorted population with the size of $2n$
11) $Q(t)$ is classified into several groups
12) Update $Q(t)$ by using Q-gate
    End While

The fast non-dominated sorting algorithm and crowding distance calculation in Steps 8) and 9) can be referred to [132]. In Step 10), $P(t)$ is rearranged according to the

sorting results. Meanwhile, the Q-bit individuals in $Q(t)$ corresponding to $P(t)$ are also rearranged. In Step 11), $Q(t)$ is divided into several groups based on the group classification method in [155]. Through fast non-dominated sorting, the first group is the best group. For the elitism, Q-bit individuals in the first group are retained and serve as reference in Step 12) to update the rest of groups.

4.3.3 Experimental results

In this section, the proposed optimization method for multiple contingency screening is tested on New England 39-bus and IEEE 118-bus systems.

Experiment setup: network data of *case39* and *case118* in MATPOWER [151] (which can be referred to Appendices B and C), is utilized for load flow calculation. For each testing system, eight operating scenarios with different loading levels are considered to train REM. The generation and load data in Appendices B and C are used as reference for testing. Training datasets of eight operating scenarios are generated by increasing or decreasing the reference loading level with ± 0.1.

Figs 4.8-4.9 show three Pareto fronts for each test case. Comparative experiments are conducted through a complete cascading failure simulation based screening for N-2 contingencies. Experimental results are reported in Table 4.5. Obviously, results obtained by the proposed optimization method are mostly consistent with the ones by complete cascading failure simulations. For the case of IEEE 118-bus system, *N-2* contingency ranking 3rd screened out by the proposed method is different from the one

obtained by exhaustive search. This may be caused by inaccurate risk evaluation of REM. For a large system, the regression accuracy of REM is sensitive to the quality of training datasets, which has been discussed in Section 4.2. Nevertheless, the overall performance of the proposed method is fairly promising since most of high-risk contingencies can be screening out accurately and efficiently.

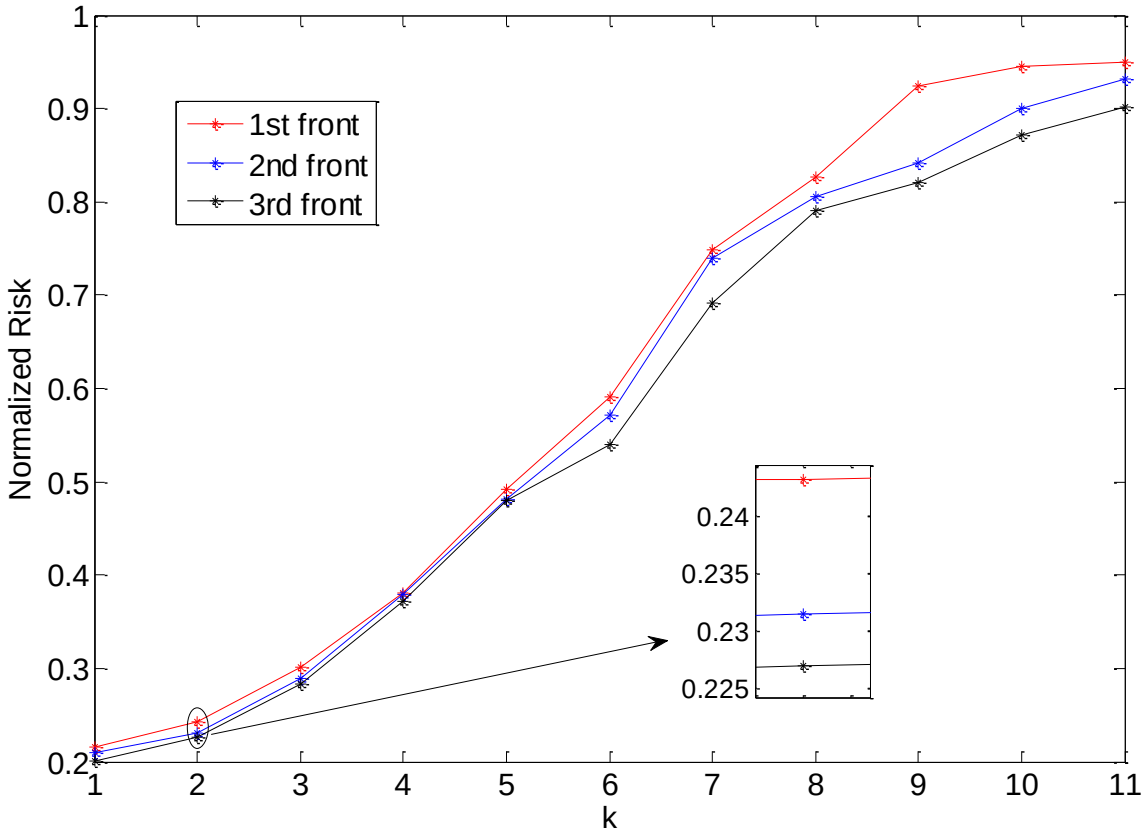

Fig 4.8 Pareto fronts of high-risk multiple contingencies (New England 39-bus system)

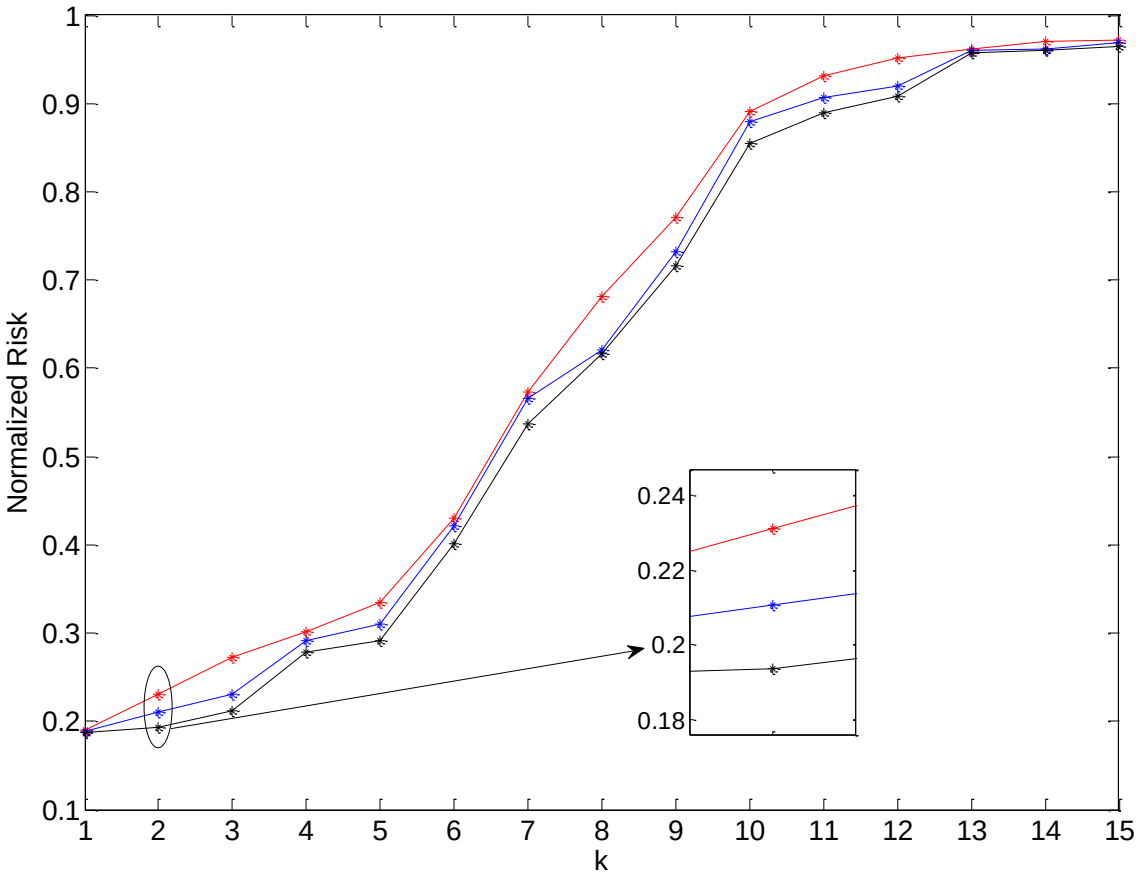

Fig 4.9 Pareto fronts of high-risk multiple contingencies (IEEE 118-bus system)

Table 4.5 *N-2* contingency screening

Testing case	Proposed optimization method			Exhaustive search through complete cascading failure simulation		
	Pareto front ranking	*N-2*	$R_{\{N-2\}}$	Contingency ranking	*N-2*	$R_{\{N-2\}}$
New England 39-bus system	1st	23-36 25-37	0.2432	1st	23-36 25-37	0.0973
	2nd	16-19	0.2314	2nd	16-19	0.0926

		25-37			25-37	
	3rd	21-22 28-29	0.2269	3rd	21-22 28-29	0.0798
IEEE 118-bus system	1st	19-24 38-65	0.2312	1st	19-24 38-65	0.0045 32
	2nd	15-33 35-36	0.2108	2nd	15-33 35-36	0.0039 39
	3rd	30-38 23-24	0.1937	3rd	34-43 38-65	0.0037 89

4.4 Conclusion

A comprehensive framework for *N-k* induced cascading contingency screening is proposed in this chapter. In this framework, topological resilience of PTN and cascading risk under multiple transmission line outages are jointly taken into account. This framework consists of three modules—CFSM, REM and CSM. Massive cascading risk datasets are generated by CFSM, which simultaneously considers the resilience of underlying network. A new neural network ensemble strategy based on RVFL is proposed and utilized in REM. A well-trained REM can efficiently evaluate the cascading risk of an *N-k* contingency. In formulating the power network interdiction problem as a pair-wise objective problem, QMEA is utilized in CSM that can effectively screen out a bunch of Pareto fronts of multiple contingencies with different rankings in a large search space. Each module has been respectively tested on New England 39-bus

and IEEE 118-bus systems. Simulation results demonstrate the effectiveness of the proposed framework.

To sum up, the proposed framework effectively remedies the drawbacks of conventional contingency screening approach such as 1) neglecting cascading failure in post-contingency phase; 2) inability of handling topological complexity of PTN; 3) the combinatorial explosion in *N-k* contingency screening; and 4) the high computational cost. Through the case studies reported in this chapter, the proposed framework inaugurates a promising research direction for multiple contingency screening in handling massive topological and operational data. Since data mining techniques are employed in this framework, risk evaluation can be fairly efficient through simple matrix calculation. On the other hand, the accuracy of this approach is sensitive to the training datasets. Effectively selecting training data to capture sufficient features for risk evaluation is useful and worth further investigation in the future.

Chapter 5 Conclusions and Future Work

5.1 Conclusions

The research presented in this thesis has studied the topological vulnerability and operational security of power systems that are essentially important in the context of smart gird development. To accommodate the stringent security standards in electricity industries in recent years, it is imperative to conduct multiple contingency analyses in an effective and efficient way. For the purpose of system planning, this research comprehensively investigates the topological properties of PTN based on complex network theory, and proposes an advanced *N-k* induced cascading contingency screening framework based on steady-state security analysis and data mining techniques.

In particular, a new model for structural vulnerability analysis based on power adjacency matrix is firstly proposed in Chapter 3 (Section 3.1). As compared with pure complex network model, the proposed one can be more effective to reflect the vulnerability of PTN by capturing both topological information and power flow sensitivity on each branch. It is worth mentioning that there are several limitations of such model which restrict the generalization of its results. Since this model is mainly based on complex network theory, only high-level statistical results can be provided for system planning. To identify and predict the uncontrolled network separations in PTN, a spectral clustering based approach is proposed in Chapter 3 (Section 3.2). Meanwhile,

an active network partitioning approach is also proposed in Section 3.3, which is based on Laplacian spectrum and SOM algorithm. Case studies on both small and large power systems have demonstrated the effectiveness of these two approaches, which shows a high potential of practical application on system planning, especially for smart grid. Furthermore, to study the resilience of underlying networks of power systems, a bond percolation model based on small-world PTN is proposed in Chapter 3 (Section 3.4). A direct solution of this percolation model is given, which effectively reflects the percolation process of small-world PTN and indicate a threshold value for critical phase transition. A useful metric (i.e. $Resilience(\mathcal{G})$) is obtained by this model to quantitatively measure the resilience of PTN, which is also incorporated into the risk evaluation of multiple contingencies in Chapter 4.

A comprehensive framework of *N-k* induced cascading contingency screening is proposed in Chapter 4. The main contributions of this work include: i) comprehensive modeling of multiple contingencies including cascading failures in post-contingency phase; ii) incorporation of network resilience in risk evaluation; and iii) computationally efficient in dealing with massive operational data in power systems. This framework has been tested through case studies on New England 39-bus and IEEE 118-bus systems, of which simulation results are fairly promising. On the other hand, the limitation of this framework lies in the accuracy of risk evaluation. For large-scale power systems, the evaluation accuracy highly depends on effective selection of training datasets. Therefore,

according to specific requirements of practical application, it is necessary to reach a tradeoff between computational efficiency and adequate training datasets.

5.2 Future Work

This thesis has laid out a substantial foundation for topology oriented vulnerability and security analysis. In the part of topological analysis, studies need to be extended to incorporate more engineering considerations in complex network based models. The following works may be worthy of further investigation in the future:

1) Electrical distance of renewable energy embedded power systems can be further studied. This is useful for topological modeling of smart grid in the application of vulnerability analysis and network partition.
2) In the proposed k-way network partitioning approach, advanced observation techniques for SOM can be further studied and employed for better clustering performance.
3) It would be interesting to further explore the topological properties (other than small-world features) and investigate the corresponding percolation model.

In another part for *N-k* contingency screening, additional researches are recommended to further enhance the proposed framework, which include the following aspects:

1) Studies on fast load flow calculation for cascading failure simulations.

2) Effective selection of training datasets to capture sufficient operational information for DNNE regression.
3) An effective model can be constructed to assess the economic loss of N-k induced cascading contingencies, so as to yield a more comprehensive risk value for practical application.

Appendices

A. Derivation of incremental real and reactive power (matrix form)

In power system, nodal injection power in polar form can be expressed as:

$$\begin{cases} P_i = V_i \sum_{j \in i} V_j (G_{ij} \cos\theta_{ij} + B_{ij} \sin\theta_{ij}) \\ Q_i = V_i \sum_{j \in i} V_j (G_{ij} \sin\theta_{ij} - B_{ij} \cos\theta_{ij}) \end{cases} (i = 1, 2, ..., |N|) \qquad \text{(A-1)}$$

where P_i and Q_i represent the real and reactive power injection of bus i respectively, V_i is bus voltage of bus i, is the phase-angle difference between bus i and j.

Then:

$$\begin{cases} \Delta P_i = P_{is} - V_i \sum_{j \in i} V_j (G_{ij} \cos\theta_{ij} + B_{ij} \sin\theta_{ij}) = 0 \\ \Delta Q_i = Q_{is} - V_i \sum_{j \in i} V_j (G_{ij} \sin\theta_{ij} - B_{ij} \cos\theta_{ij}) = 0 \end{cases} (i = 1, 2, ..., |N|) \qquad \text{(A-2)}$$

Expend ΔP_i and ΔQ_i in Taylor series and omit high order terms, one can obtain:

$$\begin{bmatrix} \Delta P_1 \\ \Delta P_2 \\ \vdots \\ \Delta P_n \\ \hdashline \Delta Q_1 \\ \Delta Q_2 \\ \vdots \\ \Delta Q_n \end{bmatrix} = \left[\begin{array}{cccc:cccc} H_{11} & H_{12} & \cdots & H_{1n} & N_{11} & N_{12} & \cdots & N_{1n} \\ H_{21} & H_{22} & \cdots & H_{2n} & N_{21} & N_{22} & \cdots & N_{2n} \\ \vdots & \vdots & \vdots & \vdots & \vdots & \vdots & \vdots & \vdots \\ H_{n1} & H_{n2} & \cdots & H_{nn} & N_{n1} & N_{n2} & \cdots & N_{nn} \\ \hdashline J_{11} & J_{12} & \cdots & J_{1n} & L_{11} & L_{12} & \cdots & L_{1n} \\ J_{21} & J_{22} & \cdots & J_{2n} & L_{21} & L_{22} & \cdots & L_{2n} \\ \vdots & \vdots & \vdots & \vdots & \vdots & \vdots & \vdots & \vdots \\ J_{n1} & J_{n2} & \cdots & J_{nn} & L_{n1} & L_{n2} & \cdots & L_{nn} \end{array}\right] \begin{bmatrix} \Delta\theta_1 \\ \Delta\theta_2 \\ \vdots \\ \Delta\theta_n \\ \hdashline \Delta V_1 / V_1 \\ \Delta V_2 / V_2 \\ \vdots \\ \Delta V_n / V_n \end{bmatrix} \qquad \text{(A-3)}$$

where

$$H_{ij} = \frac{\partial \Delta P_i}{\partial \theta_j} = -V_i V_j (G_{ij} \sin\theta_{ij} - B_{ij} \cos\theta_{ij})$$

$$H_{ii} = \frac{\partial \Delta P_i}{\partial \theta_i} = V_i \sum_{\substack{j \in i \\ j \neq i}} V_j (G_{ij} \sin\theta_{ij} - B_{ij} \cos\theta_{ij}) = V_i^2 B_{ii} + Q_i$$

$$N_{ij} = \frac{\partial \Delta P_i}{\partial V_j} V_j = -V_i V_j (G_{ij} \cos\theta_{ij} + B_{ij} \sin\theta_{ij})$$

$$N_{ii} = \frac{\partial \Delta P_i}{\partial V_i} V_i = -V_i \sum_{\substack{j \in i \\ j \neq i}} V_j (G_{ij} \cos\theta_{ij} + B_{ij} \sin\theta_{ij}) - 2V_i^2 G_{ii}$$

$$J_{ij} = \frac{\partial \Delta Q_i}{\partial \theta_j} = V_i V_j (G_{ij} \cos\theta_{ij} + B_{ij} \sin\theta_{ij})$$

$$J_{ii} = \frac{\partial \Delta Q_i}{\partial \theta_i} = -V_i \sum_{\substack{j \in i \\ j \neq}} V_j (G_{ij} \cos\theta_{ij} + B_{ij} \sin\theta_{ij})$$

$$L_{ij} = \frac{\partial \Delta Q_i}{\partial V_j} V_j = -V_i V_j (G_{ij} \sin\theta_{ij} - B_{ij} \cos\theta_{ij})$$

$$L_{ii} = \frac{\partial \Delta Q_i}{\partial V_i} V_i = -V_i \sum_{\substack{j \in i \\ j \neq i}} V_j (G_{ij} \sin\theta_{ij} - B_{ij} \cos\theta_{ij}) + 2V_t^2 B_{ii} = V_i^2 B_{ii} - Q_i$$

Thus Eq (A-3) can be rewritten as:

$$\begin{bmatrix} \Delta P \\ \Delta Q \end{bmatrix} = \begin{bmatrix} H & N \\ J & L \end{bmatrix} \begin{bmatrix} \Delta\theta \\ \Delta V / V \end{bmatrix}$$

In a PTN, real power flow is mainly subject to the bus angle and reactive power flow is mainly subject to bus voltage. In most cases, the phase angle difference between two

buses of a branch is no more than $10° \sim 20°$. Furthermore, the admittance responding to reactive power of each bus is much less than its imaginary part of self admittance, i.e. $B_{Li} = \frac{Q_i}{L_i^2} << B_{ii}$.

Thus,

$$\begin{cases} \cos\theta_{ij} \approx 1 \\ G_{ij} \sin\theta_{ij} << B_{ij} \\ Q_i << V_i^2 B_{ii} \end{cases}$$

Based on the derivation above, one can easily reach the conclusion:

$$H = L = \begin{bmatrix} V_1 & & & 0 \\ & V_2 & & \\ & & \ddots & \\ 0 & & & V_n \end{bmatrix} \begin{bmatrix} B_{11} & B_{12} & \cdots & B_{1n} \\ B_{21} & B_{22} & & B_{2n} \\ \vdots & \vdots & \ddots & \vdots \\ B_{n1} & B_{n2} & \cdots & B_{nn} \end{bmatrix} \begin{bmatrix} V_1 & & & 0 \\ & V_2 & & \\ & & \ddots & \\ 0 & & & V_n \end{bmatrix}$$

B. Data of New England 39-bus System

All data of this test case is from *case39* in MATPOWER [151].

Table B.1 Generator data of New England 39-bus system

Bus #	P_g (MW)	Q_g (MVar)	Q_{max}	Q_{min}	V_g (p.u.)	mBase(MW)	status	P_{max}	P_{min}
30	250	161.762	400	140	1.0499	100	1	1040	0
31	677.871	221.574	300	-100	0.982	100	1	646	0
32	650	206.965	300	150	0.9841	100	1	725	0
33	632	108.293	250	0	0.9972	100	1	652	0
34	508	166.688	167	0	1.0123	100	1	508	0
35	650	210.661	300	-100	1.0494	100	1	687	0
36	560	100.165	240	0	1.0636	100	1	580	0
37	540	-1.3695	250	0	1.0275	100	1	564	0
38	830	21.7327	300	-150	1.0265	100	1	865	0

Table B.2 Bus data of New England 39-bus system

Bus #	P_d(MW)	Q_d(MVar)	G_s	B_s	area	V_m(p.u)	V_a(p.u)	BaseKV	zone	V_{max} (p.u)	V_{min} (p.u)
1	97.6	44.2	0	0	2	1.039384	-13.5366	345	1	1.06	0.94
2	0	0	0	0	2	1.048494	-9.78527	345	1	1.06	0.94
3	322	2.4	0	0	2	1.030708	-12.2764	345	1	1.06	0.94
4	500	184	0	0	1	1.00446	-12.6267	345	1	1.06	0.94
5	0	0	0	0	1	1.006006	-11.1923	345	1	1.06	0.94
6	0	0	0	0	1	1.008226	-10.4083	345	1	1.06	0.94
7	233.8	84	0	0	1	0.998397	-12.7556	345	1	1.06	0.94
8	522	176.6	0	0	1	0.997872	-13.3358	345	1	1.06	0.94
9	6.5	-66.6	0	0	1	1.038332	-14.1784	345	1	1.06	0.94
10	0	0	0	0	1	1.017843	-8.17088	345	1	1.06	0.94
11	0	0	0	0	1	1.013386	-8.93697	345	1	1.06	0.94
12	8.53	88	0	0	1	1.000815	-8.99882	345	1	1.06	0.94
13	0	0	0	0	1	1.014923	-8.92993	345	1	1.06	0.94
14	0	0	0	0	1	1.012319	-10.7153	345	1	1.06	0.94
15	320	153	0	0	3	1.016185	-11.3454	345	1	1.06	0.94
16	329	32.3	0	0	3	1.03252	-10.0333	345	1	1.06	0.94
17	0	0	0	0	2	1.034237	-11.1164	345	1	1.06	0.94
18	158	30	0	0	2	1.031573	-11.9862	345	1	1.06	0.94
19	0	0	0	0	3	1.050107	-5.41007	345	1	1.06	0.94
20	680	103	0	0	3	0.991011	-6.82118	345	1	1.06	0.94
21	274	115	0	0	3	1.032319	-7.62875	345	1	1.06	0.94
22	0	0	0	0	3	1.050143	-3.18312	345	1	1.06	0.94

23	247.5	84.6	0	0	3	1.045145	-3.38128	345	1	1.06	0.94
24	308.6	-92.2	0	0	3	1.038001	-9.91376	345	1	1.06	0.94
25	224	47.2	0	0	2	1.057683	-8.36924	345	1	1.06	0.94
26	139	17	0	0	2	1.052561	-9.43877	345	1	1.06	0.94
27	281	75.5	0	0	2	1.038345	-11.3622	345	1	1.06	0.94
28	206	27.6	0	0	3	1.050374	-5.92836	345	1	1.06	0.94
29	283.5	26.9	0	0	3	1.050115	-3.16987	345	1	1.06	0.94
30	0	0	0	0	2	1.0499	-7.37047	345	1	1.06	0.94
31	9.2	4.6	0	0	1	0.982	0	345	1	1.06	0.94
32	0	0	0	0	1	0.9841	-0.18844	345	1	1.06	0.94
33	0	0	0	0	3	0.9972	-0.19317	345	1	1.06	0.94
34	0	0	0	0	3	1.0123	-1.63112	345	1	1.06	0.94
35	0	0	0	0	3	1.0494	1.776507	345	1	1.06	0.94
36	0	0	0	0	3	1.0636	4.468437	345	1	1.06	0.94
37	0	0	0	0	2	1.0275	-1.5829	345	1	1.06	0.94
38	0	0	0	0	3	1.0265	3.892818	345	1	1.06	0.94
39	1104	250	0	0	1	1.03	-14.5353	345	1	1.06	0.94

Table B.3 Branch data of New England 39-bus system

From bus	To bus	r	x	b	rateA	rateB	rateC	Transformer ratio	angle
1	2	0.0035	0.0411	0.6987	600	600	600	0	0
1	39	0.001	0.025	0.75	1000	1000	1000	0	0
2	3	0.0013	0.0151	0.2572	500	500	500	0	0
2	25	0.007	0.0086	0.146	500	500	500	0	0
2	30	0	0.0181	0	900	900	2500	1.025	0
3	4	0.0013	0.0213	0.2214	500	500	500	0	0
3	18	0.0011	0.0133	0.2138	500	500	500	0	0
4	5	0.0008	0.0128	0.1342	600	600	600	0	0
4	14	0.0008	0.0129	0.1382	500	500	500	0	0
5	6	0.0002	0.0026	0.0434	1200	1200	1200	0	0
5	8	0.0008	0.0112	0.1476	900	900	900	0	0
6	7	0.0006	0.0092	0.113	900	900	900	0	0
6	11	0.0007	0.0082	0.1389	480	480	480	0	0
6	31	0	0.025	0	1800	1800	1800	1.07	0
7	8	0.0004	0.0046	0.078	900	900	900	0	0
8	9	0.0023	0.0363	0.3804	900	900	900	0	0
9	39	0.001	0.025	1.2	900	900	900	0	0
10	11	0.0004	0.0043	0.0729	600	600	600	0	0
10	13	0.0004	0.0043	0.0729	600	600	600	0	0
10	32	0	0.02	0	900	900	2500	1.07	0
12	11	0.0016	0.0435	0	500	500	500	1.006	0
12	13	0.0016	0.0435	0	500	500	500	1.006	0
13	14	0.0009	0.0101	0.1723	600	600	600	0	0
14	15	0.0018	0.0217	0.366	600	600	600	0	0
15	16	0.0009	0.0094	0.171	600	600	600	0	0
16	17	0.0007	0.0089	0.1342	600	600	600	0	0

16	19	0.0016	0.0195	0.304	600	600	2500	0	0
16	21	0.0008	0.0135	0.2548	600	600	600	0	0
16	24	0.0003	0.0059	0.068	600	600	600	0	0
17	18	0.0007	0.0082	0.1319	600	600	600	0	0
17	27	0.0013	0.0173	0.3216	600	600	600	0	0
19	20	0.0007	0.0138	0	900	900	2500	1.06	0
19	33	0.0007	0.0142	0	900	900	2500	1.07	0
20	34	0.0009	0.018	0	900	900	2500	1.009	0
21	22	0.0008	0.014	0.2565	900	900	900	0	0
22	23	0.0006	0.0096	0.1846	600	600	600	0	0
22	35	0	0.0143	0	900	900	2500	1.025	0
23	24	0.0022	0.035	0.361	600	600	600	0	0
23	36	0.0005	0.0272	0	900	900	2500	1	0
25	26	0.0032	0.0323	0.531	600	600	600	0	0
25	37	0.0006	0.0232	0	900	900	2500	1.025	0
26	27	0.0014	0.0147	0.2396	600	600	600	0	0
26	28	0.0043	0.0474	0.7802	600	600	600	0	0
26	29	0.0057	0.0625	1.029	600	600	600	0	0
28	29	0.0014	0.0151	0.249	600	600	600	0	0
29	38	0.0008	0.0156	0	1200	1200	2500	1.025	0
1	2	0.0035	0.0411	0.6987	600	600	600	0	0
1	39	0.001	0.025	0.75	1000	1000	1000	0	0
2	3	0.0013	0.0151	0.2572	500	500	500	0	0

C. Data of IEEE 118-bus System

All data of this test case is from *case118* in MATPOWER [151].

Table C.1 Generator data of IEEE 118-bus system

Bus #	P_g (MW)	Q_g (MVar)	Q_{max}	Q_{min}	V_g (p.u.)	mBase(MW)	status	P_{max}	P_{min}
1	0	0	15	-5	0.955	100	1	100	0
4	0	0	300	-300	0.998	100	1	100	0
6	0	0	50	-13	0.99	100	1	100	0
8	0	0	300	-300	1.015	100	1	100	0
10	450	0	200	-147	1.05	100	1	550	0
12	85	0	120	-35	0.99	100	1	185	0
15	0	0	30	-10	0.97	100	1	100	0
18	0	0	50	-16	0.973	100	1	100	0
19	0	0	24	-8	0.962	100	1	100	0
24	0	0	300	-300	0.992	100	1	100	0
25	220	0	140	-47	1.05	100	1	320	0
26	314	0	1000	-1000	1.015	100	1	414	0
27	0	0	300	-300	0.968	100	1	100	0
31	7	0	300	-300	0.967	100	1	107	0
32	0	0	42	-14	0.963	100	1	100	0
34	0	0	24	-8	0.984	100	1	100	0
36	0	0	24	-8	0.98	100	1	100	0
40	0	0	300	-300	0.97	100	1	100	0
42	0	0	300	-300	0.985	100	1	100	0
46	19	0	100	-100	1.005	100	1	119	0
49	204	0	210	-85	1.025	100	1	304	0
54	48	0	300	-300	0.955	100	1	148	0
55	0	0	23	-8	0.952	100	1	100	0
56	0	0	15	-8	0.954	100	1	100	0
59	155	0	180	-60	0.985	100	1	255	0
61	160	0	300	-100	0.995	100	1	260	0
62	0	0	20	-20	0.998	100	1	100	0
65	391	0	200	-67	1.005	100	1	491	0
66	392	0	200	-67	1.05	100	1	492	0
69	516.4	0	300	-300	1.035	100	1	805.2	0
70	0	0	32	-10	0.984	100	1	100	0
72	0	0	100	-100	0.98	100	1	100	0
73	0	0	100	-100	0.991	100	1	100	0
74	0	0	9	-6	0.958	100	1	100	0
76	0	0	23	-8	0.943	100	1	100	0
77	0	0	70	-20	1.006	100	1	100	0
80	477	0	280	-165	1.04	100	1	577	0
85	0	0	23	-8	0.985	100	1	100	0

87	4	0	1000	-100	1.015	100	1	104	0
89	607	0	300	-210	1.005	100	1	707	0
90	0	0	300	-300	0.985	100	1	100	0
91	0	0	100	-100	0.98	100	1	100	0
92	0	0	9	-3	0.99	100	1	100	0
99	0	0	100	-100	1.01	100	1	100	0
100	252	0	155	-50	1.017	100	1	352	0
103	40	0	40	-15	1.01	100	1	140	0
104	0	0	23	-8	0.971	100	1	100	0
105	0	0	23	-8	0.965	100	1	100	0
107	0	0	200	-200	0.952	100	1	100	0
110	0	0	23	-8	0.973	100	1	100	0
111	36	0	1000	-100	0.98	100	1	136	0
112	0	0	1000	-100	0.975	100	1	100	0
113	0	0	200	-100	0.993	100	1	100	0
116	0	0	1000	-1000	1.005	100	1	100	0

Table C.2 Bus data of IEEE 118-bus system

Bus #	P_d(MW)	Q_d(MVar)	G_s	B_s	area	V_m(p.u)	V_a(p.u)	BaseKV	zone	V_{max} (p.u)	V_{min} (p.u)
1	51	27	0	0	1	0.955	10.67	138	1	1.06	0.94
2	20	9	0	0	1	0.971	11.22	138	1	1.06	0.94
3	39	10	0	0	1	0.968	11.56	138	1	1.06	0.94
4	39	12	0	0	1	0.998	15.28	138	1	1.06	0.94
5	0	0	0	-40	1	1.002	15.73	138	1	1.06	0.94
6	52	22	0	0	1	0.99	13	138	1	1.06	0.94
7	19	2	0	0	1	0.989	12.56	138	1	1.06	0.94
8	28	0	0	0	1	1.015	20.77	345	1	1.06	0.94
9	0	0	0	0	1	1.043	28.02	345	1	1.06	0.94
10	0	0	0	0	1	1.05	35.61	345	1	1.06	0.94
11	70	23	0	0	1	0.985	12.72	138	1	1.06	0.94
12	47	10	0	0	1	0.99	12.2	138	1	1.06	0.94
13	34	16	0	0	1	0.968	11.35	138	1	1.06	0.94
14	14	1	0	0	1	0.984	11.5	138	1	1.06	0.94
15	90	30	0	0	1	0.97	11.23	138	1	1.06	0.94
16	25	10	0	0	1	0.984	11.91	138	1	1.06	0.94
17	11	3	0	0	1	0.995	13.74	138	1	1.06	0.94
18	60	34	0	0	1	0.973	11.53	138	1	1.06	0.94
19	45	25	0	0	1	0.963	11.05	138	1	1.06	0.94
20	18	3	0	0	1	0.958	11.93	138	1	1.06	0.94
21	14	8	0	0	1	0.959	13.52	138	1	1.06	0.94
22	10	5	0	0	1	0.97	16.08	138	1	1.06	0.94
23	7	3	0	0	1	1	21	138	1	1.06	0.94
24	13	0	0	0	1	0.992	20.89	138	1	1.06	0.94
25	0	0	0	0	1	1.05	27.93	138	1	1.06	0.94
26	0	0	0	0	1	1.015	29.71	345	1	1.06	0.94
27	71	13	0	0	1	0.968	15.35	138	1	1.06	0.94

28	17	7	0	0	1	0.962	13.62	138	1	1.06	0.94
29	24	4	0	0	1	0.963	12.63	138	1	1.06	0.94
30	0	0	0	0	1	0.968	18.79	345	1	1.06	0.94
31	43	27	0	0	1	0.967	12.75	138	1	1.06	0.94
32	59	23	0	0	1	0.964	14.8	138	1	1.06	0.94
33	23	9	0	0	1	0.972	10.63	138	1	1.06	0.94
34	59	26	0	14	1	0.986	11.3	138	1	1.06	0.94
35	33	9	0	0	1	0.981	10.87	138	1	1.06	0.94
36	31	17	0	0	1	0.98	10.87	138	1	1.06	0.94
37	0	0	0	-25	1	0.992	11.77	138	1	1.06	0.94
38	0	0	0	0	1	0.962	16.91	345	1	1.06	0.94
39	27	11	0	0	1	0.97	8.41	138	1	1.06	0.94
40	66	23	0	0	1	0.97	7.35	138	1	1.06	0.94
41	37	10	0	0	1	0.967	6.92	138	1	1.06	0.94
42	96	23	0	0	1	0.985	8.53	138	1	1.06	0.94
43	18	7	0	0	1	0.978	11.28	138	1	1.06	0.94
44	16	8	0	10	1	0.985	13.82	138	1	1.06	0.94
45	53	22	0	10	1	0.987	15.67	138	1	1.06	0.94
46	28	10	0	10	1	1.005	18.49	138	1	1.06	0.94
47	34	0	0	0	1	1.017	20.73	138	1	1.06	0.94
48	20	11	0	15	1	1.021	19.93	138	1	1.06	0.94
49	87	30	0	0	1	1.025	20.94	138	1	1.06	0.94
50	17	4	0	0	1	1.001	18.9	138	1	1.06	0.94
51	17	8	0	0	1	0.967	16.28	138	1	1.06	0.94
52	18	5	0	0	1	0.957	15.32	138	1	1.06	0.94
53	23	11	0	0	1	0.946	14.35	138	1	1.06	0.94
54	113	32	0	0	1	0.955	15.26	138	1	1.06	0.94
55	63	22	0	0	1	0.952	14.97	138	1	1.06	0.94
56	84	18	0	0	1	0.954	15.16	138	1	1.06	0.94
57	12	3	0	0	1	0.971	16.36	138	1	1.06	0.94
58	12	3	0	0	1	0.959	15.51	138	1	1.06	0.94
59	277	113	0	0	1	0.985	19.37	138	1	1.06	0.94
60	78	3	0	0	1	0.993	23.15	138	1	1.06	0.94
61	0	0	0	0	1	0.995	24.04	138	1	1.06	0.94
62	77	14	0	0	1	0.998	23.43	138	1	1.06	0.94
63	0	0	0	0	1	0.969	22.75	345	1	1.06	0.94
64	0	0	0	0	1	0.984	24.52	345	1	1.06	0.94
65	0	0	0	0	1	1.005	27.65	345	1	1.06	0.94
66	39	18	0	0	1	1.05	27.48	138	1	1.06	0.94
67	28	7	0	0	1	1.02	24.84	138	1	1.06	0.94
68	0	0	0	0	1	1.003	27.55	345	1	1.06	0.94
69	0	0	0	0	1	1.035	30	138	1	1.06	0.94
70	66	20	0	0	1	0.984	22.58	138	1	1.06	0.94
71	0	0	0	0	1	0.987	22.15	138	1	1.06	0.94
72	12	0	0	0	1	0.98	20.98	138	1	1.06	0.94
73	6	0	0	0	1	0.991	21.94	138	1	1.06	0.94
74	68	27	0	12	1	0.958	21.64	138	1	1.06	0.94
75	47	11	0	0	1	0.967	22.91	138	1	1.06	0.94
76	68	36	0	0	1	0.943	21.77	138	1	1.06	0.94

77	61	28	0	0	1	1.006	26.72	138	1	1.06	0.94
78	71	26	0	0	1	1.003	26.42	138	1	1.06	0.94
79	39	32	0	20	1	1.009	26.72	138	1	1.06	0.94
80	130	26	0	0	1	1.04	28.96	138	1	1.06	0.94
81	0	0	0	0	1	0.997	28.1	345	1	1.06	0.94
82	54	27	0	20	1	0.989	27.24	138	1	1.06	0.94
83	20	10	0	10	1	0.985	28.42	138	1	1.06	0.94
84	11	7	0	0	1	0.98	30.95	138	1	1.06	0.94
85	24	15	0	0	1	0.985	32.51	138	1	1.06	0.94
86	21	10	0	0	1	0.987	31.14	138	1	1.06	0.94
87	0	0	0	0	1	1.015	31.4	161	1	1.06	0.94
88	48	10	0	0	1	0.987	35.64	138	1	1.06	0.94
89	0	0	0	0	1	1.005	39.69	138	1	1.06	0.94
90	163	42	0	0	1	0.985	33.29	138	1	1.06	0.94
91	10	0	0	0	1	0.98	33.31	138	1	1.06	0.94
92	65	10	0	0	1	0.993	33.8	138	1	1.06	0.94
93	12	7	0	0	1	0.987	30.79	138	1	1.06	0.94
94	30	16	0	0	1	0.991	28.64	138	1	1.06	0.94
95	42	31	0	0	1	0.981	27.67	138	1	1.06	0.94
96	38	15	0	0	1	0.993	27.51	138	1	1.06	0.94
97	15	9	0	0	1	1.011	27.88	138	1	1.06	0.94
98	34	8	0	0	1	1.024	27.4	138	1	1.06	0.94
99	42	0	0	0	1	1.01	27.04	138	1	1.06	0.94
100	37	18	0	0	1	1.017	28.03	138	1	1.06	0.94
101	22	15	0	0	1	0.993	29.61	138	1	1.06	0.94
102	5	3	0	0	1	0.991	32.3	138	1	1.06	0.94
103	23	16	0	0	1	1.001	24.44	138	1	1.06	0.94
104	38	25	0	0	1	0.971	21.69	138	1	1.06	0.94
105	31	26	0	20	1	0.965	20.57	138	1	1.06	0.94
106	43	16	0	0	1	0.962	20.32	138	1	1.06	0.94
107	50	12	0	6	1	0.952	17.53	138	1	1.06	0.94
108	2	1	0	0	1	0.967	19.38	138	1	1.06	0.94
109	8	3	0	0	1	0.967	18.93	138	1	1.06	0.94
110	39	30	0	6	1	0.973	18.09	138	1	1.06	0.94
111	0	0	0	0	1	0.98	19.74	138	1	1.06	0.94
112	68	13	0	0	1	0.975	14.99	138	1	1.06	0.94
113	6	0	0	0	1	0.993	13.74	138	1	1.06	0.94
114	8	3	0	0	1	0.96	14.46	138	1	1.06	0.94
115	22	7	0	0	1	0.96	14.46	138	1	1.06	0.94
116	184	0	0	0	1	1.005	27.12	138	1	1.06	0.94
117	20	8	0	0	1	0.974	10.67	138	1	1.06	0.94
118	33	15	0	0	1	0.949	21.92	138	1	1.06	0.94

Table C.3 Branch data of IEEE 118-bus system

From bus	To bus	r	x	b	rateA	rateB	rateC	Transformer ratio	angle
1	2	0.0303	0.0999	0.0254	9900	0	0	0	0
1	3	0.0129	0.0424	0.01082	9900	0	0	0	0
4	5	0.00176	0.00798	0.0021	9900	0	0	0	0
3	5	0.0241	0.108	0.0284	9900	0	0	0	0
5	6	0.0119	0.054	0.01426	9900	0	0	0	0
6	7	0.00459	0.0208	0.0055	9900	0	0	0	0
8	9	0.00244	0.0305	1.162	9900	0	0	0	0
8	5	0	0.0267	0	9900	0	0	0.985	0
9	10	0.00258	0.0322	1.23	9900	0	0	0	0
4	11	0.0209	0.0688	0.01748	9900	0	0	0	0
5	11	0.0203	0.0682	0.01738	9900	0	0	0	0
11	12	0.00595	0.0196	0.00502	9900	0	0	0	0
2	12	0.0187	0.0616	0.01572	9900	0	0	0	0
3	12	0.0484	0.16	0.0406	9900	0	0	0	0
7	12	0.00862	0.034	0.00874	9900	0	0	0	0
11	13	0.02225	0.0731	0.01876	9900	0	0	0	0
12	14	0.0215	0.0707	0.01816	9900	0	0	0	0
13	15	0.0744	0.2444	0.06268	9900	0	0	0	0
14	15	0.0595	0.195	0.0502	9900	0	0	0	0
12	16	0.0212	0.0834	0.0214	9900	0	0	0	0
15	17	0.0132	0.0437	0.0444	9900	0	0	0	0
16	17	0.0454	0.1801	0.0466	9900	0	0	0	0
17	18	0.0123	0.0505	0.01298	9900	0	0	0	0
18	19	0.01119	0.0493	0.01142	9900	0	0	0	0
19	20	0.0252	0.117	0.0298	9900	0	0	0	0
15	19	0.012	0.0394	0.0101	9900	0	0	0	0
20	21	0.0183	0.0849	0.0216	9900	0	0	0	0
21	22	0.0209	0.097	0.0246	9900	0	0	0	0
22	23	0.0342	0.159	0.0404	9900	0	0	0	0
23	24	0.0135	0.0492	0.0498	9900	0	0	0	0
23	25	0.0156	0.08	0.0864	9900	0	0	0	0
26	25	0	0.0382	0	9900	0	0	0.96	0
25	27	0.0318	0.163	0.1764	9900	0	0	0	0
27	28	0.01913	0.0855	0.0216	9900	0	0	0	0
28	29	0.0237	0.0943	0.0238	9900	0	0	0	0
30	17	0	0.0388	0	9900	0	0	0.96	0
8	30	0.00431	0.0504	0.514	9900	0	0	0	0
26	30	0.00799	0.086	0.908	9900	0	0	0	0
17	31	0.0474	0.1563	0.0399	9900	0	0	0	0
29	31	0.0108	0.0331	0.0083	9900	0	0	0	0
23	32	0.0317	0.1153	0.1173	9900	0	0	0	0
31	32	0.0298	0.0985	0.0251	9900	0	0	0	0
27	32	0.0229	0.0755	0.01926	9900	0	0	0	0
15	33	0.038	0.1244	0.03194	9900	0	0	0	0
19	34	0.0752	0.247	0.0632	9900	0	0	0	0

35	36	0.00224	0.0102	0.00268	9900	0	0	0	0
35	37	0.011	0.0497	0.01318	9900	0	0	0	0
33	37	0.0415	0.142	0.0366	9900	0	0	0	0
34	36	0.00871	0.0268	0.00568	9900	0	0	0	0
34	37	0.00256	0.0094	0.00984	9900	0	0	0	0
38	37	0	0.0375	0	9900	0	0	0.935	0
37	39	0.0321	0.106	0.027	9900	0	0	0	0
37	40	0.0593	0.168	0.042	9900	0	0	0	0
30	38	0.00464	0.054	0.422	9900	0	0	0	0
39	40	0.0184	0.0605	0.01552	9900	0	0	0	0
40	41	0.0145	0.0487	0.01222	9900	0	0	0	0
40	42	0.0555	0.183	0.0466	9900	0	0	0	0
41	42	0.041	0.135	0.0344	9900	0	0	0	0
43	44	0.0608	0.2454	0.06068	9900	0	0	0	0
34	43	0.0413	0.1681	0.04226	9900	0	0	0	0
44	45	0.0224	0.0901	0.0224	9900	0	0	0	0
45	46	0.04	0.1356	0.0332	9900	0	0	0	0
46	47	0.038	0.127	0.0316	9900	0	0	0	0
46	48	0.0601	0.189	0.0472	9900	0	0	0	0
47	49	0.0191	0.0625	0.01604	9900	0	0	0	0
42	49	0.0715	0.323	0.086	9900	0	0	0	0
42	49	0.0715	0.323	0.086	9900	0	0	0	0
45	49	0.0684	0.186	0.0444	9900	0	0	0	0
48	49	0.0179	0.0505	0.01258	9900	0	0	0	0
49	50	0.0267	0.0752	0.01874	9900	0	0	0	0
49	51	0.0486	0.137	0.0342	9900	0	0	0	0
51	52	0.0203	0.0588	0.01396	9900	0	0	0	0
52	53	0.0405	0.1635	0.04058	9900	0	0	0	0
53	54	0.0263	0.122	0.031	9900	0	0	0	0
49	54	0.073	0.289	0.0738	9900	0	0	0	0
49	54	0.0869	0.291	0.073	9900	0	0	0	0
54	55	0.0169	0.0707	0.0202	9900	0	0	0	0
54	56	0.00275	0.00955	0.00732	9900	0	0	0	0
55	56	0.00488	0.0151	0.00374	9900	0	0	0	0
56	57	0.0343	0.0966	0.0242	9900	0	0	0	0
50	57	0.0474	0.134	0.0332	9900	0	0	0	0
56	58	0.0343	0.0966	0.0242	9900	0	0	0	0
51	58	0.0255	0.0719	0.01788	9900	0	0	0	0
54	59	0.0503	0.2293	0.0598	9900	0	0	0	0
56	59	0.0825	0.251	0.0569	9900	0	0	0	0
56	59	0.0803	0.239	0.0536	9900	0	0	0	0
55	59	0.04739	0.2158	0.05646	9900	0	0	0	0
59	60	0.0317	0.145	0.0376	9900	0	0	0	0
59	61	0.0328	0.15	0.0388	9900	0	0	0	0
60	61	0.00264	0.0135	0.01456	9900	0	0	0	0
60	62	0.0123	0.0561	0.01468	9900	0	0	0	0
61	62	0.00824	0.0376	0.0098	9900	0	0	0	0
63	59	0	0.0386	0	9900	0	0	0.96	0
63	64	0.00172	0.02	0.216	9900	0	0	0	0

64	61	0	0.0268	0	9900	0	0	0.985	0
38	65	0.00901	0.0986	1.046	9900	0	0	0	0
64	65	0.00269	0.0302	0.38	9900	0	0	0	0
49	66	0.018	0.0919	0.0248	9900	0	0	0	0
49	66	0.018	0.0919	0.0248	9900	0	0	0	0
62	66	0.0482	0.218	0.0578	9900	0	0	0	0
62	67	0.0258	0.117	0.031	9900	0	0	0	0
65	66	0	0.037	0	9900	0	0	0.935	0
66	67	0.0224	0.1015	0.02682	9900	0	0	0	0
65	68	0.00138	0.016	0.638	9900	0	0	0	0
47	69	0.0844	0.2778	0.07092	9900	0	0	0	0
49	69	0.0985	0.324	0.0828	9900	0	0	0	0
68	69	0	0.037	0	9900	0	0	0.935	0
69	70	0.03	0.127	0.122	9900	0	0	0	0
24	70	0.00221	0.4115	0.10198	9900	0	0	0	0
70	71	0.00882	0.0355	0.00878	9900	0	0	0	0
24	72	0.0488	0.196	0.0488	9900	0	0	0	0
71	72	0.0446	0.18	0.04444	9900	0	0	0	0
71	73	0.00866	0.0454	0.01178	9900	0	0	0	0
70	74	0.0401	0.1323	0.03368	9900	0	0	0	0
70	75	0.0428	0.141	0.036	9900	0	0	0	0
69	75	0.0405	0.122	0.124	9900	0	0	0	0
74	75	0.0123	0.0406	0.01034	9900	0	0	0	0
76	77	0.0444	0.148	0.0368	9900	0	0	0	0
69	77	0.0309	0.101	0.1038	9900	0	0	0	0
75	77	0.0601	0.1999	0.04978	9900	0	0	0	0
77	78	0.00376	0.0124	0.01264	9900	0	0	0	0
78	79	0.00546	0.0244	0.00648	9900	0	0	0	0
77	80	0.017	0.0485	0.0472	9900	0	0	0	0
77	80	0.0294	0.105	0.0228	9900	0	0	0	0
79	80	0.0156	0.0704	0.0187	9900	0	0	0	0
68	81	0.00175	0.0202	0.808	9900	0	0	0	0
81	80	0	0.037	0	9900	0	0	0.935	0
77	82	0.0298	0.0853	0.08174	9900	0	0	0	0
82	83	0.0112	0.03665	0.03796	9900	0	0	0	0
83	84	0.0625	0.132	0.0258	9900	0	0	0	0
83	85	0.043	0.148	0.0348	9900	0	0	0	0
84	85	0.0302	0.0641	0.01234	9900	0	0	0	0
85	86	0.035	0.123	0.0276	9900	0	0	0	0
86	87	0.02828	0.2074	0.0445	9900	0	0	0	0
85	88	0.02	0.102	0.0276	9900	0	0	0	0
85	89	0.0239	0.173	0.047	9900	0	0	0	0
88	89	0.0139	0.0712	0.01934	9900	0	0	0	0
89	90	0.0518	0.188	0.0528	9900	0	0	0	0
89	90	0.0238	0.0997	0.106	9900	0	0	0	0
90	91	0.0254	0.0836	0.0214	9900	0	0	0	0
89	92	0.0099	0.0505	0.0548	9900	0	0	0	0
89	92	0.0393	0.1581	0.0414	9900	0	0	0	0
91	92	0.0387	0.1272	0.03268	9900	0	0	0	0

92	93	0.0258	0.0848	0.0218	9900	0	0	0	0
92	94	0.0481	0.158	0.0406	9900	0	0	0	0
93	94	0.0223	0.0732	0.01876	9900	0	0	0	0
94	95	0.0132	0.0434	0.0111	9900	0	0	0	0
80	96	0.0356	0.182	0.0494	9900	0	0	0	0
82	96	0.0162	0.053	0.0544	9900	0	0	0	0
94	96	0.0269	0.0869	0.023	9900	0	0	0	0
80	97	0.0183	0.0934	0.0254	9900	0	0	0	0
80	98	0.0238	0.108	0.0286	9900	0	0	0	0
80	99	0.0454	0.206	0.0546	9900	0	0	0	0
92	100	0.0648	0.295	0.0472	9900	0	0	0	0
94	100	0.0178	0.058	0.0604	9900	0	0	0	0
95	96	0.0171	0.0547	0.01474	9900	0	0	0	0
96	97	0.0173	0.0885	0.024	9900	0	0	0	0
98	100	0.0397	0.179	0.0476	9900	0	0	0	0
99	100	0.018	0.0813	0.0216	9900	0	0	0	0
100	101	0.0277	0.1262	0.0328	9900	0	0	0	0
92	102	0.0123	0.0559	0.01464	9900	0	0	0	0
101	102	0.0246	0.112	0.0294	9900	0	0	0	0
100	103	0.016	0.0525	0.0536	9900	0	0	0	0
100	104	0.0451	0.204	0.0541	9900	0	0	0	0
103	104	0.0466	0.1584	0.0407	9900	0	0	0	0
103	105	0.0535	0.1625	0.0408	9900	0	0	0	0
100	106	0.0605	0.229	0.062	9900	0	0	0	0
104	105	0.00994	0.0378	0.00986	9900	0	0	0	0
105	106	0.014	0.0547	0.01434	9900	0	0	0	0
105	107	0.053	0.183	0.0472	9900	0	0	0	0
105	108	0.0261	0.0703	0.01844	9900	0	0	0	0
106	107	0.053	0.183	0.0472	9900	0	0	0	0
108	109	0.0105	0.0288	0.0076	9900	0	0	0	0
103	110	0.03906	0.1813	0.0461	9900	0	0	0	0
109	110	0.0278	0.0762	0.0202	9900	0	0	0	0
110	111	0.022	0.0755	0.02	9900	0	0	0	0
110	112	0.0247	0.064	0.062	9900	0	0	0	0
17	113	0.00913	0.0301	0.00768	9900	0	0	0	0
32	113	0.0615	0.203	0.0518	9900	0	0	0	0
32	114	0.0135	0.0612	0.01628	9900	0	0	0	0
27	115	0.0164	0.0741	0.01972	9900	0	0	0	0
114	115	0.0023	0.0104	0.00276	9900	0	0	0	0
68	116	0.00034	0.00405	0.164	9900	0	0	0	0
12	117	0.0329	0.14	0.0358	9900	0	0	0	0
75	118	0.0145	0.0481	0.01198	9900	0	0	0	0
76	118	0.0164	0.0544	0.01356	9900	0	0	0	0
1	2	0.0303	0.0999	0.0254	9900	0	0	0	0
1	3	0.0129	0.0424	0.01082	9900	0	0	0	0
4	5	0.00176	0.00798	0.0021	9900	0	0	0	0

Reference

[1] F. Li, W. Qiao, H. Sun, H. Wan, J. Wang, Y. Xia, *et al.*, "Smart transmission grid: Vision and framework," *Smart Grid, IEEE Transactions on,* vol. 1, pp. 168-177, 2010.

[2] F. Aloula, A. Al-Alia, R. Al-Dalkya, M. Al-Mardinia, and W. El-Hajj, "Smart grid security: threats, vulnerabilities and solutions," *International Journal of Smart Grid and Clean Energy,* vol. 1, pp. 1-6, 2012.

[3] W. Su, H. Eichi, W. Zeng, and M.-Y. Chow, "A survey on the electrification of transportation in a smart grid environment," *Industrial Informatics, IEEE Transactions on,* vol. 8, pp. 1-10, 2012.

[4] V. C. Gungor, D. Sahin, T. Kocak, S. Ergut, C. Buccella, C. Cecati, *et al.*, "Smart Grid Technologies: Communication Technologies and Standards," *Industrial Informatics, IEEE Transactions on,* vol. 7, pp. 529-539, 2011.

[5] H. Morais, P. Vancraeyveld, A. H. Birger Pedersen, M. Lind, H. Johannsson, and J. Ostergaard, "SOSPO-SP: Secure Operation of Sustainable Power Systems Simulation Platform for Real-Time System State Evaluation and Control," *Industrial Informatics, IEEE Transactions on,* vol. 10, pp. 2318-2329, 2014.

[6] X. Yan, D. Zhao Yang, X. Zhao, M. Ke, and W. Kit Po, "An Intelligent Dynamic Security Assessment Framework for Power Systems With Wind Power," *Industrial Informatics, IEEE Transactions on,* vol. 8, pp. 995-1003, 2012.

[7] D. Yue Min, H. Seung Ho, and L. Xiao Hui, "A Demand Response Energy Management Scheme for Industrial Facilities in Smart Grid," *Industrial Informatics, IEEE Transactions on,* vol. 10, pp. 2257-2269, 2014.

[8] Final Report on the August 14th, 2003 Blackout in the United States and Canada, US-Canada Power System Outage Task Force, Tech. Pep., 2004

[9] Final Report System Disturbance on November 4th, 2006, Union for the Co-ordination of Transmission of Electricity, Tech. Rep., 2007

[10] W. Lin, H. Sun, Y. Tang, G. Bu, and Y. Yin, "Analysis and Lessons of the Blackout in Brazil Power Grid on November 10, 2009 [J]," Automation of Electric Power Systems, vol. 7, p. 000, 2010.

[11] L. L. Lai, H. T. Zhang, C. S. Lai, F. Y. Xu, and S. Mishra, "Investigation on July 2012 Indian blackout," in Machine Learning and Cybernetics (ICMLC), 2013 International Conference on, 2013, pp. 92-97.

[12] IEEE PES PSDP Task Force on Blackout experience, mitigation, and role of new technologies, blackout experiences and lessons, Best practices for system dynamic performance, and the role of new technologies, IEEE Special Publication 07TP190, July 2007

[13] System Operating Limits Methodology for the Operations Horizon, NERC, Standard FAC-011-2, Available online: http://www.nerc.com/files/FAC-011_2.pdf

[14] S. Boccaletti, V. Latora, Y. Moreno, M. Chavez, and D.-U. Hwang, "Complex networks: Structure and dynamics," *Physics reports,* vol. 424, pp. 175-308, 2006.
[15] J. Youwei, X. Zhao, H. Siu-Lau, F. Zheng Xiong, and L. Loi Lei, "Security analysis of smart grids-A complex network perspective," in *Advances in Power System Control, Operation and Management (APSCOM 2012), 9th IET International Conference on,* 2012, pp. 1-4.
[16] G. Chen, Z. Y. Dong, D. J. Hill, G. H. Zhang, and K. Q. Hua, "Attack structural vulnerability of power grids: A hybrid approach based on complex networks," *Physica A: Statistical Mechanics and its Applications,* vol. 389, pp. 595-603, 2010.
[17] L. Mili, K. Dooley, Risk based power system planning integrating social and economic direct and indirect costs, Chapter 2 in Electric Power Networks Efficiency and Security (EPNES)-Volume 2: Risk-Based Power System Planning and Control, Eds. J. Momoh, L. Mili, John Wiley 2008
[18] "Parallel processing in power systems computation," *Power Systems, IEEE Transactions on,* vol. 7, pp. 629-638, 1992.
[19] C. Lemaitre and B. Thomas, "Two applications of parallel processing in power system computation," in *Power Industry Computer Application Conference, 1995. Conference Proceedings., 1995 IEEE,* 1995, pp. 62-69.
[20] O. R. Saavedra, "Solving the security constrained optimal power flow problem in a distributed computing environment," *Generation, Transmission and Distribution, IEE Proceedings-,* vol. 143, pp. 593-598, 1996.
[21] A. B. Alves and A. Monticelli, "Static security analysis using pipeline decomposition," *Generation, Transmission and Distribution, IEE Proceedings-,* vol. 145, pp. 105-110, 1998.
[22] Q. Morante, N. Ranaldo, A. Vaccaro, and E. Zimeo, "Pervasive grid for large-scale power systems contingency analysis," *Industrial Informatics, IEEE Transactions on,* vol. 2, pp. 165-175, 2006.
[23] C. Qiming and J. D. McCalley, "Identifying high risk N-k contingencies for online security assessment," *Power Systems, IEEE Transactions on,* vol. 20, pp. 823-834, 2005.
[24] C. M. Davis and T. J. Overbye, "Multiple Element Contingency Screening," *Power Systems, IEEE Transactions on,* vol. 26, pp. 1294-1301, 2011.
[25] D. Bienstock and A. Verma, "The nk problem in power grids: New models, formulations, and numerical experiments," *SIAM Journal on Optimization,* vol. 20, pp. 2352-2380, 2010.
[26] B. C. Lesieutre, S. Roy, V. Donde, and A. Pinar, "Power System Extreme Event Screening using Graph Partitioning," in *Power Symposium, 2006. NAPS 2006. 38th North American,* 2006, pp. 503-510.
[27] V. Donde, V. Lopez, B. Lesieutre, A. Pinar, Y. Chao, and J. Meza, "Severe Multiple Contingency Screening in Electric Power Systems," *Power Systems, IEEE Transactions on,* vol. 23, pp. 406-417, 2008.

[28] M. Eppstein and P. Hines, "A “Random Chemistry” algorithm for identifying collections of multiple contingencies that initiate cascading failure," in *Power and Energy Society General Meeting (PES), 2013 IEEE*, 2013, pp. 1-1.

[29] M. J. Eppstein and P. D. H. Hines, "A “Random Chemistry” Algorithm for Identifying Collections of Multiple Contingencies That Initiate Cascading Failure," *Power Systems, IEEE Transactions on,* vol. 27, pp. 1698-1705, 2012.

[30] D. P. Nedic, I. Dobson, D. S. Kirschen, B. A. Carreras, and V. E. Lynch, "Criticality in a cascading failure blackout model," *International Journal of Electrical Power & Energy Systems,* vol. 28, pp. 627-633, 2006.

[31] M. Papic, K. Bell, Y. Chen, I. Dobson, L. Fonte, E. Haq, *et al.*, "Survey of tools for risk assessment of cascading outages," in *Power and Energy Society General Meeting, 2011 IEEE*, 2011, pp. 1-9.

[32] A. G. Phadke and J. S. Thorp, "Expose hidden failures to prevent cascading outages [in power systems]," *Computer Applications in Power, IEEE,* vol. 9, pp. 20-23, 1996.

[33] J. Chen, J. S. Thorp, and I. Dobson, "Cascading dynamics and mitigation assessment in power system disturbances via a hidden failure model," *International Journal of Electrical Power & Energy Systems,* vol. 27, pp. 318-326, 2005.

[34] I. Dobson, J. Kim, and K. R. Wierzbicki, "Testing branching process estimators of cascading failure with data from a simulation of transmission line outages," *Risk Analysis,* vol. 30, pp. 650-662, 2010.

[35] I. Dobson, "Estimating the Propagation and Extent of Cascading Line Outages From Utility Data With a Branching Process," *Power Systems, IEEE Transactions on,* vol. 27, pp. 2146-2155, 2012.

[36] Q. Junjian, I. Dobson, and M. Shengwei, "Towards Estimating the Statistics of Simulated Cascades of Outages With Branching Processes," *Power Systems, IEEE Transactions on,* vol. 28, pp. 3410-3419, 2013.

[37] I. Dobson, B. A. Carreras, and D. E. Newman, "A loading-dependent model of probabilistic cascading failure," *Probability in the Engineering and Informational Sciences,* vol. 19, pp. 15-32, 2005.

[38] I. Dobson, B. Carreras, V. Lynch, and D. Newman, "An initial model for complex dynamics in electric power system blackouts," in *2013 46th Hawaii International Conference on System Sciences*, 2001, pp. 2017-2017.

[39] B. A. Carreras, V. E. Lynch, I. Dobson, and D. E. Newman, "Critical points and transitions in an electric power transmission model for cascading failure blackouts," *Chaos: An interdisciplinary journal of nonlinear science,* vol. 12, pp. 985-994, 2002.

[40] H. Ren, I. Dobson, and B. A. Carreras, "Long-Term Effect of the n-1 Criterion on Cascading Line Outages in an Evolving Power Transmission Grid," *Power Systems, IEEE Transactions on,* vol. 23, pp. 1217-1225, 2008.

[41] B. A. Carreras, D. E. Newman, I. Dobson, and N. S. Degala, "Validating OPA with WECC Data," in *System Sciences (HICSS), 2013 46th Hawaii International Conference on*, 2013, pp. 2197-2204.

[42] M. Shengwei, H. Fei, Z. Xuemin, W. Shengyu, and W. Gang, "An Improved OPA Model and Blackout Risk Assessment," *Power Systems, IEEE Transactions on*, vol. 24, pp. 814-823, 2009.

[43] M. Shengwei, N. Yixin, W. Gang, and W. Shengyu, "A Study of Self-Organized Criticality of Power System Under Cascading Failures Based on AC-OPF With Voltage Stability Margin," *Power Systems, IEEE Transactions on*, vol. 23, pp. 1719-1726, 2008.

[44] Q. Junjian, M. Shengwei, and L. Feng, "Blackout Model Considering Slow Process," *Power Systems, IEEE Transactions on*, vol. 28, pp. 3274-3282, 2013.

[45] M. A. Rios, D. S. Kirschen, D. Jayaweera, D. P. Nedic, and R. N. Allan, "Value of security: modeling time-dependent phenomena and weather conditions," *Power Systems, IEEE Transactions on*, vol. 17, pp. 543-548, 2002.

[46] D. S. Kirschen, D. Jayaweera, D. P. Nedic, and R. N. Allan, "A probabilistic indicator of system stress," *Power Systems, IEEE Transactions on*, vol. 19, pp. 1650-1657, 2004.

[47] M. Anghel, K. A. Werley, and A. E. Motter, "Stochastic Model for Power Grid Dynamics," in *System Sciences, 2007. HICSS 2007. 40th Annual Hawaii International Conference on*, 2007, pp. 113-113.

[48] M. Rahnamay-Naeini, W. Zhuoyao, N. Ghani, A. Mammoli, and M. M. Hayat, "Stochastic Analysis of Cascading-Failure Dynamics in Power Grids," *Power Systems, IEEE Transactions on*, vol. 29, pp. 1767-1779, 2014.

[49] J. Youwei and X. Zhao, "Risk assessment based on information entropy of cascading failure in power systems," in *Power and Energy Society General Meeting, 2012 IEEE*, 2012, pp. 1-5.

[50] G. A. Pagani and M. Aiello, "The Power Grid as a complex network: A survey," *Physica A: Statistical Mechanics and its Applications*.

[51] H. Jeong, B. Tombor, R. Albert, Z. N. Oltvai, and A. L. Barabasi, "The large-scale organization of metabolic networks," *Nature*, vol. 407, pp. 651-654, Oct 2000.

[52] E. Ravasz and A. L. Barabasi, "Hierarchical organization in complex networks," *Physical Review E*, vol. 67, Feb 2003.

[53] J. D. Noh and H. Rieger, "Random walks on complex networks," *Physical Review Letters*, vol. 92, Mar 2004.

[54] A. E. Motter and Y.-C. Lai, "Cascade-based attacks on complex networks," *Physical Review E*, vol. 66, p. 065102, 12/20/ 2002.

[55] Y.-C. Lai, A. Motter, and T. Nishikawa, "Attacks and Cascades in Complex Networks," in *Complex Networks*. vol. 650, E. Ben-Naim, H. Frauenfelder, and Z. Toroczkai, Eds., ed: Springer Berlin Heidelberg, 2004, pp. 299-310.

[56] M. Jalili, "Social power and opinion formation in complex networks," *Physica A: Statistical Mechanics and its Applications*, vol. 392, pp. 959-966, 2/15/ 2013.

[57] R. Baldick, B. Chowdhury, I. Dobson, D. Zhaoyang, G. Bei, D. Hawkins, *et al.*, "Initial review of methods for cascading failure analysis in electric power transmission systems IEEE PES CAMS task force on understanding, prediction, mitigation and restoration of cascading failures," in *Power and Energy Society General Meeting - Conversion and Delivery of Electrical Energy in the 21st Century, 2008 IEEE*, 2008, pp. 1-8.

[58] S. H. Strogatz, "Exploring complex networks," *Nature,* vol. 410, pp. 268-276, Mar 2001.

[59] A. L. Barabasi and R. Albert, "Emergence of scaling in random networks," *Science,* vol. 286, pp. 509-512, Oct 1999.

[60] D. J. Watts, *Small worlds: The dynamics of networks between order and randomness*: Princeton University Press, 2001.

[61] D. J. Watts, "A simple model of global cascades on random networks," *Proceedings of the National Academy of Sciences,* vol. 99, pp. 5766-5771, 2002.

[62] P. Crucitti, V. Latora, and M. Marchiori, "Model for cascading failures in complex networks," *Physical Review E,* vol. 69, p. 045104, 2004.

[63] P. Hines and S. Blumsack, "A centrality measure for electrical networks," in *Hawaii International Conference on System Sciences, Proceedings of the 41st Annual*, 2008, pp. 185-185.

[64] P. Crucitti, V. Latora, and M. Marchiori, "A topological analysis of the Italian electric power grid," *Physica a-Statistical Mechanics And Its Applications,* vol. 338, pp. 92-97, Jul 2004.

[65] S. Arianos, E. Bompard, A. Carbone, and F. Xue, "Power grid vulnerability: A complex network approach," *Chaos,* vol. 19, Mar 2009.

[66] J. Ash and D. Newth, "Optimizing complex networks for resilience against cascading failure," *Physica A: Statistical Mechanics and its Applications,* vol. 380, pp. 673-683, 7/1/ 2007.

[67] D. J. Watts and S. H. Strogatz, "Collective dynamics of 'small-world' networks," *Nature,* vol. 393, pp. 440-442, Jun 1998.

[68] M. Girvan and M. E. J. Newman, "Community structure in social and biological networks," *Proceedings Of the National Academy Of Sciences Of the United States Of America,* vol. 99, pp. 7821-7826, Jun 2002.

[69] M. E. J. Newman, "Modularity and community structure in networks," *Proceedings Of the National Academy Of Sciences Of the United States Of America,* vol. 103, pp. 8577-8582, Jun 2006.

[70] M. E. J. Newman, "Detecting community structure in networks," *European Physical Journal B,* vol. 38, pp. 321-330, Mar 2004.

[71] F. Radicchi, C. Castellano, F. Cecconi, V. Loreto, and D. Parisi, "Defining and identifying communities in networks," *Proceedings Of the National Academy Of Sciences Of the United States Of America,* vol. 101, pp. 2658-2663, Mar 2004.

[72] F. Wu and B. A. Huberman, "Finding communities in linear time: a physics approach," *European Physical Journal B,* vol. 38, pp. 331-338, Mar 2004.

[73] J. Reichardt and S. Bornholdt, "Detecting fuzzy community structures in complex networks with a Potts model," *Physical Review Letters,* vol. 93, Nov 2004.

[74] A. Capocci, V. D. P. Servedio, G. Caldarelli, and F. Colaiori, "Detecting communities in large networks," *Physica a-Statistical Mechanics And Its Applications,* vol. 352, pp. 669-676, Jul 2005.

[75] H. H. Happ, "The operation and control of large interconnected power systems," *Circuit Theory, IEEE Transactions on,* vol. 20, pp. 212-222, 1973.

[76] H. H. Happ, "Diakoptics—The solution of system problems by tearing," *Proceedings of the IEEE,* vol. 62, pp. 930-940, 1974.

[77] A. O. M. Saleh and M. A. Laughton, "Cluster analysis of power-system networks for array processing solutions," *Generation, Transmission and Distribution, IEE Proceedings C,* vol. 132, pp. 172-178, 1985.

[78] L. Hang, A. Bose, and V. Venkatasubramanian, "A fast voltage security assessment method using adaptive bounding," in *Power Industry Computer Applications, 1999. PICA '99. Proceedings of the 21st 1999 IEEE International Conference,* 1999, pp. 325-330.

[79] Z. Jin, E. Nobile, A. Bose, and K. Bhattacharya, "Localized reactive power markets using the concept of voltage control areas," *Power Systems, IEEE Transactions on,* vol. 19, pp. 1555-1561, 2004.

[80] W. Yurong, L. Fangxing, W. Qiulan, and C. Hao, "Reactive Power Planning Based on Fuzzy Clustering, Gray Code, and Simulated Annealing," *Power Systems, IEEE Transactions on,* vol. 26, pp. 2246-2255, 2011.

[81] M. Bjorndal and K. Jornsten, "Zonal pricing in a deregulated electricity market," *Energy Journal,* vol. 22, pp. 51-73, 2001.

[82] Gu, x, T. ler, and G. Gross, "Detection of Island Formation and Identification of Causal Factors Under Multiple Line Outages," *Power Systems, IEEE Transactions on,* vol. 22, pp. 505-513, 2007.

[83] M. Burger, D. Zelazo, and F. Allgower, "Hierarchical Clustering of Dynamical Networks Using a Saddle-Point Analysis," *Automatic Control, IEEE Transactions on,* vol. 58, pp. 113-124, 2013.

[84] H. You, V. Vittal, and W. Xiaoming, "Slow coherency-based islanding," *Power Systems, IEEE Transactions on,* vol. 19, pp. 483-491, 2004.

[85] B. Yang, V. Vittal, and G. T. Heydt, "Slow-Coherency-Based Controlled Islanding—A Demonstration of the Approach on the August 14, 2003 Blackout Scenario," *Power Systems, IEEE Transactions on,* vol. 21, pp. 1840-1847, 2006.

[86] F. Vallee, G. Brunieau, M. Pirlot, O. Deblecker, and J. Lobry, "Optimal Wind Clustering Methodology for Adequacy Evaluation in System Generation Studies Using Nonsequential Monte Carlo Simulation," *Power Systems, IEEE Transactions on,* vol. 26, pp. 2173-2184, 2011.

[87] E. Cotilla-Sanchez, P. D. H. Hines, C. Barrows, S. Blumsack, and M. Patel, "Multi-Attribute Partitioning of Power Networks Based on Electrical Distance," *Power Systems, IEEE Transactions on,* vol. 28, pp. 4979-4987, 2013.

[88] L. Juan, L. Chen-Ching, and K. P. Schneider, "Controlled Partitioning of a Power Network Considering Real and Reactive Power Balance," *Smart Grid, IEEE Transactions on,* vol. 1, pp. 261-269, 2010.

[89] S. Kai, Z. Da-Zhong, and L. Qiang, "Splitting strategies for islanding operation of large-scale power systems using OBDD-based methods," *Power Systems, IEEE Transactions on,* vol. 18, pp. 912-923, 2003.

[90] V. Donde, V. Lopez, B. Lesieutre, A. Pinar, Y. Chao, and J. Meza, "Identification of severe multiple contingencies in electric power networks," in *Power Symposium, 2005. Proceedings of the 37th Annual North American*, 2005, pp. 59-66.

[91] M. E. Newman, "The structure and function of complex networks," *SIAM review,* vol. 45, pp. 167-256, 2003.

[92] J. J. Grainger and W. D. Stevenson, *Power system analysis* vol. 31: McGraw-Hill New York, 1994.

[93] F. Goderya, A. A. Metwally, and O. Mansour, "Fast Detection and Identification of Islands in Power Networks," *Power Apparatus and Systems, IEEE Transactions on,* vol. PAS-99, pp. 217-221, 1980.

[94] A. M. Sasson, S. T. Ehrmann, P. Lynch, and L. S. Van Slyck, "Automatic Power System Network Topology Determination," *Power Apparatus and Systems, IEEE Transactions on,* vol. PAS-92, pp. 610-618, 1973.

[95] T. E. D. Liacco and T. J. Kraynak, "Processing by Logic Programming of Circuit-Breaker and Protective-Relaying Information," *Power Apparatus and Systems, IEEE Transactions on,* vol. PAS-88, pp. 171-175, 1969.

[96] M. Montagna and G. Granelli, "Detection of Jacobian singularity and network islanding in power flow computations," *Generation, Transmission and Distribution, IEE Proceedings-*, vol. 142, pp. 589-594, 1995.

[97] F. di Pierro, S.-T. Khu, D. Savić, and L. Berardi, "Efficient multi-objective optimal design of water distribution networks on a budget of simulations using hybrid algorithms," *Environmental Modelling & Software,* vol. 24, pp. 202-213, 2// 2009.

[98] M. Bertran and X. Corbella, "On the Validation and Analysis of a New Method for Power Network Connecticity Determination," *Power Apparatus and Systems, IEEE Transactions on,* vol. PAS-101, pp. 316-324, 1982.

[99] T. Men-Shen, "Development of islanding early warning mechanism for power systems," in *Power Engineering Society Summer Meeting, 2000. IEEE*, 2000, pp. 22-26 vol. 1.

[100] B. Mohar and Y. Alavi, "The Laplacian spectrum of graphs," *Graph theory, combinatorics, and applications,* vol. 2, pp. 871-898, 1991.

[101] "Engineering graph clustering: Models and experimental evaluation," *J. Exp. Algorithmics,* vol. 12, pp. 1-26, 2008.

[102] H. Wang, *The Eigenvalues and Laplacian Eigenvalues of A Graph*, 2009.
[103] A. E. Brouwer and W. H. Haemers, "A lower bound for the Laplacian eigenvalues of a graph - Proof of a conjecture by Guo," *Linear Algebra And Its Applications,* vol. 429, pp. 2131-2135, Oct 16 2008.
[104] H.-H. Li, J.-S. Li, and Y.-Z. Fan, "The effect on the second smallest eigenvalue of the normalized Laplacian of a graph by grafting edges," *Linear & Multilinear Algebra,* vol. 56, pp. 627-638, 2008 2008.
[105] K. C. Das and R. Bapat, "A sharp upper bound on the largest Laplacian eigenvalue of weighted graphs," *Linear algebra and its applications,* vol. 409, pp. 153-165, 2005.
[106] U. Luxburg, "A tutorial on spectral clustering," *Statistics and Computing,* vol. 17, pp. 395-416, 2007/12/01 2007.
[107] L. Donetti and M. A. Munoz, "Detecting network communities: a new systematic and efficient algorithm," *Journal of Statistical Mechanics: Theory and Experiment,* vol. 2004, p. P10012, 2004.
[108] J. G. Wilpon and L. R. Rabiner, "A MODIFIED K-MEANS CLUSTERING-ALGORITHM FOR USE IN ISOLATED WORK RECOGNITION," *Ieee Transactions on Acoustics Speech and Signal Processing,* vol. 33, pp. 587-594, 1985 1985.
[109] J. Chen and J. S. Thorp, "A reliability study of transmission system protection via a hidden failure DC load flow model," in *Power System Management and Control, 2002. Fifth International Conference on (Conf. Publ. No. 488),* 2002, pp. 384-389.
[110] A. A. Aquino-Lugo, R. Klump, and T. J. Overbye, "A Control Framework for the Smart Grid for Voltage Support Using Agent-Based Technologies," *Smart Grid, IEEE Transactions on,* vol. 2, pp. 173-180, 2011.
[111] S. M. Amin and B. F. Wollenberg, "Toward a smart grid: power delivery for the 21st century," *Power and Energy Magazine, IEEE,* vol. 3, pp. 34-41, 2005.
[112] S. A. Arefifar, Y. A. R. I. Mohamed, and T. H. M. El-Fouly, "Comprehensive Operational Planning Framework for Self-Healing Control Actions in Smart Distribution Grids," *Power Systems, IEEE Transactions on,* vol. 28, pp. 4192-4200, 2013.
[113] A. Zidan and E. F. El-Saadany, "A Cooperative Multiagent Framework for Self-Healing Mechanisms in Distribution Systems," *Smart Grid, IEEE Transactions on,* vol. 3, pp. 1525-1539, 2012.
[114] Y. Dayong, Z. Minjie, and D. Sutanto, "A Hybrid Multiagent Framework With Q-Learning for Power Grid Systems Restoration," *Power Systems, IEEE Transactions on,* vol. 26, pp. 2434-2441, 2011.
[115] T. Nagata, H. Watanabe, M. Ohno, and H. Sasaki, "A multi-agent approach to power system restoration," in *Power System Technology, 2000. Proceedings. PowerCon 2000. International Conference on,* 2000, pp. 1551-1556 vol.3.

[116] D. Lei, F. M. Gonzalez-Longatt, P. Wall, and V. Terzija, "Two-Step Spectral Clustering Controlled Islanding Algorithm," *Power Systems, IEEE Transactions on,* vol. 28, pp. 75-84, 2013.
[117] K. Schloegel, G. Karypis, and V. Kumar, *A New Algorithm for Multi-objective Graph Partitioning*: Springer, 1999.
[118] F. R. Chung, *Spectral graph theory* vol. 92: AMS Bookstore, 1997.
[119] C. Davis and W. M. Kahan, "The rotation of eigenvectors by a perturbation. III," *SIAM Journal on Numerical Analysis,* vol. 7, pp. 1-46, 1970.
[120] J. Shi and J. Malik, "Normalized cuts and image segmentation," *Pattern Analysis and Machine Intelligence, IEEE Transactions on,* vol. 22, pp. 888-905, 2000.
[121] T. Kohonen, "The self-organizing map," *Proceedings of the IEEE,* vol. 78, pp. 1464-1480, 1990.
[122] T. Kohonen, "Self-organization and associative memory," *Self-Organization and Associative Memory, 100 figs. XV, 312 pages.. Springer-Verlag Berlin Heidelberg New York. Also Springer Series in Information Sciences, volume 8,* vol. 1, 1988.
[123] T. Kohonen, "Self-organized formation of topologically correct feature maps," *Biological cybernetics,* vol. 43, pp. 59-69, 1982.
[124] Y. Jun, Z. Yihai, H. Haibo, and S. Yan, "Multi-Contingency Cascading Analysis of Smart Grid Based on Self-Organizing Map," *Information Forensics and Security, IEEE Transactions on,* vol. 8, pp. 646-656, 2013.
[125] D. Srinivasan, T. Swee Sien, C. S. Cheng, and C. Eng Kiat, "Parallel neural network-fuzzy expert system strategy for short-term load forecasting: system implementation and performance evaluation," *Power Systems, IEEE Transactions on,* vol. 14, pp. 1100-1106, 1999.
[126] B. P. Padhy, S. C. Srivastava, and N. K. Verma, "A Coherency-Based Approach for Signal Selection for Wide Area Stabilizing Control in Power Systems," *Systems Journal, IEEE,* vol. 7, pp. 807-816, 2013.
[127] K. Tasdemir, P. Milenov, and B. Tapsall, "Topology-Based Hierarchical Clustering of Self-Organizing Maps," *Neural Networks, IEEE Transactions on,* vol. 22, pp. 474-485, 2011.
[128] J. Vesanto and E. Alhoniemi, "Clustering of the self-organizing map," *Neural Networks, IEEE Transactions on,* vol. 11, pp. 586-600, 2000.
[129] F. Murtagh, "Interpreting the Kohonen self-organizing feature map using contiguity-constrained clustering," *Pattern Recognition Letters,* vol. 16, pp. 399-408, 1995.
[130] K. Tasdemir and E. Merényi, "Data topology visualization for the Self-Organizing Map," in *ESANN*, 2006, pp. 277-282.
[131] K. Tasdemir and E. Merenyi, "Exploiting Data Topology in Visualization and Clustering of Self-Organizing Maps," *Neural Networks, IEEE Transactions on,* vol. 20, pp. 549-562, 2009.

[132] K. Deb, A. Pratap, S. Agarwal, and T. Meyarivan, "A fast and elitist multiobjective genetic algorithm: NSGA-II," *Evolutionary Computation, IEEE Transactions on,* vol. 6, pp. 182-197, 2002.
[133] S. Agrawal, K. B. Panigrahi, and M. K. Tiwari, "Multiobjective Particle Swarm Algorithm With Fuzzy Clustering for Electrical Power Dispatch," *Evolutionary Computation, IEEE Transactions on,* vol. 12, pp. 529-541, 2008.
[134] T. Hastie, R. Tibshirani, and J. J. H. Friedman, *The elements of statistical learning* vol. 1: Springer New York, 2001.
[135] D. L. Davies and D. W. Bouldin, "A Cluster Separation Measure," *Pattern Analysis and Machine Intelligence, IEEE Transactions on,* vol. PAMI-1, pp. 224-227, 1979.
[136] Available online http://psdyn.ece.wisc.edu/IEEE_benchmarks/
[137] Available online https://www.ee.washington.edu/research/pstca/pf118/pg_tca118bus.htm
[138] S. Milgram, "The small world problem," *Psychology today,* vol. 2, pp. 60-67, 1967.
[139] D. J. Watts and S. H. Strogatz, "Collective dynamics of 'small-world'networks," *nature,* vol. 393, pp. 440-442, 1998.
[140] C. Moore and M. E. Newman, "Exact solution of site and bond percolation on small-world networks," *Physical Review E,* vol. 62, p. 7059, 2000.
[141] M. Vaiman, K. Bell, Y. Chen, B. Chowdhury, I. Dobson, P. Hines, *et al.*, "Risk Assessment of Cascading Outages: Methodologies and Challenges," *Power Systems, IEEE Transactions on,* vol. 27, pp. 631-641, 2012.
[142] B. A. Carreras, V. E. Lynch, I. Dobson, and D. E. Newman, "Complex dynamics of blackouts in power transmission systems," *Chaos: An Interdisciplinary Journal of Nonlinear Science,* vol. 14, pp. 643-652, 2004.
[143] North American Electric Reliability Council. Disturbances Analysis Working Group Database. Available online: http://www.nerc.com/~dawg/database.html
[144] A. Lipowski and D. Lipowska, "Roulette-wheel selection via stochastic acceptance," *Physica A: Statistical Mechanics and its Applications,* vol. 391, pp. 2193-2196, 2012.
[145] M. Alhamdoosh and D. H. Wang, "Fast decorrelated neural network ensembles with random weights," *Information Sciences,* vol. 264, pp. 104-117, Apr 2014.
[146] W. F. Schmidt, M. A. Kraaijveld, and R. P. Duin, "Feedforward neural networks with random weights," in *Pattern Recognition, 1992. Vol. II. Conference B: Pattern Recognition Methodology and Systems, Proceedings., 11th IAPR International Conference on*, 1992, pp. 1-4.
[147] G.-B. Huang, Q.-Y. Zhu, and C.-K. Siew, "Extreme learning machine: theory and applications," *Neurocomputing,* vol. 70, pp. 489-501, 2006.
[148] I. Tyukin and D. Prokhorov, "Feasibility of random basis function approximators for modeling and control," *arXiv preprint arXiv:0905.0677,* 2009.

[149] C. Radhakrishna Rao and S. K. Mitra, "Generalized inverse of a matrix and its applications," in *Proceedings of the Berkeley Symposium on Mathematical Statistics and Probability*, 1972, pp. 601-620.
[150] Y. Jia, K. Meng, and Z. Xu, "N-k Induced Cascading Contingency Screening," *Power Systems, IEEE Transactions on,* vol. PP, pp. 1-2, 2014.
[151] R. D. Zimmerman, S. Murillo, x, C. E. nchez, and R. J. Thomas, "MATPOWER: Steady-State Operations, Planning, and Analysis Tools for Power Systems Research and Education," *Power Systems, IEEE Transactions on,* vol. 26, pp. 12-19, 2011.
[152] C. M. Rocco, J. E. Ramirez-Marquez, D. E. Salazar, and C. Yajure, "Assessing the Vulnerability of a Power System Through a Multiple Objective Contingency Screening Approach," *Reliability, IEEE Transactions on,* vol. 60, pp. 394-403, 2011.
[153] H. Kuk-Hyun and K. Jong-Hwan, "Quantum-inspired evolutionary algorithm for a class of combinatorial optimization," *Evolutionary Computation, IEEE Transactions on,* vol. 6, pp. 580-593, 2002.
[154] H. Kuk-Hyun and K. Jong-Hwan, "Quantum-inspired evolutionary algorithms with a new termination criterion, H_ε gate, and two-phase scheme," *Evolutionary Computation, IEEE Transactions on,* vol. 8, pp. 156-169, 2004.
[155] K. Yehoon, K. Jong-Hwan, and H. Kuk-Hyun, "Quantum-inspired Multiobjective Evolutionary Algorithm for Multiobjective 0/1 Knapsack Problems," in *Evolutionary Computation, 2006. CEC 2006. IEEE Congress on*, 2006, pp. 2601-2606.